

to appear in
Reports on Progress in Physics

COLOUR DECONFINEMENT IN NUCLEAR COLLISIONS

Helmut Satz

Fakultät für Physik, Universität Bielefeld
D-33501 Bielefeld, Germany

Abstract:

QCD predicts that strongly interacting matter will undergo a transition from a state of hadronic constituents to a plasma of unbound quarks and gluons. We first survey the conceptual features of this transition and its description in finite temperature lattice QCD, before we address its experimental investigation through high energy nucleus-nucleus collisions. After considering the conditions achievable in such collisions, we discuss the possible probes to check if the produced medium in its early stages was indeed deconfined. We then elaborate the method that has emerged and the results which were obtained using the most extensively studied deconfinement probe, the suppression of charmonium production. In closing, we discuss possible supporting information provided through the study of soft hadronic probes.

Contents

1. Introduction
2. States of Matter in QCD
 - 2.1 From Hadronic Matter to Quark-Gluon Plasma
 - 2.2 Critical Behaviour in QCD
 - 2.3 Deconfinement and Chiral Symmetry Restoration
 - 2.4 Deconfinement and Percolation
3. Conditions in Nuclear Collisions
 - 3.1 High Energy Collisions and Nuclear Transparency
 - 3.2 Collision Evolution and Initial Conditions
 - 3.3 The Onset of Deconfinement
4. Probes of Primordial Matter
 - 4.1 Evolution Stages
 - 4.2 Quarkonium Dissociation
 - 4.3 Jet Quenching
5. J/ψ Suppression in Nuclear Collisions
 - 5.1 The Hadroproduction of Charmonium
 - 5.2 Pre-Resonance Suppression
 - 5.3 Anomalous J/ψ Suppression
 - 5.4 P_T Dependence
6. Soft Hadronic Probes
 - 6.1 Retrospective Probes
 - 6.2 Hadronisation and Freeze-Out
 - 6.3 Parton Cascade Models
7. Summary

1. INTRODUCTION

Over the past hundred years, our ideas about the ultimate constituents of matter have undergone a considerable evolution. Atoms were found to be divisible into electrons and nuclei. Nuclei in turn consist of nucleons, bound together by strong short-range forces. With the advent of the basic theory of strong interactions, quantum chromodynamics (QCD), has come the conviction that nucleons - and more generally, all strongly interacting elementary particles (hadrons) - are bound states of quarks. Quarks are point-like and confined to “their” hadron by a binding potential $V_0(r)$ which increases linearly with quark separation r ,

$$V_0(r) \sim \sigma r, \quad (1)$$

where the string tension σ measures the energy per unit separation distance. Hence an infinite amount of energy would be needed to isolate a quark; it cannot exist by itself, and it is therefore not possible to split an isolated hadron into its quark constituents. The elementary particles of strong interaction physics remain elementary in the sense that they are the smallest entities with an independent existence; however, they have become composite, since they are bound states of quarks. What effect will this have on the states of strongly interacting matter?

To get a first idea of what the quark infrastructure of elementary particles implies for the behaviour of matter at extreme density, consider a very simple picture. If nucleons, with their intrinsic spatial extension, were both elementary and incompressible, then a state of close packing would constitute the high density limit of matter (Fig. 1a). On the other hand, composite nucleons made up of point-like quarks will start to overlap with increasing density, until eventually each quark finds within its immediate vicinity a considerable number of other quarks (Fig. 1b). It has no way to identify which of these had been its partners in a specific nucleon at some previous state of lower density. Beyond a certain point, the concept of a hadron thus loses its meaning; at extreme density, we are quite naturally led to a medium whose basic constituents are unbound quarks.

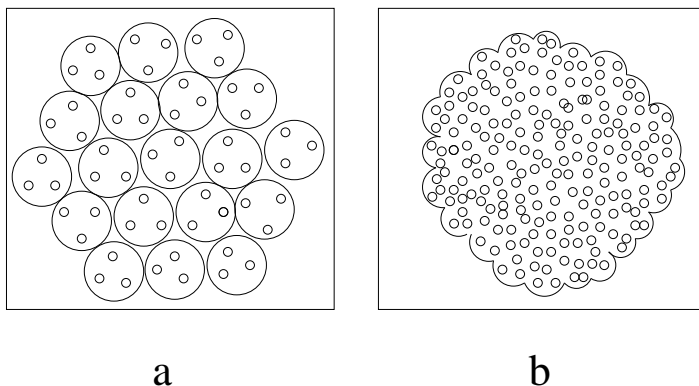


Figure 1: Strongly interacting matter as nuclear matter at a density of closely packed nucleons (a) and as quark matter at much higher density (b).

Ever since the big bang, our universe has been expanding; if we could reverse time and let the film run backwards, we would find matter of higher and higher densities. Up

to nuclear density, we have experimental information to guide our understanding of such matter. What happens beyond this point? This question, the nature of matter at extreme density, will be the central topic of this report. The primordial matter in the very early universe provides a particularly striking instance of such a system, but not the only one, as we shall see shortly.

On the theoretical side, studies of statistical QCD, in particular through computer simulations, have confirmed the transition from hadronic matter to a plasma of unbound quarks and gluons. This led to the challenge to produce and study the predicted new state of matter in the laboratory. The only way to achieve this, as far as we know, is to collide two heavy nuclei and study the resulting small and short-lived droplets of hot and dense medium. For such studies it is essential to have viable probes which can determine if the droplets in the early stages of nuclear collisions indeed consisted of unbound quarks and gluons: we have to find signatures of colour deconfinement.

In the next section, we shall survey concepts and theoretical results concerning the states of matter in strong interaction physics. Following that, we shall address the thermodynamic conditions which can be achieved in nuclear collisions. This will set the stage for the main problem: probing experimentally whether high energy nuclear collisions have produced deconfined matter and studying the properties of the new phase. Finally we shall consider the possible support that soft hadronic observables from later stages can provide to corroborate the conclusions obtained using early hard probes.

In view of the many-faceted nature of high energy nuclear physics, it is perhaps appropriate to emphasize here that the aim of this survey is colour deconfinement and its manifestation in such collisions. Many other interesting aspects of the field will unfortunately but unavoidably have to suffer from this restriction.

2. STATES OF MATTER IN QCD

2.1 From Hadronic Matter to Quark-Gluon Plasma

Confinement is a *long-range* feature, which prevents the isolation of a *single* quark. In the high density situation of Fig. 1a each quark finds very close to it many others and is thus far from isolated. To see how the *short-range* nature of dense matter overcomes confinement, recall the effect of a dense medium on electric forces. In a vacuum, two electric charges e_0 interact through the Coulomb potential

$$V_0(r) = \left(\frac{e_0^2}{r} \right), \quad (2)$$

where r again denotes the separation distance. In a dense environment of many other charges, the potential becomes screened,

$$V(r) = \left(\frac{e_0^2}{r} \right) \exp(-\mu r); \quad (3)$$

where $r_D = \mu^{-1}$ is the Debye screening radius of the medium; it decreases as the charge density of the medium increases. Thus the potential between two test charges a fixed distance apart becomes weaker with increasing density. This occurs because the other charges in the medium partially neutralize the test charges and thereby shorten the range of the interaction. If a bound state, such as a hydrogen atom, is put into such a medium, the screening radius r_D will for sufficiently high density become less than the binding radius r_B of the atom. Once $r_D \ll r_B$, the effective force between proton and electron has become so short-ranged that the two can no longer bind. Thus insulating matter, consisting of bound electric charges, will at sufficiently high density become conducting: it will undergo a phase transition [1], in which charge screening dissolves the binding of the constituents, leading to a plasma of unbound charges as a new state of matter.

The interaction of quarks in QCD is based on their intrinsic colour charge, and in a dense medium this charge can be screened in much the same way as an electric charge. Hadrons are colour-neutral bound states of coloured quarks; hence dilute hadronic matter is a colour insulator. At sufficiently high density, however, we expect colour screening to set in, so that the potential (1) becomes ¹

$$V(r) \simeq \sigma r \left[\frac{1 - \exp(-\mu r)}{\mu r} \right]; \quad (4)$$

as above, the colour screening mass μ here is also the inverse of the screening radius for colour charges. The resulting exponential damping of the binding force will remove all long range effects and in a sufficiently dense medium ‘melt’ hadrons (see Fig. 2) just as Debye screening dissociated hydrogen atoms. Colour screening will thus transform a colour insulator into a colour conductor, turning hadronic matter into a quark plasma [3]. The transition from insulator to conductor by charge screening is a collective effect, so that we expect a phase transition at the point of plasma formation.

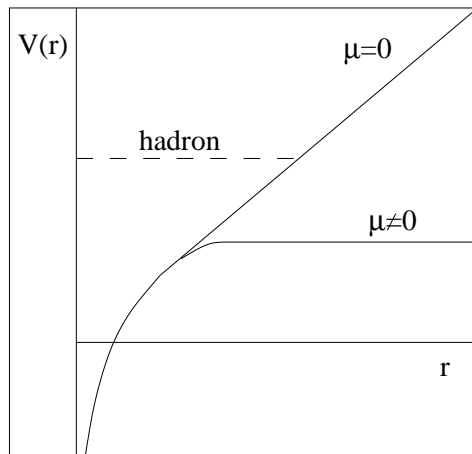


Figure 2: Colour screening of the confining potential.

¹The functional form of the screening depends on the form of the unscreened potential [2]; this leads to the difference between Eqs. (3) and (4).

When atomic matter is transformed from an insulator into a conductor, the effective mass of the conduction electrons is changed. In insulators, the electrons occur with their physical mass; in the conducting phase, however, they acquire a different, *effective* mass, due to the presence of the other conducting electrons, the periodic field of the charged ions and the lattice vibrations. All these effects combine to produce a mean background field quite different from the vacuum. As a result, the insulator-conductor transition is accompanied by a mass shift for the electrons. Similarly, the effective quark mass is expected to change between the confined and the deconfined phase. When confined in hadrons, the basic quarks ‘dress’ themselves with gluons to acquire an effective constituent quark mass of about 300 MeV (1/3 of the proton or 1/2 of the ρ -meson mass). On the other hand, the basic bare quarks in the QCD Lagrangian are almost massless, so that the mass of the constituent quarks in the confined phase must be generated spontaneously through the confinement interaction. Hence it is likely that when deconfinement occurs, this additional mass is ‘lost’ and the quarks revert to their intrinsic ‘bare’ mass.

A Lagrangian with massless fermions – the limiting case of the light up and down quarks in the physical Lagrangian – possesses chiral symmetry; this allows a decomposition of the quarks into independent left- and right-handed massless spin one-half states, which for massive fermions become mixed. For massless quarks, confinement must thus lead to spontaneous breaking of chiral symmetry, deconfinement to its restoration. Hence the mass shift transition in QCD is often referred to as chiral symmetry restoration. It can, but does not need to coincide with deconfinement: when the hadrons are dissolved into quark constituents, the liberated and hence now coloured quarks may still interact to form coloured bound states. Thus at low temperature and high density, the quark triplets in nucleons, once deconfined, might choose to recombine into massive coloured quark pairs (“diquarks”) [4], similar to Cooper pairs in QED. When the density is increased further, the diquarks would break up into the massless basic quarks. This results in a three-phase picture of strongly interacting matter, with hadronic matter as confined phase, then deconfinement, followed by a phase consisting of massive coloured diquark systems, and finally, after chiral symmetry restoration, a plasma of coloured massless quarks and gluons. Such a three-phase structure would correspond to the succession of insulator, superconductor and conductor in atomic matter.

In relativistic thermodynamics, higher densities can be obtained either by increasing the net baryon number density, or by ‘heating’ the system, so that collisions between its constituents produce further hadrons. This leads to the phase diagram shown in Fig. 3: for low values of the temperature T and the baryochemical potential μ_B , associated to the net baryon number density, we have confinement and hence hadronic matter; for high T and/or μ_B , deconfinement sets in and we get a quark-gluon plasma. In the compression of cold nuclear matter, by increasing μ_B for $T = 0$, an intermediate diquark phase could occur, similar to the superconducting phase in atomic matter. By increasing T at $\mu_B = 0$, we are heating mesonic matter until it becomes a quark-gluon plasma. Strong interaction thermodynamics thus predicts the existence of new, deconfined states of matter at high temperatures and densities.

Before turning to the theoretical basis of these conceptual considerations, we illustrate the transition from hadronic matter to quark-gluon plasma by a very simple model. For

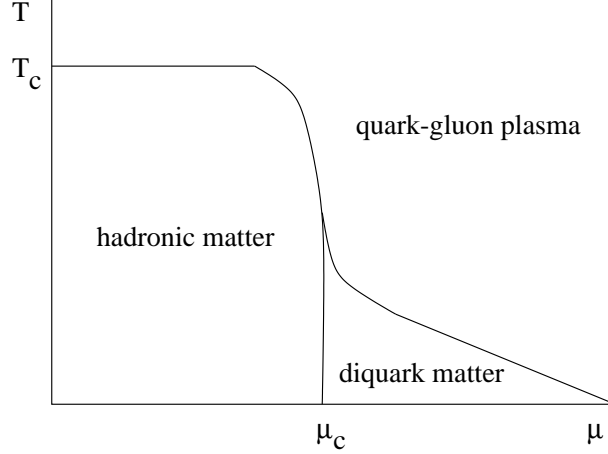


Figure 3: The phase diagram of strongly interacting matter.

an ideal gas of massless pions, the pressure as function of the temperature is given by the Stefan-Boltzmann form

$$P_\pi = 3 \frac{\pi^2}{90} T^4 \quad (5)$$

where the factor 3 accounts for the three charge states of the pion. The corresponding form for an ideal quark-gluon plasma with two flavours and three colours is

$$P_{qg} = \left\{ 2 \times 8 + \frac{7}{8} (3 \times 2 \times 2 \times 2) \right\} \frac{\pi^2}{90} T^4 - B = 37 \frac{\pi^2}{90} T^4 - B. \quad (6)$$

In Eq. (6), the first temperature term in the curly brackets accounts for the two spin and eight colour degrees of freedom of the gluons, the second for the three colour, two flavour, two spin and two particle-antiparticle degrees of freedom of the quarks, with 7/8 to obtain the correct statistics. The bag pressure B takes into account the difference between the physical vacuum and the ground state for quarks and gluons in a medium.

Since in thermodynamics, a system chooses the state of lowest free energy and hence highest pressure, we compare in Fig. 4a the temperature behaviour of Eq's. (5) and (6). Our simple model thus leads to a two-phase picture of strongly interacting matter, with a hadronic phase up to

$$T_c = \left(\frac{45}{17\pi^2} \right)^{1/4} B^{1/4} \simeq 0.72 B^{1/4} \quad (7)$$

and a quark gluon plasma above this critical temperature. From hadron spectroscopy, the bag pressure is given by $B^{1/4} \simeq 0.2$ GeV, so that we obtain

$$T_c \simeq 145 \text{ MeV} \quad (8)$$

as the deconfinement temperature. In the next section we shall find this simple estimate to be remarkably close to the value obtained in lattice QCD.

The energy densities of the two phases of our model are given by

$$\epsilon_\pi = \frac{\pi^2}{10} T^4 \quad (9)$$

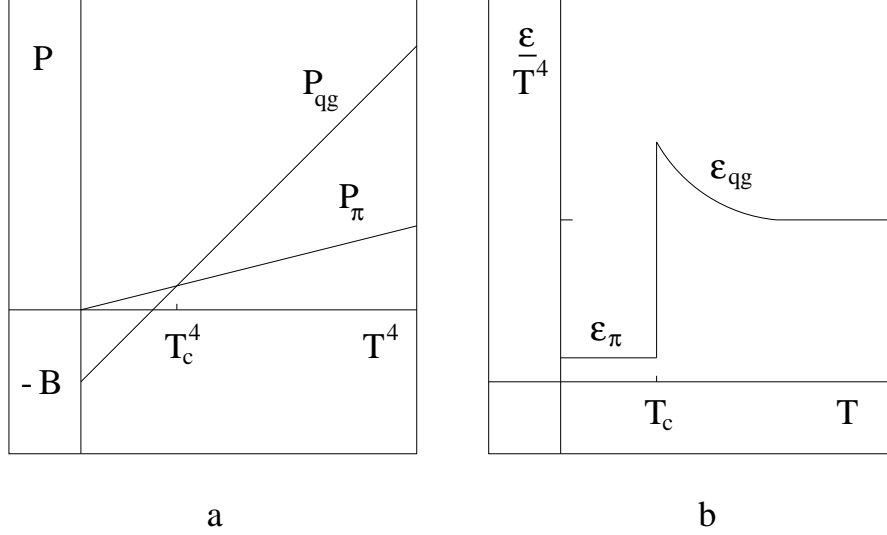


Figure 4: Pressure (a) and energy density (b) in a two-phase ideal gas model.

and

$$\epsilon_{qg} = 37 \frac{\pi^2}{30} T^4 + B. \quad (10)$$

By construction, the transition is first order, and the resulting temperature dependence is shown in Fig. 4b. We note that even though both phases consist of massless non-interacting constituents, in the quark-gluon plasma

$$(\epsilon - 3P) = 4B \quad (11)$$

does not vanish, as consequence of the difference between physical vacuum and in-medium QCD ground state [5].

2.2 Critical Behaviour in QCD

Here we shall derive the conceptual considerations of the last section from strong interaction thermodynamics, based on QCD as the input dynamics. QCD is defined by the Lagrangian

$$\mathcal{L} = -\frac{1}{4} F_{\mu\nu}^a F_a^{\mu\nu} - \sum_f \bar{\psi}_\alpha^f (i\gamma^\mu \partial_\mu + m_f - g\gamma^\mu A_\mu)^{\alpha\beta} \psi_\beta^f, \quad (12)$$

with

$$F_{\mu\nu}^a = (\partial_\mu A_\nu^a - \partial_\nu A_\mu^a - gf_{bc}^a A_\mu^b A_\nu^c). \quad (13)$$

Here A_μ^a denotes the gluon field of colour a ($a=1,2,\dots,8$) and ψ_α^f the quark field of colour α ($\alpha=1,2,3$) and flavour f ; the input (‘bare’) quark masses are given by m_f . With the dynamics thus determined, the corresponding thermodynamics is obtained from the partition function, which is most suitably expressed as a functional path integral,

$$Z(T, V) = \int dA d\psi d\bar{\psi} \exp \left(- \int_V d^3x \int_0^{1/T} d\tau \mathcal{L}(A, \psi, \bar{\psi}) \right), \quad (14)$$

since this form involves directly the Lagrangian density defining the theory. The spatial integration in the exponent of Eq. (14) is performed over the entire spatial volume V of the system; in the thermodynamic limit it becomes infinite. The time component x_0 is “rotated” to become purely imaginary, $\tau = ix_0$, thus turning the Minkowski manifold, on which the fields A and ψ are originally defined, into a Euclidean space. The integration over τ in Eq. (14) runs over a finite slice whose thickness is determined by the temperature of the system.

From $Z(T, V)$, all thermodynamical observables can be calculated in the usual fashion. Thus

$$\epsilon = (T^2/V) \left(\frac{\partial \ln Z}{\partial T} \right)_V \quad (15)$$

gives the energy density, and

$$P = T \left(\frac{\partial \ln Z}{\partial V} \right)_T \quad (16)$$

the pressure. For the study of critical behaviour, long range correlations and multi-particle interactions are of crucial importance; hence perturbation theory cannot be used. The necessary non-perturbative regularisation scheme is provided by the lattice formulation of QCD [6]; it leads to a form which can be evaluated numerically by computer simulation [7]. Unfortunately, this method is so far viable only for the case of vanishing baryon number density, so that results are today available only for that part of the phase diagram in Fig. 3.

Without going into the details of computer simulation of finite temperature QCD (for a survey, see [8]), we summarize what has been obtained so far. The first variable to consider is the deconfinement measure given by the Polyakov loop [9, 10]

$$L(T) \sim \lim_{r \rightarrow \infty} \exp\{-V(r)/T\} \quad (17)$$

where $V(r)$ is the potential between a static quark-antiquark pair separated by a distance r . In the limit of large input quark mass, $V(\infty) = \infty$ in the confined phase, so that then $L = 0$. Colour screening, on the other hand, makes $V(r)$ finite at large r , so that in the deconfined phase, L does not vanish. It thus becomes an ‘order parameter’ like the magnetisation in the Ising model; this is zero at high temperatures, but becomes non-zero below the Curie point, when the ‘up-down’ Z_2 symmetry of the Ising Hamiltonian is spontaneously broken. In the large quark mass limit, QCD reduces to pure $SU(3)$ gauge theory, which is invariant under a global Z_3 symmetry. The Polyakov loop provides a measure of the state of the system under this symmetry: it vanishes for Z_3 symmetric states and becomes finite when Z_3 is spontaneously broken. Hence the critical behaviour of the Ising model (and more generally, Z_N spin systems) as well as that of $SU(N)$ gauge theories is based on the spontaneous symmetry breaking of a global Z_N symmetry [16].

For finite quark mass m_q , $V(r)$ remains finite for $r \rightarrow \infty$, since the ‘string’ between the two colour charges ‘breaks’ when the corresponding potential energy becomes equal to the mass M_h of the lowest hadron; beyond this point, it becomes energetically more favourable to produce an additional hadron. Hence now L no longer vanishes in the

confined phase, but only becomes exponentially small there,

$$L(T) \sim \exp\{-M_h/T\}; \quad (18)$$

here M_h is of the order of the ρ -mass, so that $L \sim 10^{-2}$, rather than zero. Deconfinement is thus indeed much like the insulator-conductor transition, for which the order parameter, the conductivity $\sigma(T)$, also does not really vanish for $T > 0$, but with $\sigma(T) \sim \exp\{-\Delta E/T\}$ is only exponentially small, since thermal ionisation (with ionisation energy ΔE) produces a small number of unbound electrons even in the insulator phase.

Fig. 5 shows recent lattice results for $L(T)$ and the corresponding susceptibility $\chi_L(T) \sim \langle L^2 \rangle - \langle L \rangle^2$ [11]. The calculations were performed for the case of two flavours of light quarks, using a current quark mass about four times larger than that needed for the physical pion mass [11]. We note that $L(T)$ undergoes the expected sudden increase from a small confinement to a much larger deconfinement value. The sharp peak of $\chi_L(T)$ defines quite well the transition temperature T_c , which we shall shortly specify in physical units.

The next quantity to consider is the effective quark mass; it is measured by the expectation value of the corresponding term in the Lagrangian, $\langle \bar{\psi}\psi \rangle(T)$. In the limit of vanishing current quark mass, the Lagrangian becomes chirally symmetric and $\langle \bar{\psi}\psi \rangle(T)$ the corresponding order parameter. In the confined phase, with effective constituent quark masses $M_q \simeq 0.3$ GeV, this chiral symmetry is spontaneously broken, while in the deconfined phase, at high enough temperature, we expect its restoration. In the real world, with finite pion and hence finite current quark mass, this symmetry is also only approximate, since $\langle \bar{\psi}\psi \rangle(T)$ now never vanishes at finite T .

The behaviour of $\langle \bar{\psi}\psi \rangle(T)$ and the corresponding susceptibility $\chi_m \sim \partial \langle \bar{\psi}\psi \rangle / \partial m_q$ are shown in Fig. 6 [11], calculated for the same case as above in Fig. 5. We note here the expected sudden drop of the effective quark mass and the associated sharp peak in the susceptibility. The temperature at which this occurs coincides with that obtained through the deconfinement measure. We therefore conclude that at vanishing baryon number density, quark deconfinement and the shift from constituent to current quark mass coincide. In section 2.3, we shall consider why this is so.

We thus obtain for $\mu_B = 0$ a rather well defined phase structure, consisting of a confined phase for $T < T_c$, with $L(T) \simeq 0$ and $\langle \bar{\psi}\psi \rangle(T) \neq 0$, and a deconfined phase for $T > T_c$ with $L(T) \neq 0$ and $\langle \bar{\psi}\psi \rangle(T) \simeq 0$. The underlying symmetries associated to the critical behaviour at $T = T_c$, the Z_3 symmetry of deconfinement and the chiral symmetry of the quark mass shift, become exact in the limits $m_q \rightarrow \infty$ and $m_q \rightarrow 0$, respectively. In the real world, both symmetries are only approximate; nevertheless, we see from Figs. 5 and 6 that both associated measures retain an almost critical behaviour.

Next we turn to the behaviour of energy density ϵ and pressure P at deconfinement. In Fig. 7 it is seen that ϵ/T^4 changes quite abruptly at the above determined critical temperature $T = T_c$, increasing from a low hadronic value to nearly that expected for an ideal gas of quarks and gluons [12]. Besides the sudden increase at deconfinement, there are two further points to note. In the region $T_c < T < 2 T_c$, ϵ and $3P$ do not yet coincide, as also found in the simple model of the previous section; much of the difference is presumably due to the difference between physical vacuum and QCD in-medium ground state [5].

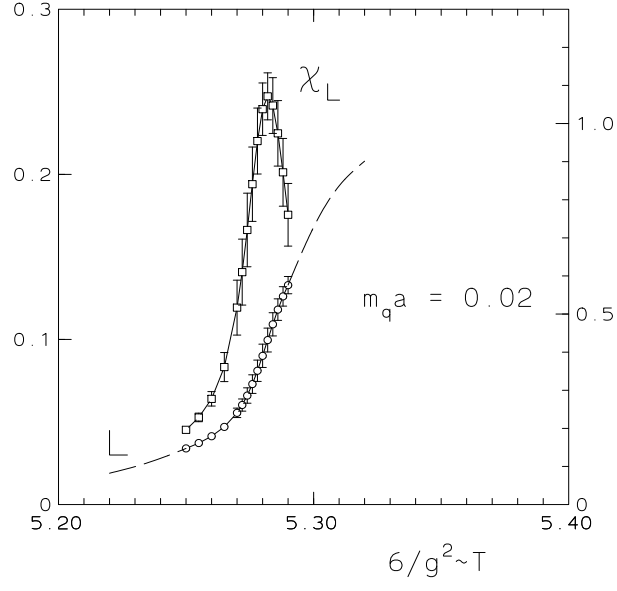


Figure 5: The temperature dependence of the Polyakov loop and the associated susceptibility in two-flavour QCD [11].

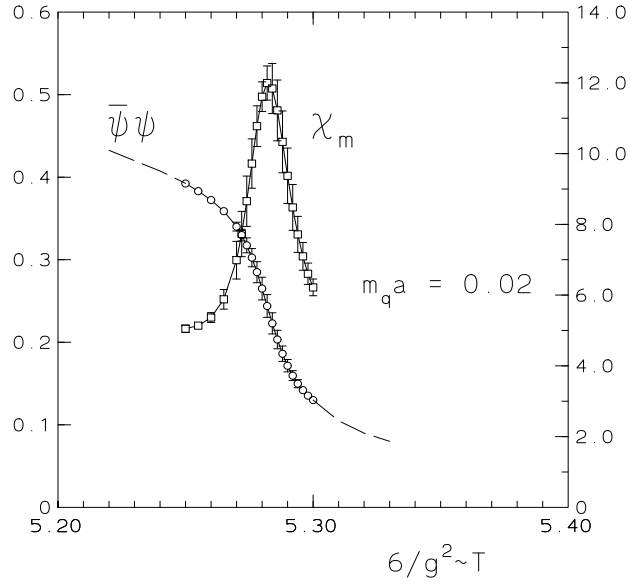


Figure 6: The temperature dependence of the chiral condensate and the associated susceptibility in two-flavour QCD [11].

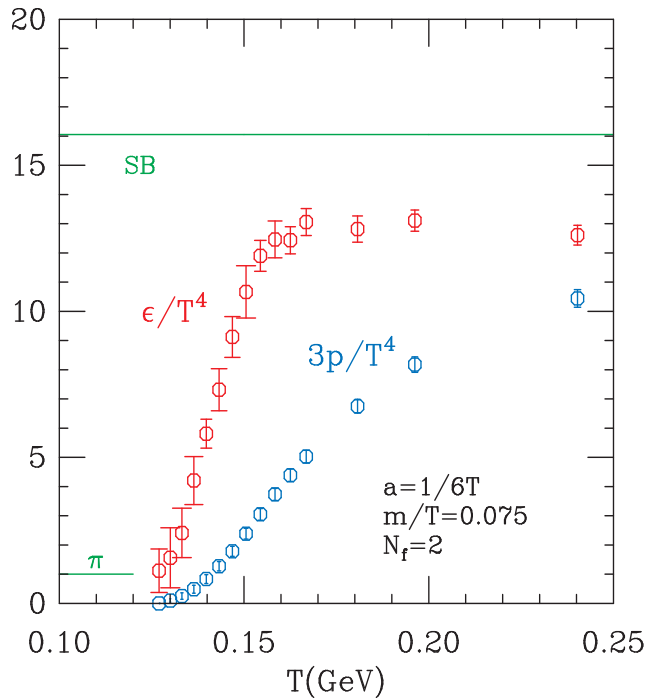


Figure 7: The temperature dependence of energy density and pressure in two-flavour QCD [12].

Furthermore the thermodynamic observables do not quite reach their Stefan-Boltzmann values (marked “SB” in Fig. 7) even at very high temperatures. These deviations from ideal gas behaviour can be expressed to a large extent in terms of effective ‘thermal’ masses m_{th} of quarks and gluons, with $m_{\text{th}} \sim gT$ [13] - [15].

Finally we turn to the value of the transition temperature. Since QCD (in the limit of massless quarks) does not contain any dimensional parameters, T_c can only be obtained in physical units by expressing it in terms of some other known observable which can also be calculated on the lattice, such as the ρ -mass, the proton mass, or the string tension. In the continuum limit, all different ways should lead to the same result. Within the present accuracy, they define the uncertainty so far still inherent in the lattice evaluation of QCD. Using the ρ -mass to fix the scale leads to $T_c \simeq 0.15$ GeV, while the string tension still allows values as large as $T_c \simeq 0.20$ GeV. This means that energy densities of some 1 - 2 GeV/fm³ are needed in order to produce a medium of deconfined quarks and gluons.

In summary, finite temperature lattice QCD at $\mu_b = 0$ shows

- that there is a deconfinement transition coincident with an associated shift in the effective quark mass at $T_c \simeq 0.15 - 0.20$ GeV;
- that the transition is accompanied by a sudden increase in the energy density (“latent heat of deconfinement”) from a small hadronic value to a much larger value near that of an ideal quark-gluon plasma.

From *ab initio* QCD calculations we thus have a relatively good understanding of the

phase structure expected for strongly interacting matter at vanishing baryon density. Two aspects call for some additional discussion. What relation between deconfinement and chiral symmetry restoration makes the two phenomena coincide in finite temperature QCD? And how does a hadronic medium turn into a quark-gluon plasma on a microscopic level - do hadrons somehow fuse to form a deconfined plasma? These questions will be addressed in sections 2.3 and 2.4.

2.3 Deconfinement and Chiral Symmetry Restoration

The relation between these two transition phenomena has been quite puzzling all along; why should they (at least for $\mu_B=0$) occur at the same temperature? We shall here give a somewhat speculative conceptual answer [18]-[21].

In the presence of light quarks of mass m_q , the string between a static quark-antiquark pair could in principle break when $V(r) = \sigma r = 2m_q$, leading to

$$L(T) \sim e^{-2m_q/T} \quad (19)$$

for the Polyakov loop. For sufficiently small m_q , all variations of $L(T)$ with T would then be washed out and the deconfinement transition should disappear [17]. Such an effect would be the counterpart of that caused by an external magnetic field H in the Ising model. When $H = 0$, spontaneous magnetisation sets in at the Curie point T_c ; but for $H \neq 0$, the field always aligns spins and makes the magnetisation non-zero for all T (Fig. 8). We might thus expect that $H \sim 1/m_q$ constitutes an effective external field in QCD.

However, it turns out that this is not the case; the Polyakov loop shows strong variations with T even for $m_q \rightarrow 0$, as seen in Fig. 9 [11]. Conceptually, there is a good reason for this: chiral symmetry breaking in the confined phase keeps the effective constituent quark mass M_q finite even for vanishing m_q , and to break the string through formation of a normal meson requires $2M_q$, not $2m_q$. The relevant field should thus be [18]-[21]

$$H \sim 1/M_q, \quad (20)$$

where M_q is the constituent quark mass in the relevant temperature region. Hence the temperature dependence of M_q plays a crucial role for the temperature dependence of the Polyakov loop.

Putting together what we know about the effective quark mass under different conditions, we expect the external field

$$H \sim 1/(m_q + c_1 \langle \bar{\psi}\psi \rangle^{1/3} + c_2 g T), \quad (21)$$

to be determined by a combination of bare quark mass, chiral mass and thermal mass (Fig. 10). For $m_q \rightarrow \infty$, we obviously recover the pure gauge case. For small or vanishing m_q , $\langle \bar{\psi}\psi \rangle$ is the crucial term, since the thermal mass at low T is very small. Below the chiral symmetry restoration point T_χ , the large value of $\langle \bar{\psi}\psi \rangle$ keeps the external field H small, allowing the Polyakov loop distribution to remain essentially disordered, so that the system is in a confined state. At chiral symmetry restoration, $\langle \bar{\psi}\psi \rangle$ vanishes and hence H suddenly becomes very large; it aligns the Polyakov loops and thereby explicitly

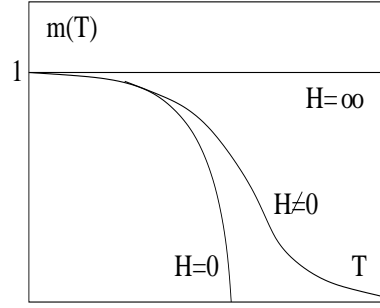


Figure 8: Magnetisation in the Ising model with and without external magnetic field H .

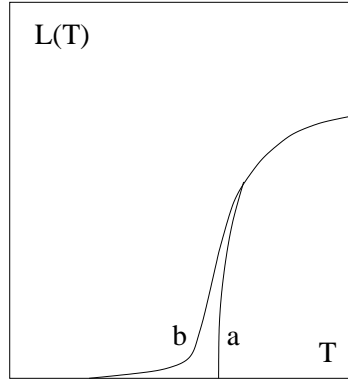


Figure 9: The temperature dependence of the Polyakov loop for (a) pure gauge theory, $m_q = \infty$, and (b) two-flavour QCD with massless quarks, $m_q = 0$.

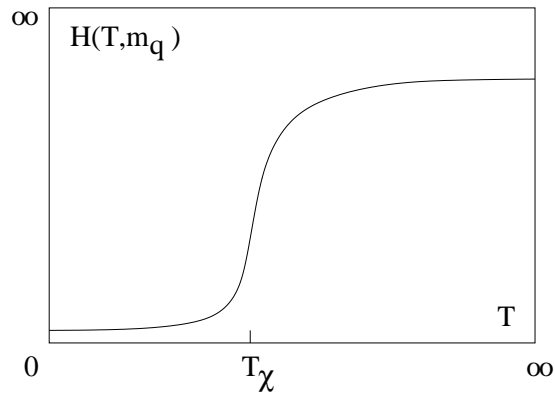


Figure 10: The expected temperature dependence of the effective external field in full QCD.

breaks the Z_3 confining symmetry. As a result, L increases sharply and deconfinement sets in.

We thus have essentially two limiting situations:

- For large m_q , H is always very small, so that deconfinement is determined by an approximate spontaneous symmetry breaking at $T = T_c$.
- For small m_q , H becomes large when $\langle \bar{\psi}\psi \rangle$ vanishes; H then aligns the Polyakov loops, resulting in deconfinement at $T = T_\chi$.

In the second case, we have assumed that chiral symmetry restoration occurs at a temperature T_χ less than the deconfinement temperature in pure gauge theory, as is in fact the case, with $T_c[SU(3)] \simeq 0.26$ GeV and $T_\chi(N_f = 2) \simeq 0.15$ GeV.

Deconfinement is thus due to *spontaneous* Z_3 symmetry breaking only in the large m_q limit. For small m_q , that symmetry is broken *explicitly* by an effective external field H which becomes large when $\langle \bar{\psi}\psi \rangle \rightarrow 0$. Hence deconfinement and chiral symmetry restoration coincide.

2.4 Deconfinement and Percolation

Conceptually, the transition from hadronic matter to quark-gluon plasma seems quite transparent. As we had seen in the introduction, deconfinement is expected when the density of quarks and gluons becomes so high that it no longer makes sense to partition them into colour-neutral hadrons, since these would strongly overlap. Instead we have clusters much larger than hadrons, within which colour is not confined; deconfinement is thus related to cluster formation. This is the central topic of percolation theory, and hence a connection between percolation and deconfinement seems very likely [20, 22, 23]. In percolation theory, one considers a system of extended geometric objects, such as spheres, which can overlap; percolation is said to occur when, with increasing density, a connected cluster begins to span the entire system [24]. If the interior of the spheres is coloured, such a cluster signals the onset of colour conductivity and hence of deconfinement. Moreover, for any value of the quark mass [20], the percolation transition is based on genuine singular behaviour as function of the temperature.

Already the first studies [22, 23] had noted that percolation of spheres of hadronic size cannot mean deconfinement. The percolation density n_p for spheres of radius r is given by [25]

$$n_c \simeq \frac{0.34}{(4\pi/3) r^3}. \quad (22)$$

Hence for a nucleon radius of 0.8 fm, the critical value is 0.16 fm^{-3} and thus just standard nuclear density. The percolation of nucleons therefore corresponds to the formation of nuclear matter; for deconfinement, the true coloured ‘interiors’ of the hadrons must overlap. These are more easily defined for mesons.

In QCD, two fundamental triplet colour charges are connected by a string, with

$$\sigma \simeq 0.16 \text{ GeV}^2 = 0.8 \text{ GeV/fm} \quad (23)$$

as string tension. The transverse radius r_t of these strings is found to be about 0.2 - 0.3 fm in the range $0.5 \leq l \leq 2$ fm [26, 27], where l is the length of the string. A meson

is thus like an ellipsoid of major axis $r = l/2$ and minor axis r_t , randomly oriented and oscillating in time about its center of mass to fill a sphere of radius r . The percolation threshold for ellipsoids of aspect ratio $r/r_t = 4$ is found to be [28]

$$n_p \simeq \frac{0.21}{(4\pi/3) r r_t^2}; \quad (24)$$

for $r = 1$ fm and $r_t = 0.25$ fm, this gives 0.8 fm^{-3} as critical density. With $m_h = 2r\sigma$ for the ‘generic’ hadron mass in such a string model, we obtain

$$\epsilon_p \simeq 1.3 \text{ GeV/fm}^3 \quad (25)$$

as the energy density at the percolation point, in good agreement with the deconfinement value ($1 - 2 \text{ GeV/fm}^3$) obtained from lattice QCD in section 2.2. Thus deconfinement indeed appears to set in at the percolation point for extended hadronic objects; for mesons, these are quark-antiquark strings. For nucleons, the quark triplet structure makes the geometry more complex, but conceptually there should be no difference.

The connection between percolation and deconfinement is presently also under investigation on a more formal level, based on the relation between spin and $SU(N)$ gauge field systems [16] and on the percolation of Polyakov loops [29, 30]. As mentioned, the introduction of dynamical quarks in QCD destroys the underlying Z_N symmetry; the expectation value of the Polyakov loop $L(T)$ now never vanishes, so that $L(T)$ can no longer be taken as an order parameter to identify the transition. The analogue in the Ising model is, as we saw, the introduction of an external field, which also breaks the Z_2 symmetry and makes the magnetization finite for all temperatures. Although now no thermal phase transition can take place, the percolation transition between a region of finite clusters of parallel spins to one of infinite clusters continues to exist. Its counterpart in $SU(N)$ gauge theory may therefore constitute a general order parameter for deconfinement in full QCD, with dynamical quarks [20].

3. CONDITIONS IN NUCLEAR COLLISIONS

3.1 High Energy Collisions and Nuclear Transparency

Quark matter presumably made up the early universe, and perhaps neutron stars have quark cores. But the big bang was long ago, and neutron stars are far away. The rapid growth which the field has experienced in the past two decades was to a very large extent stimulated by the idea of using high energy nuclear collisions to produce in the laboratory droplets of strongly interacting matter large enough and long-lived enough for a study of statistical QCD.

Normal nuclear matter consists of nucleons of mass 0.94 GeV and has a density of $0.17 \text{ nucleons/fm}^3$; hence its energy density is 0.16 GeV/fm^3 , i.e., well below the $1 - 2 \text{ GeV/fm}^3$ necessary for deconfinement. We want to collide two heavy nuclei with the aim of increasing the density of matter as far as possible beyond this value. To what extent

can this be achieved? In a low energy nucleus-nucleus collision, the two nuclei will remain intact and simply “bounce off” each other. With increasing energy, they will penetrate each other more and more, leading to highly excited nuclear matter, which rapidly breaks up into nuclear fragments and some additional mesons.

If the collision energy is increased still further, *nuclear transparency* begins to set in: the two colliding nuclei pass through each other, leaving behind them a “vapour trail” of deposited energy, which eventually decays into hadrons. Different droplets of this trail move at different speeds, from slow ones in the center of mass to the fast remnants of target and projectile. We refer to elements in the trail as ‘droplets’, keeping in mind, however, that there really is a continuous fluid of such droplets, without any gaps. Since nuclear transparency clearly limits the local (droplet) energy density available for the medium produced in the collision, its understanding is necessary in order to estimate the conditions which can be achieved experimentally. It is a phenomenon which occurs already in the collision of two *nucleons*, which at high energy also pass through each other, creating a cascade of secondary hadrons. Most of these are produced outside the primary interaction region and long after the primary collision [31, 32].

We therefore first ask why in the more elementary process of a nucleon-nucleon collision the two collision partners do not stop each other. Nucleons have a spatial extension of about 1 fm, and in a nucleon-nucleon collision it therefore takes a certain time τ_0 before the entire projectile nucleon has realised that it has hit something. In the rest-frame of the projectile, a time $\tau_0 \sim 1$ fm is required to transmit the information about the collision from one side of the nucleon to the other. In the rest-frame of the target nucleon, this time is dilated to

$$t_0 = \tau_0 \left(\frac{P_0}{m} \right), \quad (26)$$

where $P_0 = \sqrt{\mathbf{P}^2 + m^2}$ is the energy of the incident projectile nucleon, \mathbf{P} its lab momentum and m its mass. Thus at high collision energies, $t_0 \gg 1$ fm; since the target also has a size of about 1 fm, the projectile has long left the target region before it fully realises that it was hit. It also takes a time of order 1 fm to form a hadronic secondary of radius $R_h \simeq 1$ fm, like a pion, and hence only very slow secondaries are produced *inside* the target region. For faster ones, the formation time is again dilated, and they are therefore formed *outside* the target region. The production process in nucleon-nucleon collisions, beginning about 1 fm after the collision with soft secondaries produced in the target region and continuing with further production of faster secondaries later and outside the target, is therefore often referred to as *inside-outside* cascade.

One thus encounters transparency and a vapour trail of droplets of deposited energy already in high energy nucleon-nucleon collisions. Here one moreover observes that the nature of all the droplets of different rapidities is more or less the same in their respective rest-frames: they decay into the same types of hadrons, and these have the same momentum distributions, apart from possible effects due to the motion of the droplet [33]. In other words, the properties of any segment of the vapour trail, measured in its own rest system, do not depend on its relative velocity with respect to the others. We will thus assume [34, 35] that the vapour trail is invariant under Lorentz transformations along the collision axis. Evidently there are limits to the validity of such a picture: it must

break down at both ends of the trail, when the kinematic limit is reached. Moreover, at very high energies, the overall baryon number is negligible in the main (central) part of the trail, since the fast target and projectile nucleons emerge as leading particles at high rapidity. Hence the droplets have a non-zero baryon number.

Let us make this more precise. A particle of mass m , moving with a momentum p along the beam axis, has a rapidity $y = \sinh^{-1}(p/m)$; for the moment, we assume vanishing transverse momentum. Since the transformation from one reference system to another is just a displacement in rapidity, boost invariance along the beam axis means that a physical quantity, such as the deposited energy in the restframe of the droplet, cannot depend on the rapidity y . Since the deposited energy appears later in the form of hadrons, the number of hadronic secondaries (dN_h/dy) produced in a given rapidity interval dy must be independent of y ,

$$\left(\frac{dN_h}{dy}\right) = a(s), \quad (27)$$

where $a(s)$ depends on the (squared) collision energy s only. The central rapidity plateau defined by Eq. (27) is a reasonable approximation to what one observes in high energy $p-p$ and $p-\bar{p}$ collisions.

We now include transverse momenta and note that the transverse momentum (p_T) distribution of the produced hadrons must also be y -independent. The full momentum distribution of secondaries of species i thus becomes (assuming azimuthal symmetry around the collision axis)

$$\left(\frac{d^2N_i}{dy dp_T^2}\right) = a_i(s)f_i(p_T, s). \quad (28)$$

Here $a_i(s)$ determines the relative abundance of species i at the given s , and $f_i(p_T, s)$ is the corresponding rapidity-independent transverse momentum distribution, normalized to unity. In principle, $f_i(p_T, s)$ could depend both on the collision energy and on the species of hadron involved. One finds, however, that in very good approximation it is energy-independent, and the species-dependence enters only through the transverse mass, $m_T(m_i) \equiv \sqrt{m_i^2 + p_T^2}$,

$$f_i(p_T, s) = f(p_T, m_i) = \left[\frac{\lambda^2}{2(1 + m_i\lambda)}\right] \exp\{-\lambda [m_T(m_i) - m_i]\}, \quad (29)$$

with a universal (i.e., species-independent) constant $\lambda^{-1} \simeq 0.15$ GeV. Since $[m_T(m_i) - m_i]$ is just the transverse kinetic energy of species i , $f_i(p_T, s) \sim \exp\{-\lambda E_i\}$ provides a universal cut-off in the transverse kinetic energy for all species. This phenomenon is generally referred to as m_T -scaling. It is very reminiscent of a Boltzmann distribution and has led to the formulation of thermodynamic models for such production processes, with $\lambda^{-1} = T_H$ playing the role of a temperature [36]. A droplet thus freezes out at temperature T_H by turning into freely flowing (non-interacting) hadrons. From Eq. (29), the average transverse mass of a secondary is

$$\langle m_T(m_i) \rangle = \frac{2}{\lambda} \left[1 + \frac{(m_i\lambda)^2}{2(1 + m_i\lambda)} \right]. \quad (30)$$

With $\lambda \simeq 0.15$ GeV, this gives for pions $\langle m_T(\pi) \rangle \simeq 0.37$ GeV, for nucleons $\langle m_T(N) \rangle \simeq 1.11$ GeV. The corresponding average transverse momentum is 0.34 GeV for pions, 0.59 GeV for nucleons. We thus note that m_T scaling (or thermal production, if we interpret it in this way) provides higher average transverse momenta for heavier secondaries.

The possible thermal nature of hadron production in $p - p$ collisions has recently received further support in analyses of species abundances [38]. Experimentally, the production rates for up to thirty different species of hadrons and hadron resonances have been measured, for different collision energies. The simplest thermal picture has chemical freeze-out occurring when a hadron gas, whose constituents are all possible hadron and hadron resonance states, reaches a certain temperature T_h [39]. This would mean that the relative abundances of all species at all (high) collision energies are determined by just this one parameter. This is in fact not possible for $p - p$ collisions, because of the so-called strangeness suppression; the relative abundance of secondaries of non-zero strangeness is considerably smaller than predicted. A full description does become possible, however, if one further parameter γ_s is introduced to take this into account [40]. It is chosen so that $\gamma_s = 1$ implies a fully thermal abundance spectrum, $\gamma_s < 1$ strangeness suppression. One then finds that for $T_h \simeq 170$ MeV and $\gamma_s \simeq 0.5$, it is possible to reproduce quite well the observed secondary hadron abundances in $p - p$ and $p - \bar{p}$ collisions from $\sqrt{s} = 20$ to 900 GeV [38].

The origin of such thermal behaviour remains rather unclear, all the more so since it holds for hadron production in high energy e^+e^- annihilation as well [41]. It can certainly not arise from rescattering among the produced secondaries, since neither the life-time nor the density of the produced medium are high enough for this. It may be due to a statistical excitation of the vacuum due to the passage of one or more colour charges, occurring already on the partonic level. The strangeness suppression factor could then be a consequence of the large strange quark mass, compared to that of the light u and d quarks. In a partonic medium of temperature $T > T_h$, the ratio of Boltzmann weights,

$$\gamma_s \simeq \exp\{-(m_s - m_u)/T\} \quad (31)$$

would indeed lead to values around 0.5 for partonic temperatures around 200 MeV. Eq. (31) implies that with increasing T , i.e., with increasing energy density of the excited vacuum, γ_s should approach unity. One way to check this is to see if the relative abundance of strange particles increases when one increases either the collision energy or considers collision fluctuations of higher than average secondary multiplicity. In both cases, the K/π ratio indeed grows considerably [42, 43], as seen in Fig. 11.

To complete the discussion of nucleon-nucleon collisions, we specify $a(s)$ in Eq. (28). From $p - p$ and $p - \bar{p}$ experiments over a large range of collision energies, up to $\sqrt{s} = 1.8$ TeV, one finds in the central rapidity region [44] for the sum over all secondaries (which means predominantly pions),

$$\left(\frac{dN_h}{dy} \right)_{y \simeq 0} \simeq \ln(\sqrt{s}/2m), \quad (32)$$

so that $a(s) \simeq \ln(\sqrt{s}/2m)$; here m denotes the nucleon mass.

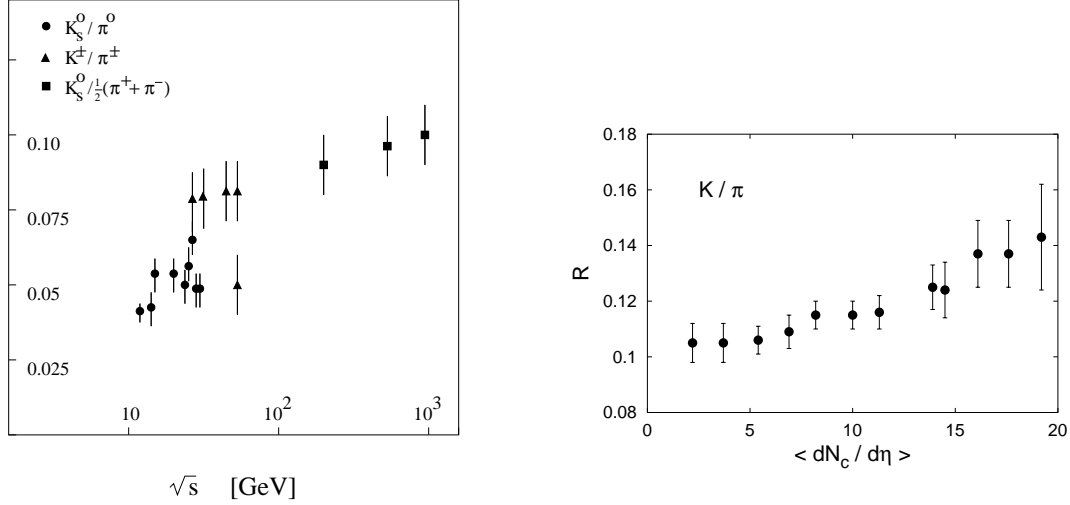


Figure 11: The K/π ratio (a) in $p-p$ and $p-\bar{p}$ collisions as function of the cms collision energy [42] and (b) in $p-\bar{p}$ collisions at $\sqrt{s} = 1.8$ TeV as function of the associated multiplicity [43].

After this brief survey of nucleon-nucleon interactions, we now return to nucleus-nucleus collisions in more detail. At high energies, each of the two incoming nuclei (for simplicity, we assume them to have equal mass numbers A) will appear Lorentz-contracted to a longitudinal thickness of

$$d_A = 2R_A \left(\frac{2m}{\sqrt{s}} \right) \quad (33)$$

in the overall center of mass. Here $s = 2m^2 + 2m\sqrt{\mathbf{P}^2 + m^2}$ denotes the squared nucleon-nucleon collision energy, \mathbf{P} the incident lab momentum per nucleon, and $R_A \simeq 1.12 A^{1/3}$ fm the nuclear radius. For c.m.s. collision energies of 20 GeV or more, d_A is thus one fermi or less, so that the different nucleon-nucleon collisions in the course of the nucleus-nucleus collision essentially occur superimposed in the same space-time region. Consider a central $A-A$ collision; in the process, each of the A projectile nucleons will interact one or more times with nucleons from the target nucleus. When the nuclei have passed through each other, we are thus left with $2A$ ‘wounded’ nucleons, each of which eventually emits secondary hadrons [45]. At present energies it is found that the number of secondaries is proportional to the number of wounded nucleons; it is not affected by the number of collisions which the nucleon has experienced². Since a proton-proton collision results in two wounded nucleons, we obtain from Eq. (32) that the number of secondary hadrons in a central high energy $A-A$ collision is given by

$$\left(\frac{dN_h}{dy} \right)_{y \simeq 0}^{AA} \simeq A \ln(\sqrt{s}/2m). \quad (34)$$

²Note that this holds for ‘soft’ secondaries; the emission of ‘hard’ products, such as Drell-Yan dileptons or charmonium states, does depend on the number of collisions.

In effect, this result is modified already in $p-A$ collisions, since the nuclear target stops the projectile nucleon more than a nucleonic target does. This is taken into account by the form

$$\left(\frac{dN_h}{dy}\right)_{y \simeq 0}^{AA} \simeq A^\alpha \ln(\sqrt{s}/2m), \quad (35)$$

with $\alpha \simeq 1.15$ for secondaries close to target rapidity in $p-A$ data [46]. The multiplicity predicted by Eq. (35) agrees quite well with results from $S-S$ to $Pb-Pb$ collisions at the CERN-SPS [47, 48, 49].

3.2 Collision Evolution and Initial Conditions

Statistical QCD, as described in Section 2, provides predictions for time-independent systems; we want to apply these to the rapidly evolving systems produced in nuclear collisions. Hence we have to consider in some detail the different evolution stages of such collisions. In the period of nuclear passage, which at high energies lasts a fermi or less, there is multiple scattering among the quark and gluon constituents of the colliding nucleons, leading to a rapid generation of entropy and thereby eventually to thermalisation. The separating nucleons thus leave behind a more or less equilibrated expanding medium which in its ‘hot’ early stages we expect to be a quark-gluon plasma. It cools off, undergoes the confining quark-hadron transition and after that forms hadronic matter, which finally freezes out into the observed hadronic secondaries. The aim of this section is to estimate the energy density of the medium in its early stage.

Thermalisation is presumably attained by multiple scattering of the incident constituents and the subsequently produced secondaries. At high energies and early times, these constituents are quarks and gluons, so that the tool to study the resulting entropy production must be some form of parton cascade model based on perturbative QCD [50, 51]. The partons contained in the incident nucleons collide, produce further partons, and this cascade continues and eventually leads to a thermal medium. Such partonic cascade models allow the calculation of entropy production as a function of the local time after the collision, and the systems produced in high energy collisions appear to reach thermalisation after about one fermi. We shall return to parton cascade models in section 6.3.

To estimate the energy density, one has to model the expansion process. The simplest model [35] assumes that the finally observed hadrons have emerged from an initial interaction volume in free flow, i.e., without any collective motion. The resulting initial energy density in an $A-A$ collision is

$$\epsilon_0 = \frac{p_0}{\pi R_A^2 \tau_0} \left(\frac{dN_h}{dy}\right)_{y=0}^{AA}, \quad (36)$$

where p_0 denotes the average (local) energy of the emitted secondaries and (dN_h/dy) their multiplicity as given by Eq. (35). The initial interaction volume is determined by the transverse size R_A and the longitudinal extension as obtained from the thermalisation

time τ_0 , which is generally taken to be about one fermi. Combining this with Eq. (35), we get

$$\epsilon_0 \simeq \frac{p_0}{4} A^{0.48} \ln(\sqrt{s}/2m) \quad [\text{GeV}/\text{fm}^3] \quad (37)$$

for the initial energy density in a central $A - A$ collision. Since pions are the dominant secondaries and have an average transverse momentum of about 0.35 GeV over a wide range of incident energies, we have $p_0 \simeq 0.5$ GeV. The estimates in Eq's. (35) and (37) give averages over the transverse nuclear area, without taking into account any details of the nuclear distribution. In the Glauber formalism, the correct nuclear geometry can be taken fully into account (see e.g. [52]). For central $A - A$ collisions, this results in little change, but for non-central or $A - B$ collisions with $A \neq B$, the actual geometry becomes important.

Before looking at the attainable energy densities, let us note where nucleus-nucleus collision experiments reaching the range of interest for our purposes can actually be performed. The only laboratories providing sufficiently energetic nuclear beams are the Brookhaven National Laboratory (BNL) near New York (USA) and the European Organization for Nuclear Research (CERN) in Geneva (Switzerland). Both began experimentation in 1986, using existing accelerators. BNL had the Alternating Gradient Synchrotron (AGS), designed for 30 GeV/c proton beams, CERN the Super Proton Synchrotron (SPS) for 450 GeV/c protons. The injectors available at that time allowed only the acceleration of nuclei containing equal numbers of protons and neutrons ($A=2Z$), so that the beams were restricted to light ions ($A \lesssim 40$). Both laboratories have in the meantime built new injectors, allowing the acceleration of arbitrarily heavy nuclei in AGS and SPS. Moreover, both laboratories are presently constructing colliding beam accelerators which will bring them to very much higher collision energies. At BNL, the Relativistic Heavy Ion Collider (RHIC) is scheduled to start operating in 2000; at CERN, the Large Hadron Collider (LHC) is planned for some five years later.

The available and planned facilities are summarized in Table 1. We have there also included the corresponding energy density values; they were obtained by a Glauber analysis taking into account the correct nuclear geometry [52]. Note that the listed values are averages over the nuclear profile; the center of the interaction region can reach energy densities up to 30 % higher. The results using light ion beams are given for heavy targets ($A \simeq 200$), the others for $A - A$ with $A \simeq 200$. The $\ln \sqrt{s}$ dependence of the energy density (Eq. 37) makes it rather difficult to achieve significant changes by varying the beam energy. The use of lighter nuclei is clearly more efficient. In Fig. 12, we show the functional behaviour of ϵ for $A = 30$ and $A = 200$, to give an indication of the ranges achievable at the different facilities, as well as their relation to the expected deconfinement threshold.

3.3 The Onset of Deconfinement

At the beginning of a high energy nucleus-nucleus collision, there are hard interactions between the partonic constituents of the participating nucleons. These partons are confined: their momentum distribution is that of partons within a nucleon, as determined e.g. in deep inelastic scattering. In particular, this means that if one quark in the nucleon

Machine	Start	Type	Beam	\sqrt{s} [GeV/A]	ϵ_0^{AB} [GeV/fm ³]
BNL – AGS	1986	Fixed Target	^{28}Si	5	0.7
CERN – SPS	1986	Fixed Target	$^{16}\text{O}, ^{32}\text{S}$	19	1.6
BNL – AGS	1992	Fixed Target	^{197}Au	5	1.5
CERN – SPS	1994	Fixed Target	^{208}Pb	17	3.7
BNL – RHIC	2000	Collider	^{197}Au	200	7.6
CERN – LHC	~ 2005	Collider	^{208}Pb	5000	13

Table 1: Experimental facilities for high energy nuclear collisions; the light ion beam results are for heavy ($A = 200$) targets, the others for symmetric ($A - A$) collisions.

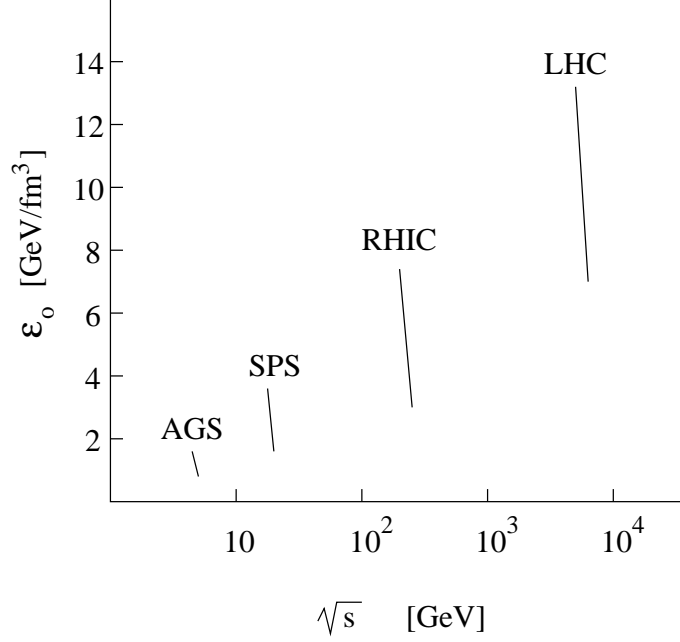


Figure 12: The variation of the initial energy density with incident collision energy for different experimental facilities.

scatters, emitting (or absorbing) a gluon, others must follow the scattered quark to retain colour neutrality (Fig. 13). As a result, high momenta k for the emitted gluon are suppressed, with a momentum distribution of the form

$$xg(x) \sim (1 - x)^{1+n}, \quad (38)$$

where $x = k/\sqrt{s}$ is the fractional momentum of the gluon and n denotes the number of other quarks or antiquarks which must follow the scattered one.

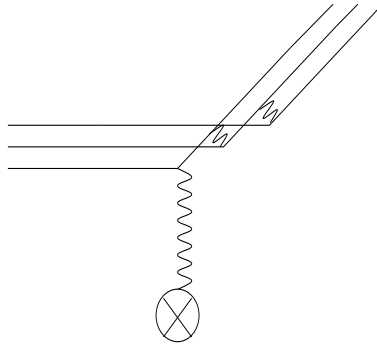


Figure 13: Scattering of quarks confined to a nucleon.

Deconfinement starts when the given environment leads to partons which are no longer subject to the confinement constraints just mentioned; with $n = 0$, this results in a hardening of the parton momentum distribution. The first step towards deconfinement is

thus the overlap of two hard nucleon-nucleon collisions. If there is a secondary interaction between the two interacting pairs *before* the nucleons in the primary interactions have had the time to ‘regroup’ into physical nucleons, a hard gluon exchanged between the two pairs is not subject to confinement. An ‘exogamous’ system of this kind is therefore the first step towards a deconfined medium.

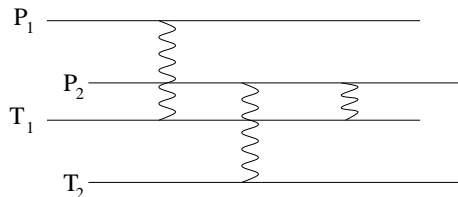


Figure 14: ‘Exogamous’ interaction between two colliding nucleon systems (P_1, T_1) and (P_2, T_2) .

The interaction of two nucleons leads to the emission or absorption of gluons of transverse momenta k_T , with a corresponding transverse area of radius $r_T \simeq 1/k_T$. In interactions of the type shown in Fig. 14, partons from different collisions overlap in the transverse plane and can thus no longer be associated to a given nucleon. To form a connected medium of such deconfined partons, their density in the transverse plane has to be sufficiently high. This density increases when the mass number A (more collisions) and/or the collision energy (more partons) is increased; hence we need high energy collisions of heavy nuclei for the formation of a quark-gluon plasma.

4. PROBES OF PRIMORDIAL MATTER

4.1 Evolution

We now assume that for sufficiently high energies, the deconfined partonic system quickly attains equilibrium; this is in accord with the parton cascade models mentioned above [50, 51]. Subsequently, it cools off and then hadronizes. For an infinite medium, the actual transition process depends considerably on the order of the confinement transition, which so far remains uncertain. The systems produced in nuclear collisions are rather small, however, and in addition it is unlikely that any measurement will fix thermal observables precisely. Hence the effect of the transition will always appear in somewhat smeared-out form. On the hadronic side, it is possible for the medium to exist for some time as a system of interacting hadrons, which eventually freezes out. However, it is known that an ideal resonance gas leads to critical behaviour because of the composition law for resonances [36, 37], and that an ideal gas of extended hadrons does so for geometric reasons [53]. Hence it is quite conceivable that the confinement transition leads directly into an ideal resonance gas.

It is evident that the different evolution stages, from primary collisions to freeze-out, require very different probes for their investigation. Consider the two extremes. Pions appear at the very end, either directly or as decay products of resonances; hence they

can hardly tell us much about the very early phases of the system, which existed and disappeared long before pions and other large ‘soft’ hadrons were formed. Hard Drell-Yan dileptons are produced essentially at the time of the collision and then remain unaffected by the subsequent history of the system; hence they are not able to provide information on thermalisation and freeze-out.

The basis for a quark-gluon plasma is the high parton density in the early stages after the collision; this effectively screens all confining long range forces, so that only short range interactions remain. Any deconfinement probe must therefore

- be hard enough to resolve sub-hadronic scales,
- be able to distinguish confinement and deconfinement,
- be present in the early stages of the evolution, and
- retain the information throughout the subsequent evolution.

The last point requires that the probe should not be in thermal equilibrium with the later evolution stages, since this would lead to a loss of memory of the previous stages.

So far, two types of probes satisfying these conditions fully or in part have been considered.

- *External* probes are produced essentially by primary parton collisions, before the existence of any medium, and then indicate by their observed behaviour whether the subsequent medium was deconfined or not. The production of quarkonium states (J/ψ , Υ) provides the best known example of such a probe. Short distance QCD predicts that the dissociation of quarkonia is possible only in a deconfined medium, since it requires harder gluons than those present in hadrons. Another example, quite likely to gain considerable importance when the high energy colliders RHIC and LHC come into operation, is the energy loss or attenuation of hard jets, which is expected to increase considerably in a deconfined medium.
- *Internal* probes are produced by the quark-gluon plasma itself. Since they must leave the medium without being affected by its subsequent states, they should undergo only weak or electromagnetic interactions after their formation; the main candidates here are thermal dileptons or photons. However, since both can also be produced by a confined medium, they can serve as thermometer of the medium rather than as probe for its confinement status. So far, another problem is their identification: both dileptons and photons are produced abundantly in hadron decays, and separating out a possible thermal component appears very difficult.

At the present stage of the investigation, quarkonium dissociation and jet quenching therefore appear the most promising direct signatures for deconfinement.

Before concentrating on these hard deconfinement probes, we will first consider electromagnetic probes in somewhat more detail. Real or virtual photons emitted during the evolution of the collision subsequently undergo no (strong) interactions with the medium and hence reflect its state at the time they were produced. On the other hand, they are emitted during the entire collision evolution, and by different dynamical mechanisms at different stages:

- Early hard parton interactions produce hard photons and Drell-Yan dileptons; these provide information about the initial (primary or pre-equilibrium) stages.
- Thermal photon and dilepton emission by the medium, through quark or hadron interactions, occur through its entire evolution, and hence give information about the successive stages, from quark-gluon plasma to final hadronic freeze-out.
- Hadrons produced at any point of the hadronic stage, from the quark-hadron transition to freeze-out, can decay and thereby emit photons or dileptons; depending on the hadron decay time, they provide information about dense interacting hadronic matter or about hadrosynthesis at the end of the strong interaction era.

Each of these formation mechanisms provides information about specific aspects of the different collision stages.

Drell-Yan dileptons and hard photons are the tools to study the effective initial state parton distributions; in particular, they will show any nuclear modifications (shadowing, anti-shadowing, coherence effects) of these distributions. They also indicate the initial state energy loss and the initial state p_T broadening suffered by partons in normal nuclear matter. Since they do not undergo any final state strong interactions, they moreover provide a reference for the effect of the produced medium on quarkonium states or jets.

Thermal emission can in principle be used to determine the temperature at the different evolution stages. The *functional form* of thermal spectra,

$$dN/dk_\gamma \sim e^{-k_\gamma/T} \quad (39)$$

for photon momenta, or the corresponding distributions in the dilepton mass M_{l+l-} , indicate the temperature T of the medium at the time the signal was emitted. Since the form (39) for thermal production is the same for a hadronic medium and for a quark-gluon plasma, it cannot specify the nature of the emitting medium, only its temperature; this feature finds support in various cascade model calculations [50, 51]. The crucial thermometric problem is to find a “thermal window”, since the measured spectra are dominated at high photon momenta or dilepton masses by hard primary reactions and at low momenta or masses by hadron decay products. As mentioned, thermal photon or dilepton emission has so far not been identified, perhaps because of the dominance of the hadronic stage at present energies.

The dileptons produced by hadron decays can probe hadronic in-medium modifications, provided the hadrons actually decay within the medium. The ρ , with a half-life of about a fermi, appears to be the best candidate for such studies. Chiral symmetry restoration is expected to change the properties of hadrons as the temperature of the medium approaches the restoration point [54]; hence such in-medium changes are of particular interest, since they might be the only experimental tool to address the chiral aspects of deconfinement. If at the onset of chiral symmetry restoration, the mass of the ρ decreases sufficiently much [55],

$$\frac{m_\rho(T)}{m_\rho(T=0)} \rightarrow 0 \text{ as } T \rightarrow T_c, \quad (40)$$

then this should lead to an observable enhancement of the low mass dilepton spectrum. There are first indications for such an enhancement [56] - [58]; however, so far alternative

explanations based on in-medium hadron interactions, leading to a change of resonance widths, can also account for the effect [59]. Moreover, a temperature dependence of the form (40) has so far not been corroborated by lattice studies of hadron masses [60].

In the following two subsections, we shall discuss how the behaviour of quarkonium states and of hard jets can provide information about the confinement status of a given medium. In order to apply the results as probes in actual nuclear collision experiments, the production of the probes in the collision process must be understood as well, which clearly complicates matters. In section 5, we shall carry out a full analysis of this type for charmonium production and suppression in nuclear collisions; for this, there now exists a wealth of beautiful data [61].

4.2 Quarkonium Dissociation

We begin our study of deconfinement probes by restating the basic question: Given a box of unidentified matter, determine if the quarks and gluons which make up this matter are in a confined or deconfined state. It is thus not evidence for quarks and gluons that we look for, but rather the confinement/deconfinement status of these elementary building blocks of all forms of matter.

As quarkonium prototype, consider the J/ψ ; it is the $1S$ bound state of a charm quark ($m_c \simeq 1.4$ GeV) and its antiquark, with $M_{J/\psi} \simeq 3.1$ GeV. Its usefulness as deconfinement probe is easily seen. If a J/ψ is placed into a hot medium of deconfined quarks and gluons, colour screening will dissolve the binding, so that the c and the \bar{c} separate. When the medium cools down to the confinement transition point, they will therefore in general be too far apart to see each other. Since thermal production of further $c\bar{c}$ pairs is negligibly small because of the high charm quark mass, the c must combine with a light antiquark to form a D , and the \bar{c} with a light quark for a \bar{D} . The presence of a quark-gluon plasma will thus lead to a suppression of J/ψ production [62].

We shall now first consider this J/ψ suppression in terms of colour screening, i.e., as consequence of global features of the medium, and then turn to a microscopic approach, in which the bound state is assumed to be broken up by collisions with constituents of the medium.

4.2a. J/ψ Suppression by Colour Screening

Because of the large charm quark mass, the charmonium spectrum can be calculated with good precision by means of the Schrödinger equation [63]

$$\left[2m_c + \frac{1}{m_c}\nabla^2 + V(r)\right]\Psi_{n,l} = M_{n,l}\Psi_{n,l}, \quad (41)$$

where the potential $V(r) = \sigma r - \alpha/r$ contains a confining long-distance part σr and a Coulomb-like short-distance term α/r . For different values of the principal quantum number n and the orbital quantum number l , the masses $M_{n,l}$ and the wave functions $\Psi_{n,l}(r)$ of different charmonium states J/ψ , χ , ψ' , ... in vacuum are given in terms of the constants m_c , σ and α .

In a medium, the potential becomes screened, as we had seen above in Eq. 4; we thus obtain

$$V(r, \mu) = \frac{\sigma}{\mu} [1 - e^{-\mu r}] - \frac{\alpha}{r} e^{-\mu r}, \quad (42)$$

where μ is the screening mass and $r_D = \mu^{-1}$ the ‘Debye’ colour screening radius. Screening is a global feature of the medium, shortening the range of the binding potential. Once μ becomes sufficiently large, the bound states begin to disappear, starting with the most weakly bound; hence for $\mu \geq \mu_d^i$, the bound state i is no longer possible [64].

state	$\psi(1S)$	$\psi'(2S)$	$\chi_c(1P)$	$\Upsilon(1S)$	$\Upsilon'(2S)$	$\Upsilon''(3S)$	$\chi_b(1P)$	$\chi'_b(2P)$
μ_d [GeV]	0.68	0.35	0.35	1.52	0.64	0.43	0.59	0.42
T_d/T_c	1.2	1	1	2.7	1.1	1	1.1	1
ΔE [GeV]	0.64	0.06	0.24	1.10	0.54	0.20	0.67	0.31

Table 2: Quarkonium Dissociation by Colour Screening

With the help of finite temperature lattice QCD, we can now determine the screening mass $\mu(T)$ as function of the temperature T . With the approximate relation [65] $\mu \simeq 3.3 T$ and $T_c \simeq 0.17$ GeV, one obtains the melting pattern for the most important $c\bar{c}$ and $b\bar{b}$ states summarized in Table 2; we see that while both ψ' and χ_c melt at the critical deconfinement point, the J/ψ , being smaller and more tightly bound, survives to about $2T_c$ and hence about twice the critical energy density. A similar pattern holds for the bottomonium states; the dissociation values of the screening masses for χ'_b and Υ'' have not yet been determined in potential theory. With increasing temperature, a hot medium will thus lead to successive quarkonium melting, so that the suppression or survival of specific quarkonium states serves as a thermometer for the medium, in much the same way as the relative intensity of spectral lines in stellar interiors measure the temperature of stellar matter [66]. Note, however, that other possible sources of quarkonium dissociation have to be considered before the method becomes unambiguous. This problem will be addressed in detail in section 5.

4.2b. J/ψ Suppression by Gluon Dissociation

The binding energy of the J/ψ , i.e., the energy difference between the J/ψ mass and the open charm threshold, $\Delta E_{J/\psi} = 2M_D - M_{J/\psi} \simeq 0.64$ GeV is considerably larger than the typical non-perturbative hadronic scale $\Lambda_{\text{QCD}} \simeq 0.2$ GeV. As a consequence, the size of the J/ψ is much smaller than that of a typical hadron, $r_{J/\psi} \simeq 0.2$ fm $\ll \Lambda_{\text{QCD}}^{-1} = 1$ fm.

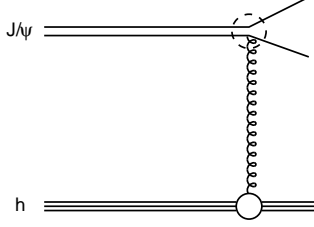


Figure 15: J/ψ dissociation by hadron interaction.

Hence the J/ψ is a hadron with characteristic short-distance features; in particular, rather hard gluons are necessary to resolve or dissociate it, making such a dissociation accessible to perturbative calculations. J/ψ collisions with ordinary hadrons made up of the usual u, d and s quarks thus probe the local partonic structure of these ‘light’ hadrons, not their global hadronic aspects, such as mass or size. It is for this reason that J/ψ ’s can be used as a confinement/deconfinement probe.

This can be illustrated by a simple example. Consider an ideal pion gas as a confined medium. The momentum spectrum of pions has the Boltzmann form $f(p) \sim \exp(-|p|/T)$, giving the pions an average momentum $\langle |p| \rangle = 3 T$. With the pionic gluon distribution function $xg(x) \sim (1-x)^3$, where $x = k/p$ denotes the fraction of the pion momentum carried by a gluon, the average momenta of gluons confined to pions becomes

$$\langle |k| \rangle_{\text{conf}} \simeq 0.6 T. \quad (43)$$

On the other hand, an ideal QGP as prototype of a deconfined medium gives the gluons themselves the Boltzmann distribution $f(k) \sim \exp(-|k|/T)$ and hence average momenta

$$\langle |k| \rangle_{\text{deconf}} = 3 T. \quad (44)$$

Deconfinement thus results in a hardening of the gluon momentum distribution. More generally speaking, the onset of deconfinement will lead to parton distribution functions which are different from those in vacuum, as determined by deep inelastic scattering experiments. Since hard gluons are needed to resolve and dissociate J/ψ ’s, one can use J/ψ ’s to probe the in-medium gluon hardness and hence the confinement status of the medium.

These qualitative considerations can be put on a solid theoretical basis provided by short-distance QCD [67] – [70]. In Fig. 15 we show the relevant diagram for the calculation of the inelastic J/ψ -hadron cross section, as obtained in the operator product expansion (essentially a multipole expansion for the charmonium quark-antiquark system). The upper part of the figure shows J/ψ dissociation by gluon interaction; the cross section for this process,

$$\sigma_{g-J/\psi} \sim (k - \Delta E_\psi)^{3/2} k^{-5}, \quad (45)$$

constitutes the QCD analogue of the photo-effect. Convoluting the J/ψ gluon-dissociation with the gluon distribution in the incident hadron, $xg(x) \simeq 0.5(1-x)^{1+n}$, we obtain

$$\sigma_{h-J/\psi} \simeq \sigma_{\text{geom}} (1 - \lambda_0/\lambda)^{n+3.5} \quad (46)$$

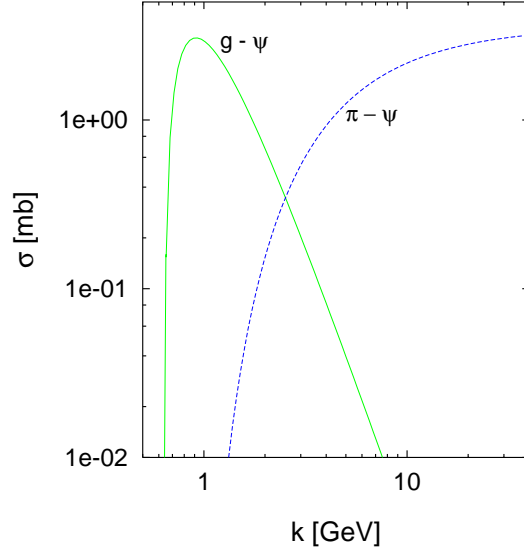


Figure 16: J/ψ dissociation by gluons and by pions; k denotes the momentum of the projectile incident on a stationary J/ψ .

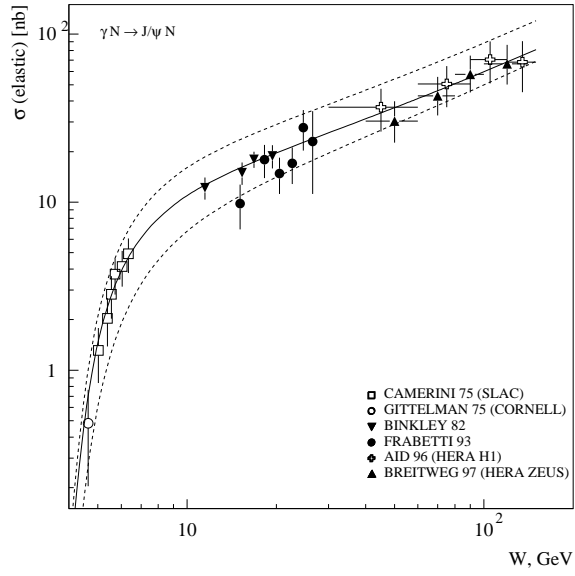


Figure 17: Elastic J/ψ photoproduction data, compared to the prediction obtained from short-distance QCD and VDM [71].

for the inelastic J/ψ -hadron cross section, with $\lambda \simeq (s - M_\psi^2)/M_\psi$ and $\lambda_0 \simeq (M_h + \Delta E_\psi)$; s denotes the squared J/ψ -hadron collision energy. In Eq. (46), $\sigma_{\text{geom}} \simeq \text{const.}$ $r_\psi^2 \simeq 2-3$ mb is the geometric cross section attained at high collision energies with the mentioned gluon distribution. In the threshold region and for relatively low collision energies, $\sigma_{h-J/\psi}$ is very strongly damped because of the suppression $(1-x)^{1+n}$ of hard gluons in hadrons, which leads to the factor $(1-\lambda_0/\lambda)^{n+3.5}$ in Eq. (46). In Fig. 16, we compare the cross sections for J/ψ dissociation by gluons (“gluo-effect”) and by pions ($n=2$), as given by Eq’s (45) and (46). Gluon dissociation shows the typical photo-effect form, vanishing until the gluon momentum k passes the binding energy ΔE_ψ ; it peaks just a little later and then vanishes again when sufficiently hard gluons just pass through the much larger charmonium bound states. In contrast, the J/ψ -hadron cross section remains negligibly small until rather high hadron momenta (3 - 4 GeV). In a thermal medium, such momenta correspond to temperatures of more than one GeV. Hence confined media in the temperature range of a few hundred MeV are essentially transparent to J/ψ ’s, while deconfined media of the same temperatures very effectively dissociate them and thus are J/ψ -opaque.

The formalism leading to Eq. (46) is also applicable to J/ψ photoproduction, where it can be compared directly to data [70]. An alternative relation between J/ψ photoproduction and J/ψ break-up by hadrons is obtained through a combination of the vector meson dominance model and the short-distance QCD approach [71]. In both cases one finds clear evidence for the strong threshold suppression due to the form of the gluon distribution function; an illustration is given in Fig. 17. In contrast, several phenomenological models based on effective hadronic Lagrangians [72] - [76] suggest a $\sigma_{g-J/\psi}$ which is very much larger than Eq. (46) in the threshold region. It seems unlikely that such models can survive a comparison to J/ψ photoproduction.

The situation for χ_c ’s is quite similar, except for an earlier gluon dissociation threshold due to the lower χ_c binding energy of about 250 MeV. Corresponding differences occur for the various bottomonium states. The difference in binding energies thus provides the microscopic basis for the successive melting of different quarkonium states noted above. The binding energies for the quarkonium states considered above are included in Table 2. We note in particular that for the ψ' , ΔE is almost negligible (about 40 MeV), so that there cannot really be any difference in its dissociation by confined or deconfined media. In other words, any form of strongly interacting matter is expected to be ψ' -opaque.

We can thus define a schematic test to determine the confinement status of a box of unidentified matter. We first shine a ψ' beam at it: if it is transparent to this, the box does not contain strongly interacting matter; otherwise it does. In that case we repeat the procedure with a J/ψ beam: if this is unaffected, the medium in the box is confined; if the beam is attenuated, it is deconfined. The problem of an unambiguous deconfinement test is thus in principle solved: there is J/ψ dissociation if and only if the medium is deconfined. However, the test pre-supposes the existence of a prepared strongly interacting medium and the availability of J/ψ and ψ' beams as probes, and in nuclear interactions, both have to be prepared by the collision process. The actual application of such a test is therefore more complex; it will be taken up in detail in section 5.

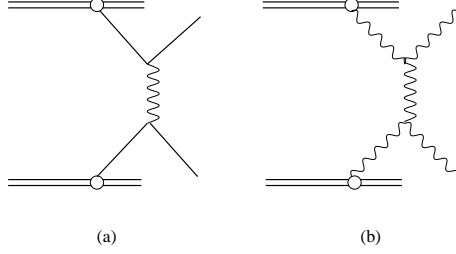


Figure 18: Some lowest order diagrams for jet production in hadron collisions.

4.3 Jet Quenching

One important aspect in the use of quarkonium states as deconfinement test is that in a collision with usual ‘big light’ hadrons, the small quarkonia probe only the local partonic structure of their collision partner, not global features such as mass or size. This aspect is also the basis for using hard jets to study the confinement status of a given medium.

Hard jets are produced through hard partonic interactions in the very early stages of nucleon-nucleon collisions; some typical processes are illustrated in Fig. 18. In nuclear collisions, the produced gluons or quarks leave their formation point with a very high momentum transverse to the collision axis, and in doing so, pass through the primary nuclear matter and through whatever secondary medium is produced by the collision. The effect of such a passage through a quark-gluon plasma has in recent years been studied in considerable detail, leading to rather well-defined predictions [77] - [79].

An electric charge, passing through matter containing other bound or unbound charges, loses energy by scattering. For charges of low incident energy E , the energy loss is largely due to ionization of the target matter. For sufficiently high energies, the incident charge scatters directly on the charges in matter and as a result radiates photons of average energy $\omega \sim E$. Per unit length of matter, the ‘radiative’ energy loss due to successive scatterings,

$$-\frac{dE}{dz} \sim E \quad (47)$$

is thus proportional to the incident energy.

This probabilistic picture of independent successive scatterings breaks down at very high incident energies [80]. The squared amplitude for n scatterings now no longer factorizes into n interactions; instead, there is destructive interference, which for a regular medium (crystal) leads to a complete cancellation of all photon emission except for the first and last of the n photons. This Landau-Pomeranchuk-Migdal (LPM) effect greatly reduces the radiative energy loss.

The physics of the LPM effect is clearly relevant in calculating the energy loss for fast colour charges in QCD media. These media are not regular crystals, so that the cancellation becomes only partial. Let us consider the effect here in a heuristic fashion; for details of the actual calculations, see [78, 79]. The time t_c needed for the emission of a gluon after the scattering of a quark (see Fig. 19) is given by

$$t_c = \frac{1}{\sqrt{P^2}} \frac{E}{\sqrt{P^2}} = \frac{E}{2P'k}, \quad (48)$$

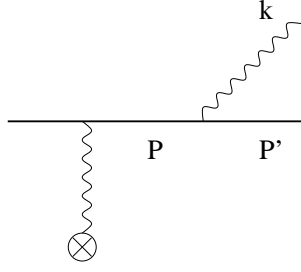


Figure 19: Gluon emission after scattering.

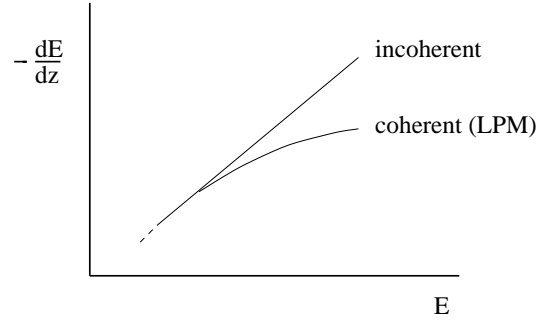


Figure 20: Energy loss in incoherent and coherent interactions.

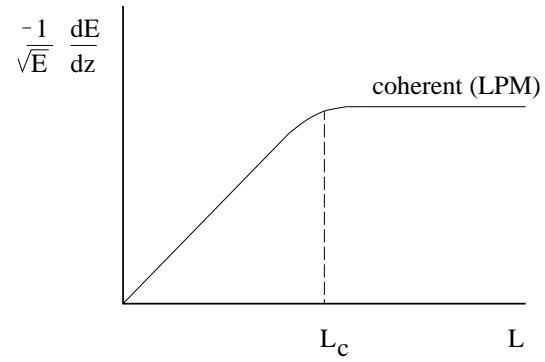


Figure 21: Energy loss in coherent interactions as function of the thickness L of the medium

in the rest system of the scattering center, where P^2 measures how far the intermediate quark state is off-shell; on-shell quarks and gluons are assumed to be massless, and $E/\sqrt{P^2}$ is the γ -factor between the lab frame and the proper frame of the intermediate quark. For gluons with $k_L \gg k_T$, we thus get

$$t_c \simeq \frac{\omega}{k_T^2}. \quad (49)$$

If the passing colour charge can interact with several scattering centers during the formation time of a gluon, the corresponding amplitudes interfere destructively, so that in effect after the passage of n centers over the coherence length z_c , only one gluon is emitted, in contrast to the emission of n gluons in the incoherent regime. Nevertheless, in both cases each scattering leads to a k_T -kick of the charge, so that after a random walk past n centers, $k_T^2 \sim n$. Hence

$$k_T^2 \simeq \mu^2 \frac{z_c}{\lambda}, \quad (50)$$

where λ is the mean free path of the charge in the medium, so that $z_c/\lambda > 1$ counts the number of scatterings. At each scattering, the transverse kick received is measured by the mass of the gluon exchanged between the charge and the scattering center, i.e., by the screening mass μ of the medium. From Eq. 49 we have

$$z_c \simeq \frac{\omega}{k_T^2}, \quad (51)$$

so that the formation length in a medium characterized by μ and λ becomes

$$z_c \simeq \sqrt{\frac{\lambda}{\mu^2}} \omega. \quad (52)$$

For the validity of Eq. (52), the mean free path has to be larger than the interaction range of the centers, i.e., $\lambda > \mu^{-1}$.

The energy loss of the passing colour charge is now determined by the relative scales of the process. If $\lambda > z_c$, we have incoherence, while for $\lambda < z_c$ there is coherent scattering with destructive interference. In both cases, we have assumed that the thickness L of the medium is larger than all other scales. When the coherence length reaches the size of the system, $z_c = L$, effectively only one gluon can be emitted. This defines a critical thickness $L_c(E) = (E\lambda/\mu^2)^{1/2}$ at fixed incident energy E , or equivalently a critical $E_c = \mu^2 L^2/\lambda$ for fixed thickness L ; for $L > L_c$, there is bulk LPM-behaviour, below L_c there are finite-size corrections.

We are thus left with three regimes for radiative energy loss. In case of incoherence, $z_c < \mu^{-1}$, there is the classical radiative loss

$$-\frac{dE}{dz} \simeq \frac{3\alpha_s}{\pi} \frac{E}{\lambda}, \quad (53)$$

where α_s is the strong coupling. In the coherent region, $\lambda > z_c$, the energy loss is given by the LPM bulk expression when $L > L_c$ [78],

$$-\frac{dE}{dz} \simeq \frac{3\alpha_s}{\pi} \sqrt{\frac{\mu^2 E}{\lambda}}. \quad (54)$$

The resulting reduction in the radiative energy loss dE/dz is illustrated in Fig. 20. Note that in earlier estimates the energy loss due to interactions of the gluon cloud accompanying the passing colour charge had been neglected [77]; this led to a considerably smaller energy loss, proportional to $\ln E$ instead of \sqrt{E} . Finally, in a medium of thickness $L < L_c$, there is less scattering and hence still less energy loss. Eq. (54) can be rewritten as

$$-\frac{dE}{dz} \simeq \frac{3\alpha_s}{\pi} \frac{\mu^2}{\lambda} L_c(E), \quad (55)$$

and for $L < L_c$, this leads to

$$-\frac{dE}{dz} \simeq \frac{3\alpha_s}{\pi} \frac{\mu^2}{\lambda} L \quad (56)$$

as the energy loss in finite size media with $L \leq L_c$. The resulting variation of the radiative energy loss with the thickness of the medium is shown in Fig. 21, with saturated (i.e., bulk) LPM behaviour setting in for $L \geq L_c$.

Eq. (56) has been used to compare the energy loss in a deconfined medium of temperature $T = 0.25$ GeV to that in cold nuclear matter of standard density [81]. For the traversal of a medium of 10 fm thickness, estimates give for the total energy loss

$$\Delta E = \int_{0 \text{ fm}}^{10 \text{ fm}} dz \frac{dE}{dz} \quad (57)$$

in a quark-gluon plasma

$$-\Delta E_{qgp} \simeq 30 \text{ GeV}, \quad (58)$$

corresponding to an average loss of 3 GeV/fm. In contrast, cold nuclear matter leads to

$$-\Delta E_{cnm} \simeq 2 \text{ GeV} \quad (59)$$

and hence an average loss of 0.2 GeV/fm. A deconfined medium thus leads to a very much higher rate of jet quenching than confined hadronic matter, as had in fact been suggested quite some time ago [82].

To convert this into an operational signature for deconfinement, considerably more work is needed [83, 84]. Some further basic ingredients needed for this effort will become clear in the next section, where the corresponding task is carried out for J/ψ suppression.

5. J/ψ SUPPRESSION IN NUCLEAR COLLISIONS

In this section, we shall present a realistic deconfinement study, based on the analysis of J/ψ production in nuclear collisions. On one hand, this provides a nice application of the general ideas presented above; on the other hand, it illustrates the steps necessary in any other, future deconfinement study. First, the production of the probe must be understood in hadronic collisions, both theoretically and experimentally. We therefore begin with the hadroproduction of charmonium. Next, one has to understand the modifications arising when the production occurs in a confined medium, for which $p-A$ collisions provide the

experimental reference. With the probe thus (a) prepared and (b) gauged to confined matter, it can be applied in an environment in which there might be deconfinement.

5.1 The Hadroproduction of Charmonium

The first stage of charmonium formation in hadronic collisions is the production of a $c\bar{c}$ pair; because of the large quark mass, this process can be described by perturbative QCD (Fig. 22). A parton from the projectile interacts with one from the target; the (non-perturbative) parton distributions within the hadrons are determined empirically in other reactions, e.g. by deep inelastic lepton-hadron scattering. Initially, the $c\bar{c}$ pair will in general be in a colour octet state. It subsequently neutralises its colour and binds to a physical resonance, such as J/ψ , χ_c or ψ' . Colour neutralisation occurs by interaction with the surrounding colour field; this and the subsequent resonance binding are presumably of non-perturbative nature. The colour evaporation model [85] provides the simplest and most general phenomenological approach to colour neutralisation. In the evaporation process, the $c\bar{c}$ pair can either combine with light quarks to form open charm mesons (D and \bar{D}) or bind with each other to form a charmonium state.

The basic quantity in this description is the total sub-threshold charm cross section, obtained by integrating the perturbative $c\bar{c}$ production cross section over the mass interval from $2m_c$ to $2m_D$. At high energy, the dominant part of $\sigma_{c\bar{c}}$ comes from gluon fusion (Fig. 22a), so that we have

$$\sigma_{c\bar{c}}(s) = \int_{2m_c}^{2m_D} d\hat{s} \int dx_1 dx_2 g_p(x_1) g_t(x_2) \sigma(\hat{s}) \delta(\hat{s} - x_1 x_2 s), \quad (60)$$

with $g_p(x)$ and $g_t(x)$ denoting the gluon densities, x_p and x_t the fractional momenta of gluons from projectile and target, respectively; σ is the $gg \rightarrow c\bar{c}$ cross section. In pion-nucleon collisions, there are also significant quark-antiquark contributions (Fig. 22c), which become dominant at low energies. The essential claim of the colour evaporation model is that the production cross section of any charmonium state i is given by

$$\sigma_i(s) = f_i \sigma_{c\bar{c}}(s), \quad (61)$$

where f_i is an energy-independent constant to be determined empirically. It follows that the energy dependence of any charmonium production cross section is predicted to be that of the perturbatively calculated sub-threshold charm cross section. As a further consequence, the production ratios of different charmonium states

$$\frac{\sigma_i(s)}{\sigma_j(s)} = \frac{f_i}{f_j} = \text{const.} \quad (62)$$

must be energy-independent. We note that only a small part of the total subthreshold cross section $\sigma_{c\bar{c}}$ goes into charmonium formation. In accord with perturbative open charm calculations, the remainder (more than 90 %) leads to $D\bar{D}$ production; the missing energy needed to reach the $D\bar{D}$ threshold is obtained by interaction with the colour field. The cross section for open charm production is thus directly predicted by the form of Eq.

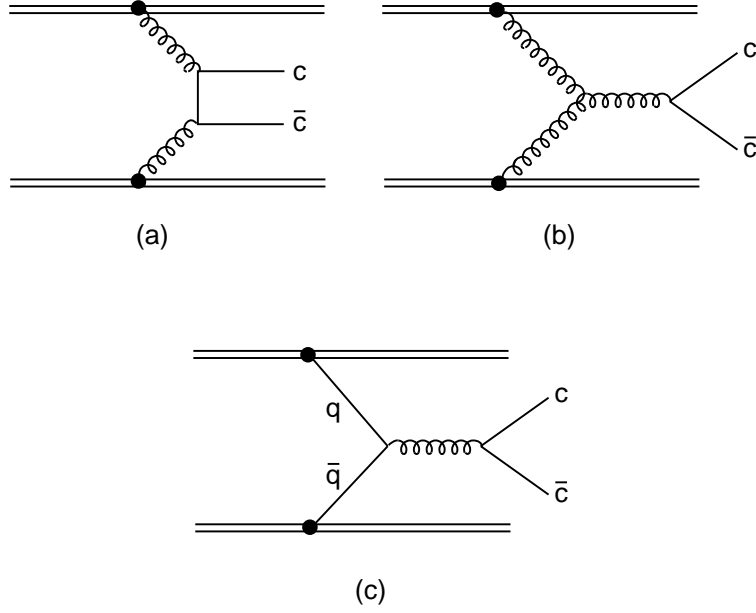


Figure 22: Lowest order diagrams for $c\bar{c}$ production in hadronic collisions, through (a,b) gluon fusion and (c) quark-antiquark annihilation.

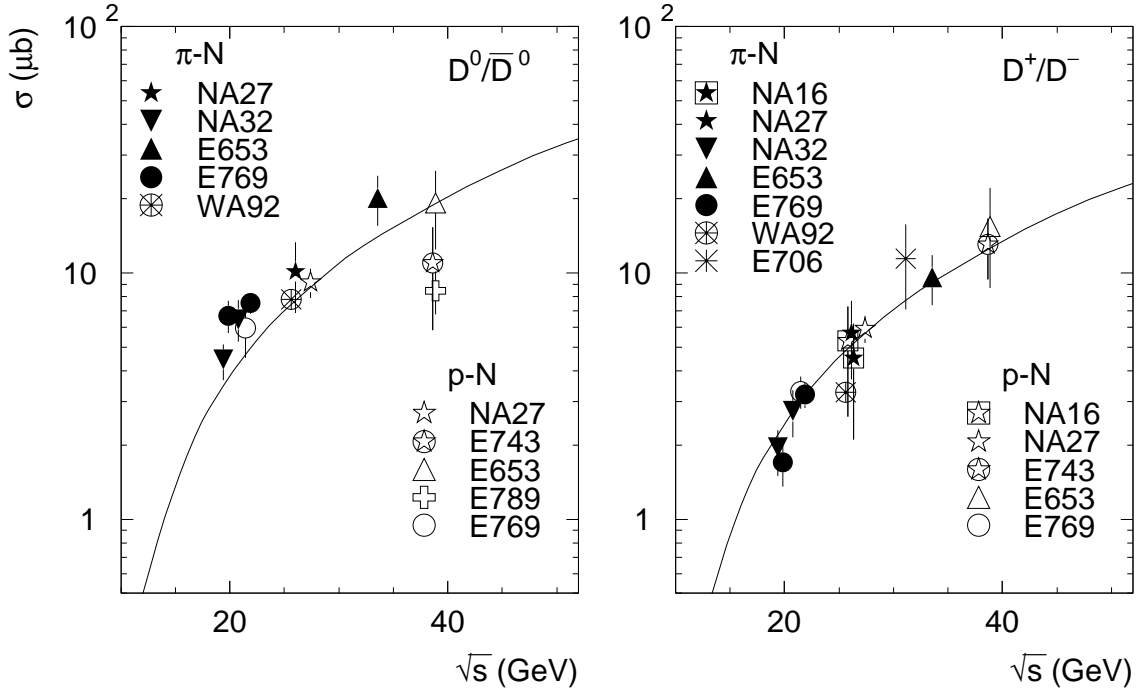


Figure 23: Open charm hadroproduction at different cms energies, compared to PYTHIA calculations [86].

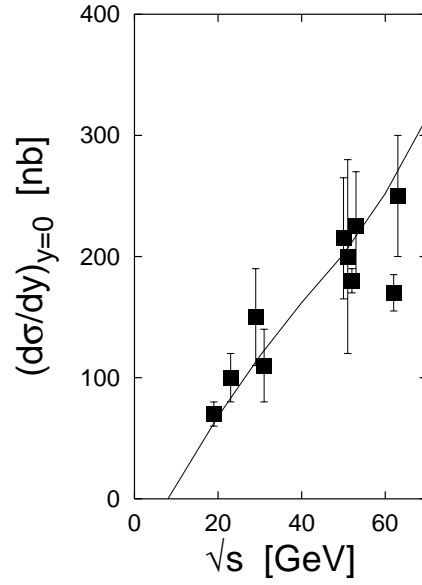


Figure 24: The energy dependence of J/ψ hadroproduction based on MRS D-' parton distributions, compared to data [87].

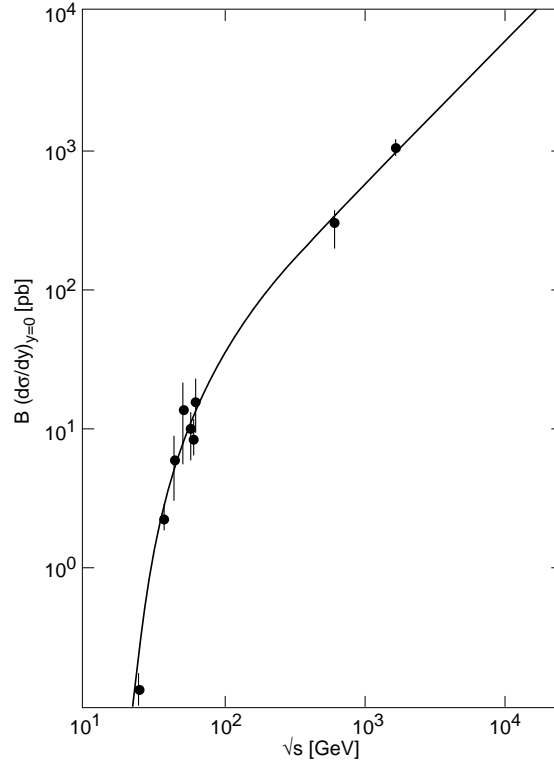


Figure 25: The energy dependence of bottomonium hadroproduction based on MRS D-' parton distributions, compared to data [87].

(60), with the integration essentially running to \sqrt{s} , instead of ending at $2m_D$. In Fig. 23 we see that the result agrees well with experiment [86].

The predictions of the colour evaporation model have been compared in a comprehensive survey [87] to the available data, using parton distribution functions which include the new HERA results [88, 89]. In Figs. 24 and 25, we see that the energy-dependence is well described for both J/ψ and Υ production; for J/ψ production, the normalisation coefficient is $f_{J/\psi}=0.025$. The Υ results are obtained for the sum of Υ , Υ' and Υ'' decaying into dimuons, with $Bf_\Upsilon = 1.6 \times 10^{-3}$ for the normalisation; here the branching ratios cannot be directly removed. In the fixed-target/ISR energy range, the results from the two different sets of parton distributions coincide; for the J/ψ at LHC energies, there is some spread due to scale uncertainties in the parton distributions, which hopefully can be removed by more precise DIS data. For the Υ production, we have already now data up to 1.8 TeV, and in Fig. 25 they are seen to agree very well with the prediction obtained using the “low energy” value $Bf_\Upsilon = 1.6 \times 10^{-3}$.

In Figs. 26 and 27, the predicted energy-independence of production ratios is found to hold as well, again up to Tevatron energy. Here it should be noted that the CDF data for the ratio $\psi'/(J/\psi)$ are taken at large transverse momenta ($5 \leq p_T \leq 15$ GeV), while the lower energy data are integrated over p_T , with the low p_T region dominant. Hence colour evaporation appears to proceed in the same way at both small and large p_T .

With the relative fractions f_i for the different quarkonium states determined, colour evaporation also predicts the longitudinal and transverse momentum distributions for the hadroproduction of these states. In both cases, the agreement is quite good [87, 90].

The colour evaporation model thus provides a viable phenomenological description of the hadroproduction of quarkonia, leading to quantitative predictions up to the highest energies under consideration. However, it does not give a theoretical basis for the fractions f_i of the hidden charm cross section, and hence one cannot use it to determine the space-time evolution of quarkonium production. For the production in nuclear collisions, this is crucial, as we shall see shortly, and so we have to consider more detailed dynamical mechanisms for hadroproduction. The first such attempt, the colour singlet model, assumed that the colour neutralisation of the $c\bar{c}$ is perturbatively calculable [91]. The resulting well-defined predictions were found to disagree by orders of magnitude with high energy data from FNAL [92], so that non-perturbative features seem to be essential for quarkonium production [93, 94]. This has led to extensive studies of possible mechanisms; see [95] for recent reviews.

We shall here concentrate on one resulting proposal, the colour octet model [93, 94], keeping in mind, however, that only rather general features of such a model will enter the subsequent applications to nuclear collisions. The basis of the colour octet model is that any quark-antiquark bound state is in reality a superposition of the basic $q\bar{q}$ state and fluctuations involving in addition one or more gluons (“higher Fock space components”). We can thus decompose the J/ψ state $|\psi\rangle$

$$|\psi\rangle = a_0|(c\bar{c})_1\rangle + a_1|(c\bar{c})_8g\rangle + a_2|(c\bar{c})_1gg\rangle + a'_2|(c\bar{c})_8gg\rangle + \dots \quad (63)$$

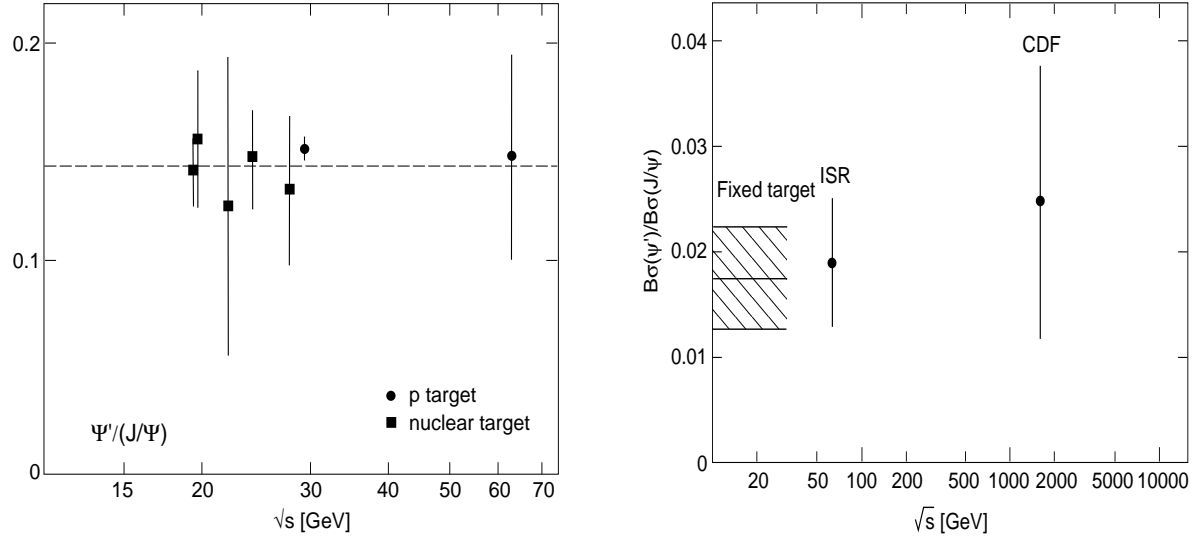


Figure 26: The ratio of J/ψ to ψ' hadroproduction as function of the cms energy [87].

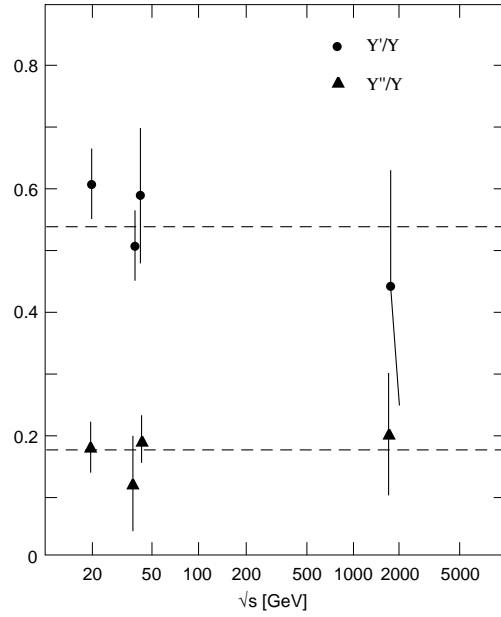


Figure 27: The ratio of Υ' to Υ and Υ'' to Υ hadroproduction as function of the cms energy [87].

into a pure $c\bar{c}$ colour singlet component (3S_1), into a component consisting of $c\bar{c}$ colour octet (1S_0 or 3P_J) plus a gluon, and so on. The higher Fock space coefficients correspond to an expansion in the relative velocity v of the charm quarks. As we shall see below, this corresponds in coordinate space to an expansion in terms of components of decreasing spatial extension. For the wave function of the J/ψ , the higher components correspond to (generally small) relativistic corrections. In high energy J/ψ production, however, the higher Fock space components of charmonium states play an important role. The short time available before confinement constraints appear, favours colour neutralisation of the $(c\bar{c})_8$ by gluons already present. Since $(c\bar{c})$ production at high energies occurs at small x , the density of such comoving gluons is in fact high, and so the higher Fock space components become dominant.

Analogous Fock space decompositions hold for the other charmonium states [93, 94]. In all cases, the first higher state consists of a colour octet $c\bar{c}$ plus a gluon. For the ψ' , the next-to-leading terms again contain a colour octet (3P_J or 1S_0 $c\bar{c}$) plus a gluon; for the χ 's, a 3S_1 colour octet $c\bar{c}$ is combined with a gluon.

This sheds some light onto the unspecified colour evaporation process. When the colour octet $c\bar{c}$ leaves the field of the nucleon in which it was produced, it will in general neutralise its colour by combining non-perturbatively with an additional collinear gluon, thus producing the $(c\bar{c})_8g$ component of the J/ψ or the other charmonium states (Fig. 28). After a “relaxation time” τ_8 , the $(c\bar{c})_8g$ will absorb the accompanying gluon to revert to the dominant $(c\bar{c})_1$ charmonium mode. Note that we are here considering those $c\bar{c}$ pairs which will later on form charmonia. The $(c\bar{c})_8$ could as well neutralise its colour by combining with a light quark-antiquark pair, but this would result predominantly in open charm production.

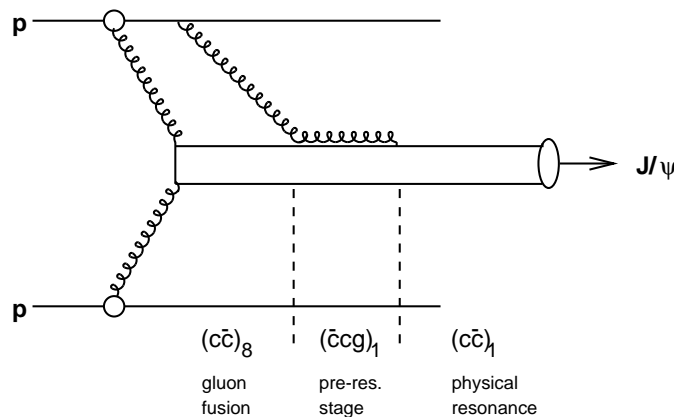


Figure 28: J/ψ production in $p - p$ collisions.

Charmonium production in hadronic collisions thus inherently involves different space-time scales [93]. The first step is the creation of a heavy $c\bar{c}$ pair, which takes place in a very short time, $\tau_{\text{pert}} \simeq 1/(2m_c)$. The colour octet $c\bar{c}$ state combines with an additional gluon to form a pre-resonance $(c\bar{c})_8g$ to neutralise its colour and yield a resonance state of the correct quantum numbers. The lifetime τ_8 of this state is determined by the virtuality

of the intermediate $c\bar{c}$ state. In the rest frame of the $c\bar{c}$, this is approximately [96]

$$\tau_8 \simeq \frac{1}{\sqrt{\Delta}}, \quad (64)$$

where $\Delta \equiv [(p+k)^2 - m_c^2] = 2pk$, with p denoting the four momentum of a quark in the final J/ψ , k that of the accompanying gluon. Because of the large charm quark mass m_c , the time uncertainty associated with gluon absorption becomes

$$\tau_8 \simeq \frac{1}{\sqrt{2m_c k_0}} \quad (65)$$

where k_0 is the gluon energy. In a confining medium, $k \geq \Lambda_{\text{QCD}}$, with $\Lambda_{\text{QCD}} \simeq 0.20 - 0.25$ GeV. We thus encounter a new scale $(2m_c \Lambda_{\text{QCD}})^{1/2}$, with $\Lambda_{\text{QCD}} \ll (2m_c \Lambda_{\text{QCD}})^{1/2} \ll m_c$; it makes $\tau_8 \gg \tau_{\text{pert}}$. For J/ψ production at mid-rapidity of a nucleon-nucleon collision, the colour neutralisation time becomes

$$t_8 \simeq \tau_8 [1 + (P_A/2m_c)^2]^{1/2} \quad (66)$$

in the rest frame of target or projectile nucleon, with P_A denoting the momentum of the $c\bar{c}$ pair in this frame. As seen from the nucleon, colour neutralisation of fast $c\bar{c}$ pairs will thus take a long time. Equivalently, the $(c\bar{c})_8 g$ travels in the time t_8 a long distance,

$$d_8 \simeq \tau_8 (P_A/2m_c), \quad (67)$$

in the rest frame of the nucleon.

Moreover, the production of high energy charmonia implies the production of composite and hence extensive states $(c\bar{c}g)_i \equiv |(c\bar{c})_8 g)_i$; here the subscript i again refers to the specific charmonium state in question (J/ψ , χ_c , ψ'). Although the intrinsic transverse size of the $(c\bar{c}g)_i$ depends in principle on the quantum numbers of the state i , confinement constraints on the gluon lead to a universal $(c\bar{c}g)$ size r_8 . Let us consider this in more detail.

The formation process of the $c\bar{c}$ pair inside the $(c\bar{c}g)$ state (see Fig. 28) makes this pair very compact, with a spatial extension of about $1/2m_c$. The size of the $(c\bar{c}g)$ is thus essentially determined by the softness of the gluon, which is restricted by $k \geq \Lambda_{\text{QCD}}$. The effect of this can be estimated by noting that in the time τ_8 obtained above, a gluon can propagate over a distance $r_8 \simeq (2m_c \Lambda_{\text{QCD}})^{-1/2}$. Equivalently, we can consider energy conservation in the passage from $(c\bar{c}g)$ to the leading Fock space component $(c\bar{c})_1$; the non-relativistic form for heavy quarks leads to

$$\frac{p^2}{2m_c} \simeq k_0, \quad (68)$$

where p is the quark three-momentum in the charmonium cms. From the lowest allowed gluon energy $k_0 = \Lambda_{\text{QCD}}$ we thus obtain the intrinsic size

$$r_8 \simeq \frac{1}{p} \simeq \frac{1}{\sqrt{2m_c \Lambda_{\text{QCD}}}} \simeq 0.20 - 0.25 \text{ fm}. \quad (69)$$

Since this size is determined only by the $(c\bar{c})_8g$ composition of the next-to-leading Fock space state, the compactness of the produced $(c\bar{c})_8$ in this state and the gluon momentum cut-off in confined systems, it is essentially the same for the different charmonium states. The Fock space state $(c\bar{c}g)$ thus constitutes something like a gluonic hard core present in all charmonium states. Its size is seen to be approximately that of the ground state charmonium J/ψ , while the higher excited charmonium states are larger. The hard gluon core in these just corresponds to the fact that in extended bound states the emission (or absorption) of gluons with momenta bigger than Λ_{QCD} can occur only in a sufficiently small inner region. In other words: while the basic $(c\bar{c})_1$ state gives for different quantum numbers quite different spatial distributions, the much more localised higher Fock space states are of universal size $(2m_c\Lambda_{\text{QCD}})^{-1/2}$. In the large quark mass limit, however, the bound state radii become smaller than $(2m_Q\Lambda_{\text{QCD}})^{-1/2}$, so that the universality would then be lost.

In summary: charmonium hadroproduction is based on a hard perturbative process, such as gluon fusion into a $c\bar{c}$ pair. The subsequent colour neutralisation brings in non-perturbative features, leading to the formation of a pre-resonance state, such as the first higher Fock state component $(c\bar{c})_8g$. Confinement constraints result in a universal pre-resonance charmonium radius of some 0.25 fm and an associated life time of the same size. In this evolution era of charmonium production, the different resonant states $(J/\psi, \chi_c, \psi')$ thus appear essentially indistinguishable. This has striking consequences for charmonium production on nuclear targets.

5.2 Pre-Resonance Suppression

The colour evaporation model alone, without further dynamical input, predicts that the charmonium production rate in high energy $p - A$ collisions is A times that in $p - p$ collisions at the same energy, just as it is for open charm production. We assume here that the hard process is dominated by gluon fusion; hard processes involving quarks would lead to a small modification due to isospin effects. Experimentally, however, the presence of the nuclear target medium is known to reduce J/ψ production rates in $p - A$ collisions significantly, up to about 40% relative to those in $p - p$ interactions [97]-[99]; in Fig. 29 we show the most recent data [100]. The suppression in $p - A$ collisions was the first indication that the presence of a strongly interacting medium influences the rate of J/ψ production. The nuclear medium introduces space-time scales, and hence we have to consider the space-time structure involved in the production process.

The mentioned experiments were carried out with incident protons with momenta between 200 and 800 GeV/c. This gives the nascent J/ψ momenta of 30 GeV/c or more in the target rest frame. As a result, the transition $c\bar{c}g \rightarrow J/\psi, \chi_c$ or ψ' occurs outside the target nucleus; the nuclear medium of the target sees only the passage of the corresponding pre-resonance states. Since these have essentially the same size and life-time for all charmonium states, the observed attenuation of the production rates should be the same for J/ψ as for ψ' . This prediction is indeed found to be quite well satisfied [105] (see Fig. 30). Earlier attempts to explain charmonium suppression in $p - A$ interactions in terms of the absorption of physical J/ψ states [101] had encountered difficulties precisely because of this feature. The equal attenuation of J/ψ and ψ' is a natural consequence

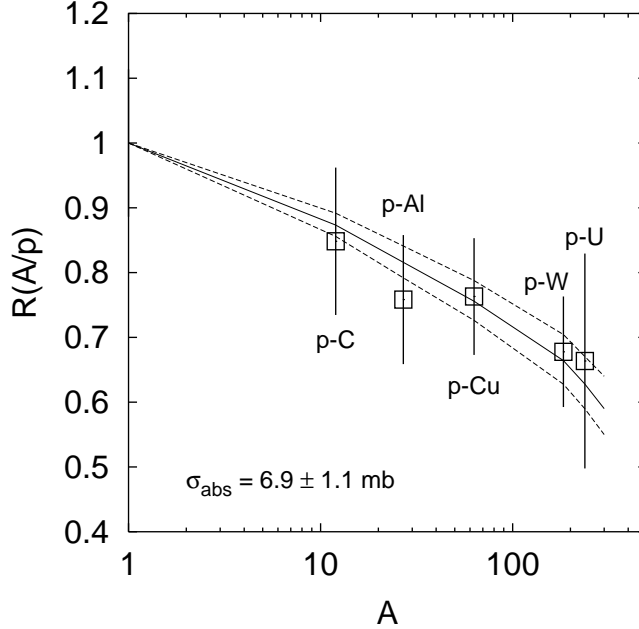


Figure 29: J/ψ production in $p - A$ vs. $p - p$ collisions [100].

of pre-resonance absorption; it can never be obtained for the physical J/ψ and ψ' states with their very different geometric sizes.

The cross section for the dissociation of the $c\bar{c}g$ state through collisions in nuclear matter can be estimated theoretically [102]; it can also be determined directly from $p - A$ data [52]. Since the components of the $c\bar{c}g$ are colour octets, the gluon interaction with this state will be 9/4 times stronger than the gluon interaction with the fundamental $c\bar{c}$, whose components are colour triplets. Hence we expect the $c\bar{c}g$ dissociation cross section to be about 9/4 times the high energy J/ψ dissociation cross section, i.e., around 6 mb.

For an experimental determination, we note that a $c\bar{c}g$ pair formed at point z_0 in the target nucleus has a survival probability

$$S_{c\bar{c}g}^A = \exp \left\{ - \int_{z_0}^{\infty} dz \rho_A(z) \sigma_{c\bar{c}g-N} \right\}, \quad (70)$$

where the integration covers the path remaining from z_0 out of the nucleus. The traversed medium of nucleus A is parametrized through a Woods-Saxon density distribution $\rho_A(z)$, and by comparing $S_{c\bar{c}g}^A$ with data for different targets A , the dissociation cross section for $c\bar{c}g - N$ interactions is found to be [103]

$$\sigma_{c\bar{c}g-N} = 6.9 \pm 1.1 \text{ mb}. \quad (71)$$

In Fig. 29 it is seen that pre-resonance absorption with this cross section agrees well with all presently available $p - A$ data on J/ψ production.

We now turn to nucleus-nucleus collisions; here there will certainly also be pre-resonance absorption in nuclear matter. However, in addition to the target and projectile

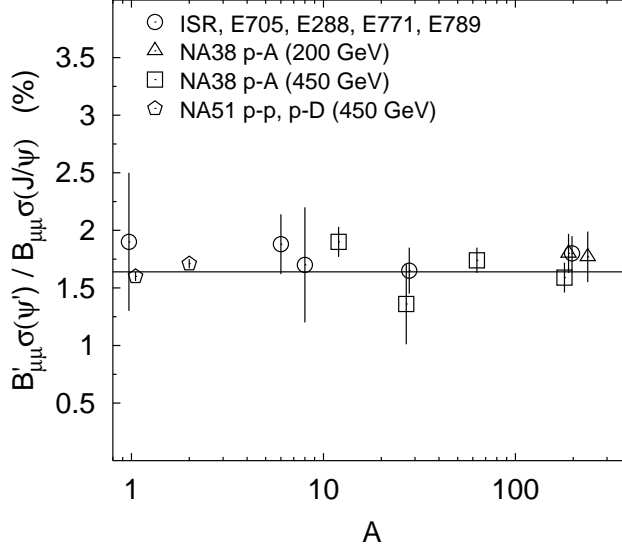


Figure 30: The relative A -dependence of J/ψ and ψ' production [105].

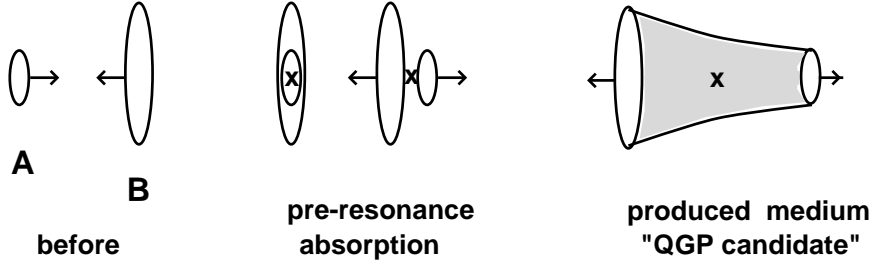


Figure 31: Schematic view of J/ψ production in $A - B$ collisions.

nuclei, there could now be a substantial amount of produced ‘secondary’ medium (Fig. 31). Our ultimate aim is to look for such a medium and test its confinement status.

The survival probability of a pre-resonance charmonium state in an $A - B$ collision at impact parameter b is given by

$$S_{c\bar{c}g}^{AB}(b) = \exp \left\{ - \int_{z_0^A}^{\infty} dz \rho_A(z) \sigma_{c\bar{c}g-N} \int_{z_0^B}^{\infty} dz \rho_B(z) \sigma_{c\bar{c}g-N} \right\}, \quad (72)$$

in extension of Eq. (70). Here z_0^A specifies the formation point of the $c\bar{c}g$ within nucleus A , z_0^B its position in B . Since experiments cannot directly measure the impact parameter b , we have to specify how Eq. (72) can be applied to data.

The Glauber formalism allows us to calculate the number $N_w^{AB}(b)$ of participant (‘wounded’) nucleons for a given collision. The number of secondary hadrons produced in association with the observed J/ψ is at present energies (up to SPS energy) found to be

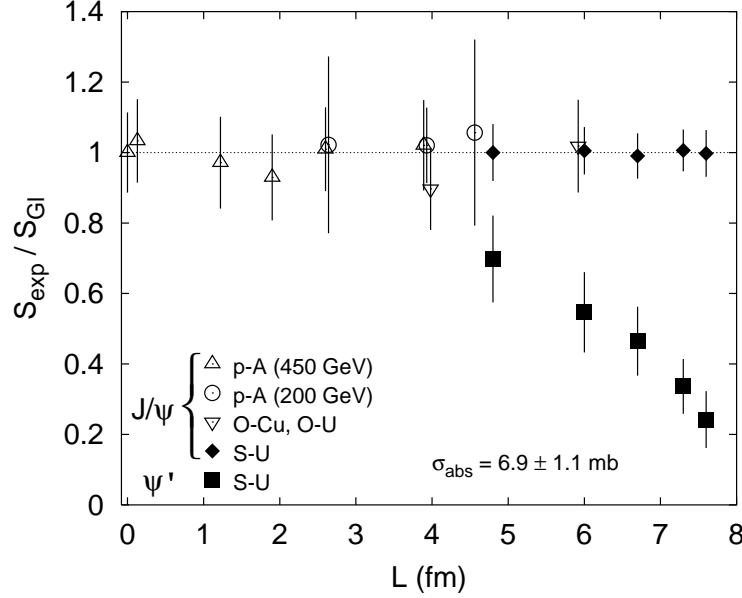


Figure 32: J/ψ and ψ' production in nuclear collisions, compared to pre-resonance absorption in nuclear matter [100, 104].

proportional to N_w^{AB} . The transverse energy E_T carried by the secondaries is measured experimentally, together with the J/ψ 's. We thus have

$$E_T(b) = q N_w^{AB}(b); \quad (73)$$

the proportionality constant q has to be determined on the basis of the given experimental acceptance. Once it is fixed, we have to check that the collision geometry (the measured relation between E_T and the number of spectator nucleons, the measured E_T -distribution) is correctly reproduced [52]. When this is assured, we can check if the J/ψ production in $O-Cu$, $O-U$ and $S-U$, as measured by the NA38 experiment at CERN over the past ten years [100, 104], shows anything beyond the expected pre-resonance nuclear absorption with the cross section $\sigma_{c\bar{c}g-N} = 6.9 \pm 1.1$ mb determined from $p-A$ interactions.

The answer is clearly negative, as seen in Fig. 32 for the integrated cross sections as well as for the centrality dependence of $S-U$ collisions. We consider here the J/ψ survival probability, i.e., the measured production rate S_{exp} , normalised to the predicted rate S_{Gl} , including pre-resonance suppression with the given absorption cross section. To compare all data in one figure, we have parametrized the different collision configurations in terms of the path length L of the charmonium state in the nuclear environment. As a rough estimate, $L \simeq (3/4)R_A$ in $p-A$ collisions, with $R_A = 1.13 A^{1/3}$ for the nuclear radius; the factor $(3/4)$ takes into account the average over centrality. Similar estimates can be obtained for $A-B$ collisions; however, the Glauber formalism allows a direct determination of this path length at each impact parameter, and we shall use the values of L thus determined and then related to E_T through Eq. (73).

All nuclear collisions measured by NA38 thus show only what is now called ‘normal’ J/ψ suppression, i.e., the pre-resonance suppression already observed in $p-A$ interactions

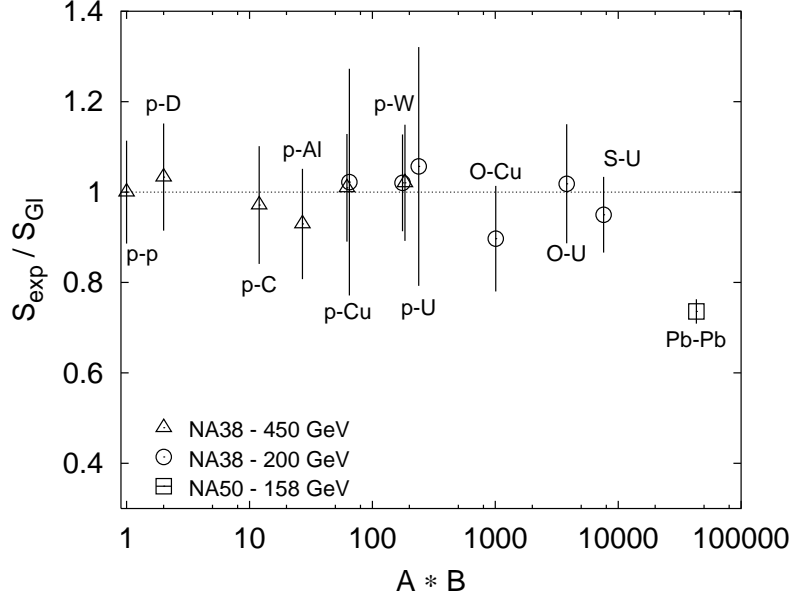


Figure 33: Centrality integrated rates for J/ψ production in $A-B$ and $Pb-Pb$ collisions, normalized to pre-resonance absorption in nuclear matter [100, 107].

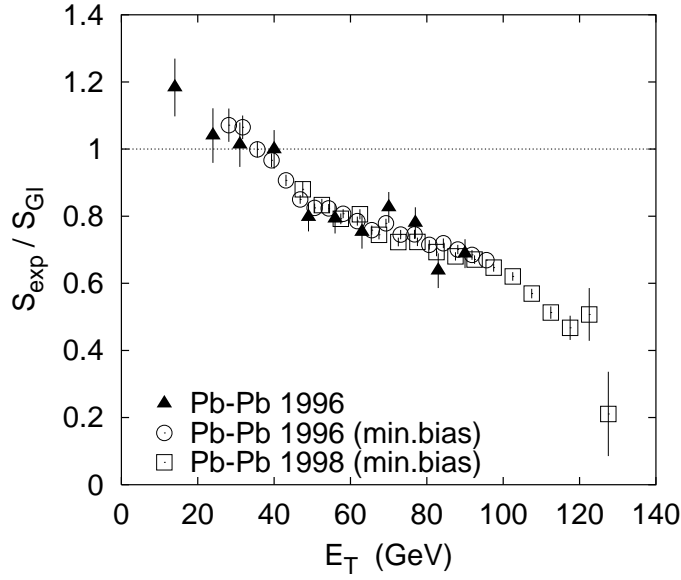


Figure 34: The E_T -dependence of J/ψ production in $Pb-Pb$ collisions, normalized to pre-resonance absorption in nuclear matter [108].

[52, 101, 102]. We thus have to ask if the $A - B$ collisions studied by NA38 lead to any produced secondary medium at all. The behaviour of ψ' production (included in Fig. 32) shows that this is indeed the case [100, 105]: in $S - U$ collisions, there is ψ' suppression beyond the expected pre-resonance nuclear absorption. The collisions thus do form a secondary medium, and this can distinguish a ψ' (which is suppressed) from a J/ψ (which remains unaffected). Since the former is suppressed, the latter unaffected, the medium does not signal colour deconfinement.

The observed ψ' suppression should thus be accountable in terms of a medium consisting of hadrons, and such a ‘hadronic comover’ description [106] is indeed found to work [52]. It involves as basic quantities the ψ' -hadron dissociation cross section and the transverse density of hadronic comovers. Since the ψ' is very loosely bound (it lies only 60 MeV below the open charm threshold, see Table 2), it seems reasonable to assume that the cross section attains its geometric value of about 10 mb soon after the threshold. The density of wounded nucleons is given as function of collision centrality by the mentioned Glauber formalism, and the observed rate of about 1.5 secondary hadrons per wounded nucleon determines the comover density. The resulting form for ψ' suppression is found to agree quite well with the existing data [52].

5.3 Anomalous J/ψ Suppression

The suppression of J/ψ production in nuclear collisions, from $p - A$ to central $S - U$ collisions, is thus understood in terms of ‘normal’ absorption in nuclear matter: the pre-resonance charmonium state is dissociated by collisions with the primary target or projectile nucleons. The J/ψ as probe of the produced environment indicates “no deconfinement”.

This situation came to an end with the advent of truly *heavy ion* experiments. In $Pb-Pb$ collisions at the CERN-SPS, the NA50 Collaboration [107, 108] observed a further ‘anomalous’ suppression of about 30% for the overall J/ψ production rate (Fig. 33). Looking in more detail, it was observed that peripheral $Pb-Pb$ collisions show only normal suppression (Fig. 34). Then, at a transverse hadronic energy $E_T \simeq 40$ GeV (corresponding to an impact parameter b of about 8 fm), the anomalous J/ψ suppression sets in quite suddenly, with a drop of 20% for an E_T increase of less than 20 GeV, or a decrease in b of about 1 fm. For very central collisions, $E_T \geq 100$ GeV or $b \leq 2$ fm, something like a second drop appeared. The most central collisions thus show a suppression by more than a factor two beyond the normal pre-resonance absorption. The general suppression pattern, combining all data from $p-p$ to central $Pb-Pb$ collisions, is illustrated in Fig. 35, where the J/ψ survival probability is shown as function of the number of participant nucleons. What conclusions can be drawn from this behaviour?

5.3a Deconfinement vs. Hadronic Comovers

Over the past decade, quarkonium suppression mechanisms have become classified into two categories. The suppression could be due to colour deconfinement, as originally predicted [62]. To verify this, one has to exclude what are generally called ‘conventional’ mechanisms, covering all possible ways to suppress J/ψ production without invoking

deconfinement. There are a considerable variety of possible conventional suppression schemes: absorption in nuclear matter [111], absorption by produced secondary hadrons (i.e., by the ‘hadronic comovers’ mentioned above [106, 110]), nuclear shadowing of parton distribution functions [112], medium-induced energy loss of the incident partons leading to $c\bar{c}$ production [113] or more general in-medium modifications of the $c\bar{c}$ production process [114]; for an extensive review, see [115]. Since all models involve several more or less adjustable parameters, the task of confirming one and ruling out all others seems quite difficult indeed. It is greatly simplified, however, by two basic *qualitative* features of deconfinement, which distinguish it from all conventional approaches.

Deconfinement is a critical phenomenon, with a well-defined onset for colour conductivity specified by theory. There is a thermodynamic region for confinement, a critical point, and then a region of deconfinement. All other approaches are always present in smoothly varying degrees. To illustrate the point, we consider two simple models, one for hadronic comover absorption, as representative and most intensively studied conventional model [120], the other for colour deconfinement [119].

In the comover picture, the J/ψ is dissociated with a cross section σ_{com} in a medium of produced hadronic secondaries; the density $n(\epsilon)$ of this medium is determined by the initial energy density ϵ of the produced environment. The medium subsequently cools off and stops affecting the J/ψ ’s when its density drops to a freeze-out value n_f . The resulting J/ψ survival probability becomes [116]

$$S_{J/\psi}^{\text{com}}(\epsilon) = \exp\{-\sigma_{\text{com}}n(\epsilon)\tau_0 \ln[n(\epsilon)/n_f]\}, \quad (74)$$

where $\tau_0 \simeq 1$ fm denotes the formation time of the medium. According to Eq. (46), the cross section for J/ψ dissociation in the comover medium is expected to be very small, ruling out significant contributions from comover absorption. An essential ingredient in all comover models is thus the assumption that the short distance QCD arguments leading to Eq. (8) become applicable only for much heavier quarks and cannot be used for charmonium states.³ The cross section σ_{com} is then treated as adjustable parameter, as is the freeze-out density n_f . Typical fit values [120] lead to $\sigma_{\text{com}} \simeq 4 - 5$ mb. We shall return shortly to the latest and most detailed comover fits.

In contrast to comover absorption, deconfinement sets in at a critical point ϵ_c ; a simple model [119] leads to

$$S_{J/\psi}^{\text{dec}}(\epsilon) = \Theta(\epsilon_c - \epsilon) + \Theta(\epsilon - \epsilon_c) \left(\frac{\epsilon}{\epsilon_c}\right)^{9/4}. \quad (75)$$

The power of the variable ϵ/ϵ_c is determined by the energy density profile in the collision, since the hot interior melts J/ψ ’s, while they survive in the cool rim. The specific form (75) arises for nuclei of constant nuclear density [121]. More recent calculations of this type [122] have led to a very similar suppression pattern, while percolation arguments, as will be seen below, lead to a still more abrupt onset of deconfinement suppression. The

³The behaviour of $\sigma^{\text{in}}(J/\psi - h)$ for low collision energies can be measured directly either by shooting a nuclear beam at a hydrogen target (‘inverse kinematics’ experiment [117]) or by annihilating antiprotons in a nuclear target [118]. Hence this question can be settled empirically.

abrupt onset of J/ψ suppression in Eq. (75) shows a fundamental qualitative difference to the smooth monotonic decrease of the comover suppression pattern Eq. (74); an explicit illustration will be given shortly. It should also be noted that hadronic comover absorption would have to be present already in $S - U$ collisions, thus ruling out pure pre-resonance absorption here. The behaviour seen in Fig. 32 seems difficult to reconcile with this.

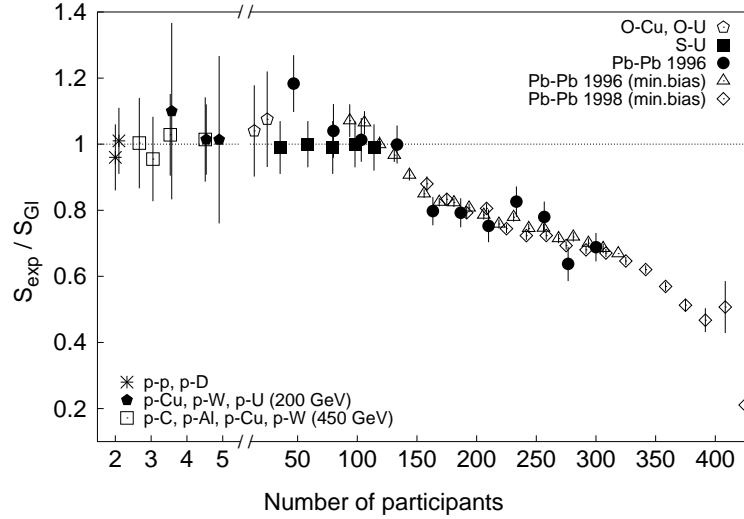


Figure 35: J/ψ production in $A - B$ and $Pb - Pb$ collisions, normalized to pre-resonance absorption in nuclear matter, as function of the number of participating nucleons [108, 109].

So far, we have addressed the fate of a well-defined J/ψ in a strongly interacting environment. However, sufficiently energetic nuclear collisions produce the entire spectrum of charmonium states; below the open charm threshold, they produce $\eta_c(1S)$, $J/\psi(1S)$, $\chi_{c0}(1P)$, $\chi_{c1}(1P)$, $\chi_{c2}(1P)$ and $\psi'(2S)$. All higher excited states have significant decay rates into the J/ψ , and so the observed J/ψ 's can be either directly produced, or they can come from the decay of higher excitations. Since the decay times of these excitations are very long (more than 1000 fm for the χ_c), the medium affects the intermediate higher excitations, not the final decay product J/ψ .

In nucleon-nucleon collisions, about 60% of the observed J/ψ 's are produced directly, about 32% come from χ_c decays, the remaining 8% from ψ' decays. To simplify matters, we neglect the ψ' component for the moment and assume 2/3 direct production and 1/3 χ_c decay. Both colour screening and gluon dissociation indicate that the χ_c will be destroyed at a lower energy density than the direct J/ψ 's. As second basic qualitative feature, colour screening thus predicts sequential J/ψ suppression, with a multi-step survival probability [64, 121]. For J/ψ suppression, the simple analytic form (75) now becomes

$$S_{J/\psi}^{dec}(\epsilon) = \frac{1}{3} \left\{ \Theta(\epsilon_\chi - \epsilon) + \Theta(\epsilon - \epsilon_\chi) \left(\frac{\epsilon}{\epsilon_\chi} \right)^{9/4} \right\} + \frac{2}{3} \left\{ \Theta(\epsilon_\psi - \epsilon) + \Theta(\epsilon - \epsilon_\psi) \left(\frac{\epsilon}{\epsilon_\psi} \right)^{9/4} \right\}, \quad (76)$$

where $\epsilon_\chi \simeq \epsilon_c$ and $\epsilon_\psi > \epsilon_c$ denote the thresholds for χ and direct ψ dissociation, respectively. This form of the resulting functional behaviour of deconfinement suppression (Fig. 36) was given eight years ago [119]; it clearly illustrates the quantitative difference to suppression by comover absorption. Today we find it to be remarkably similar to the suppression pattern now observed in $Pb - Pb$ interactions (Figs. 34 and 35).

The first $Pb - Pb$ results provided by NA50 [123] were of much lower precision than those now available. This stimulated various comover approaches to attempt a unified description of $p - A$, $S - U$ and $Pb - Pb$ data. The monotonic onset of any comover suppression requires the presence of some anomalous suppression also for $S - U$, and it excludes any thresholds. Hence even the first, relatively pronounced onset of suppression in the $Pb - Pb$ data posed problems. Nevertheless, qualitatively the comover pattern also leads to a decrease with increasing energy density, and so more precise data were needed for any reliable conclusion. Successive NA50 runs have provided this [107, 108], and the given experimental situation today, with a clear two-step suppression pattern, excludes all conventional scenarios. In Fig. 37 we show as illustration the results of one of the most general comover approaches, based on the dual parton model [125]; it includes comover production dependent on the number of collisions as well as on the number of participant nucleons, and it also takes into account $J/\psi - \psi' / \psi' - J/\psi$ transitions. In spite of the resulting number of adjustable parameters, it is clearly incompatible with the latest data. All other conventional models share this fate: none can account for all the available data, including $S - U$ and $Pb - Pb$ collisions; in particular, none can produce a mechanism leading to any kind of non-monotonic step structure. This provides the basis for the conclusion reached by the NA50 collaboration [108]: *The onset of the anomalous J/ψ suppression is the first clear observation of a threshold effect in heavy ion collisions and can be considered as a strong indication of the production of a deconfined quark-gluon plasma phase in central Pb-Pb collisions.*

5.3b Towards an Understanding of Deconfinement

The observed J/ψ suppression thus rules out conventional explanations; moreover, it is qualitatively in accord with the behaviour expected from colour deconfinement. Nevertheless, the details of the onset of deconfinement are not yet clear, and in particular the crucial collision variable triggering this onset is not yet unambiguously identified. We present in this section one possible approach, based on parton percolation [30, 128].

In a high energy nuclear collision viewed in the overall center of mass, the two Lorentz-contracted nuclei quickly pass through each other. After about 1 fm at the SPS and only about 0.1 fm at RHIC, they have separated and left behind a partonic medium as a potential QGP candidate. Inside this medium, primary nucleon-nucleon collisions have left charmonium states as probes, whose fate can provide information about the nature of the partonic medium.

The average number of produced partons will depend on the number of nucleon-nucleon collisions and/or the number of participating nucleons. Up to SPS energies, the number of wounded nucleons appears to be the main determining factor. This is understandable in terms of the dilated and hence large soft parton formation time as seen

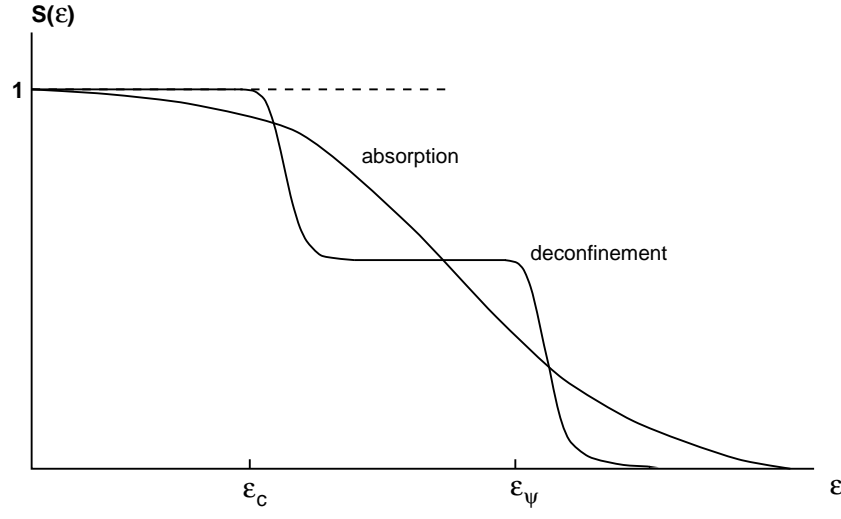


Figure 36: J/ψ suppression by deconfinement compared to that by hadronic comover absorption [119].

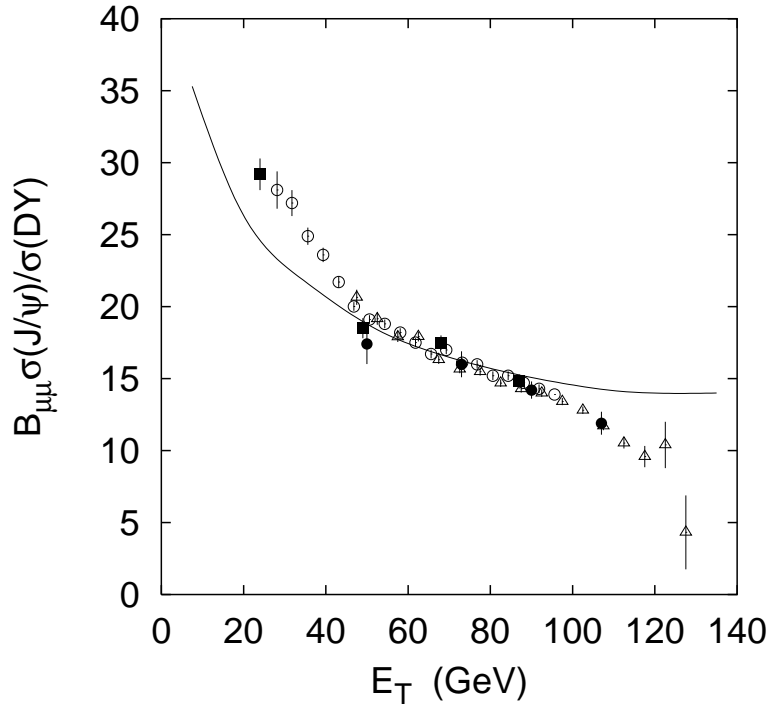


Figure 37: J/ψ production in $Pb - Pb$ collisions [61, 124], compared to the dual parton model comover approach [125].

in the rest frame of either nucleus. Interference and cancellation effects of the Landau-Pomeranchuk type thus prevent soft parton emission at each nucleon-nucleon collision. At higher energies, large additional contributions can come from hard partons (minijets or jets) with short formation time, and these will be proportional to the number of collisions. Even at SPS energy, nucleon stopping and secondary multiplicities at mid-rapidity seem to increase somewhat with increasing mass number A , and this could be the onset of collision dependent effects. The s -dependence of the mid-rapidity multiplicity is presumably a combination of the s -dependence of the parton distribution function and the onset of significant hard hadron production. We shall try to include these dependences here in rather phenomenological terms, without specifying their origin.

The number of gluons of transverse momentum k_T emitted by a wounded nucleon can be obtained from the nucleonic gluon distribution function $g(x)$ from deep inelastic scattering studies,

$$\left(\frac{dN_g}{dy dk_T^2} \right)_{y=0} \simeq x g(x) f(k_T^2) \quad (77)$$

where $x \simeq k_T/\sqrt{s}$. Here \sqrt{s} is the incident collision energy, and $f(k_T^2)$ is normalized to unity. Using the MRS-H form of the gluon distribution function [126] and integrating the resulting Eq. (77) over k_T then gives us $(dN/dy)_{y=0} \simeq 2$ for SPS and 4 for RHIC energy.

Each gluon of transverse momentum k_T has an effective transverse size $r \simeq k_T^{-1}$, and nucleus-nucleus collisions provide many such gluons overlapping in the transverse plane. We want to study their clustering behaviour. To simplify matters, we shall consider ‘average’ gluons (rather than averaging results with $f(k_T^2)$). From the transverse momentum dependence of Drell-Yan dilepton production through quark-antiquark annihilation, or from that of J/ψ production through gluon fusion, one finds that the effective intrinsic transverse momentum of gluons is $\langle k_T \rangle \simeq 0.75$ GeV/c, leading to an average transverse parton radius $r \simeq 0.27$ fm. We now want to consider the deconfinement pattern for such systems.

The collisions distribute the gluons over the transverse area according to the nucleon distribution within the nuclei. We thus have to distribute discs of radius $r \simeq 0.27$ fm in the transverse plane and determine the overall nucleon density for which colour conductivity sets in, i.e., for which there appear clusters which reach the dimension of the entire system. Hence we again encounter percolation as crucial feature for deconfinement; here it occurs as a two-dimensional phenomenon, since dynamics aligns the gluon motion along the collision axis. If we denote with n_c the critical gluon density for the production of a deconfined medium, then as in section 2.4, it appears natural to identify the onset of quark-gluon plasma formation with the percolation point, which is [25]

$$n_c = \frac{1.175}{\pi r^2}, \quad (78)$$

where πr^2 is the transverse gluon area. If we consider gluons of transverse momentum $\langle k_T \rangle = 0.75$ GeV/c as characteristic for nucleon-nucleon collisions at present CERN-SPS energies, then the threshold obtained from Eq. (78) is $n_c \simeq 5$ fm⁻². The deconfined medium thus obtained consists of gluons freed of their confinement constraints, but it does not yet need to be in thermal equilibrium.

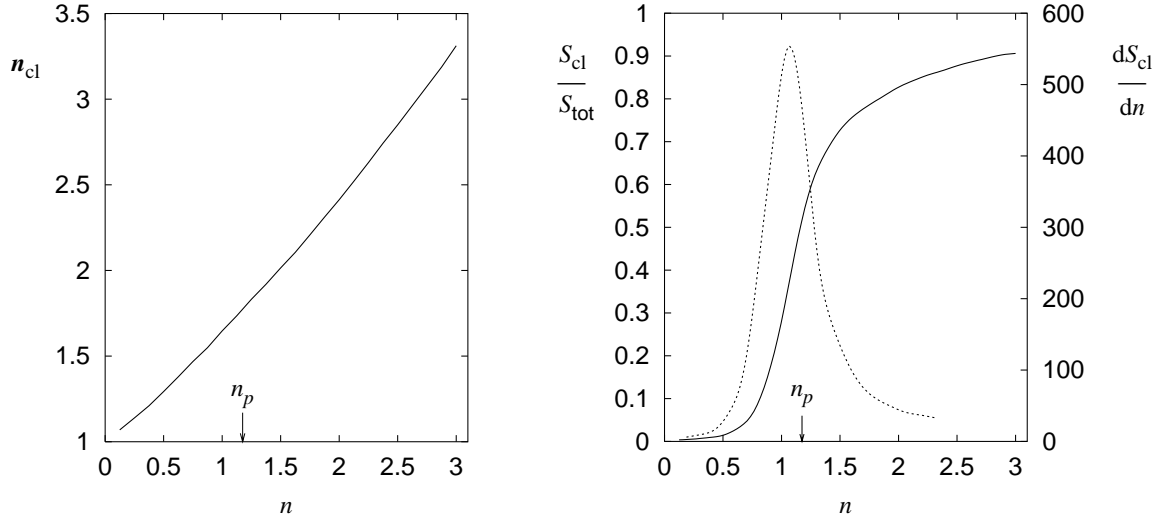


Figure 38: Average cluster density $n_{\text{cl}}(n)$ (left) and average fractional cluster size $S_{\text{cl}}(n)/S_{\text{total}}$ (right) as function of the overall density n of discs, for $r/R = 1/20$; in (b), the derivative of $S_{\text{cl}}(n)/S_{\text{total}}$ with respect to n is also shown (dotted line). The percolation point in the limit $r/R \rightarrow 0$ is indicated by n_p .

As a prelude, we assume N discs of radius r to be randomly distributed on a flat surface of radius $R \gg r$ and study the average cluster density $n_{\text{cl}}(n)$ and the average cluster size $S_{\text{cl}}(n)$ as a function of the overall density $n = N/\pi R^2$. The result is shown in Fig. 38, where we have normalized all quantities to the inverse disc area $1/\pi r^2$ in order to make them dimensionless. We note that the derivative of the cluster density peaks sharply at a certain density; in the ‘thermodynamic’ limit $R \rightarrow \infty$, this percolation point is known to be $n_p = 1.175$. We see in particular that if we want to reach a certain cluster density n_{cl} , attained at a certain overall n , then at this point the average cluster $S_{\text{cl}}(n)$ also has a certain finite size. In other words, requiring a specific density for the onset of a new phase implies that this onset occurs for a specific, finite size of the system. The percolation point, for example, is reached when about 50% of the surface is covered by discs.

Turning now to nuclear collisions, we have to distribute the partonic discs not on a flat surface, but instead in the transverse plane according to the nucleon distribution determined by the profiles of the colliding nuclei [127]. Moreover, we have to allow collisions at different impact parameters, and we want to consider different $A-B$ collisions.

In Fig. 39, the cluster density n_{cl} is shown as function of the overall density n_{parton} of ‘average’ partons of radius $r = 0.27$ fm, for different centralities of various $A-B$ combinations at SPS energy, with 2.1 partons per wounded nucleon. For each $A-B$, the point at highest n_{parton} corresponds to central (impact parameter $b = 0$) collisions, the one at lowest n_{parton} to the most peripheral collisions. We note that by varying $A-B$ and centrality we produce an essentially universal cluster density $n_{\text{cl}}(n_{\text{parton}})$. Now we assume that deconfinement occurs at the percolation point, which can be determined by studying the average fractional cluster size $S_{\text{cl}}/S_{\text{total}}$. In Fig. 40, we see the result for $Pb-Pb$ collisions. At the density for which the derivative peaks, $n_{\text{parton}} \simeq 4.2 \text{ fm}^{-2}$, the cluster density reaches its critical value $n_{\text{cl}} \simeq 6 \text{ fm}^{-2}$. The same critical value is found for

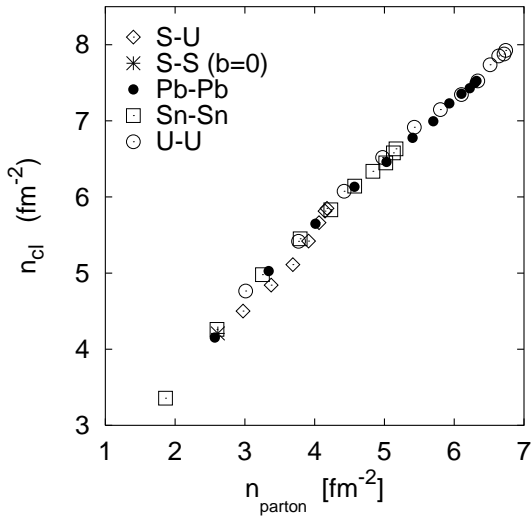


Figure 39: Cluster density vs. parton density for different centralities and different $A-B$ configurations at SPS energy.

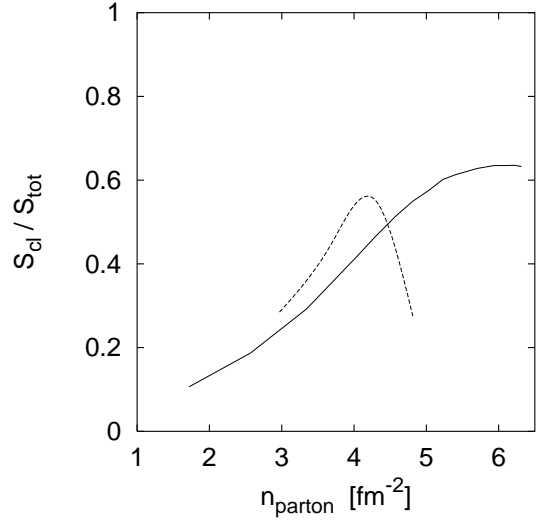


Figure 40: Fractional cluster size vs. parton density, together with its derivative, for $Pb-Pb$ collisions at SPS energy.

$Sn-Sn$ and $U-U$ collisions at SPS energy, even though this value is attained at quite different centralities in the different configurations ($b \simeq 4.5$ fm for Sn , 8.5 fm for Pb and 11.5 fm for U collisions).

In Fig's. 41 and 42, we show the result of this procedure for RHIC energy, where we have 4.0 gluons per wounded nucleon. Again the critical cluster density at deconfinement is found to be $n_{cl} \simeq 6$ fm $^{-2}$. Here we have to consider $Cu-Cu$ collisions in order to study the onset of deconfinement, since for $Pb-Pb$ all possible centralities are above the threshold.

We thus conclude that the critical cluster density is, as expected, a universal quantity, independent of the choice of $A-B$, of centrality, and of incident energy. The fractional size of the deconfined cluster at threshold does, however, depend on the collision configuration: for $Pb-Pb$ at SPS, we have $S_{cl}/S_{total} \simeq 0.45$, while $Cu-Cu$ at RHIC gives 0.70. In other words, at the higher RHIC energy, deconfinement sets in for a larger bubble than at the lower SPS energy.

We further note that at SPS energy, $S-S$ and $S-U$ are below the deconfinement threshold even for the most central collisions, while at RHIC even the most peripheral $Pb-Pb$ collisions are above the threshold. To study the threshold, we thus require heavy nuclei (such as Pb) at the SPS, lighter nuclei (such as Cu) or lower incident energy at RHIC.

Having specified deconfinement through percolation, we now turn to J/ψ suppression as a probe for its onset. As noted above, the χ_c is dissociated essentially at deconfinement, so when the cluster density reaches $n_{cl}^{crit} \simeq 6$ fm $^{-2}$, all χ_c 's which are inside the percolating cluster disappear. The amount of χ_c suppression thus depends on the fractional cluster

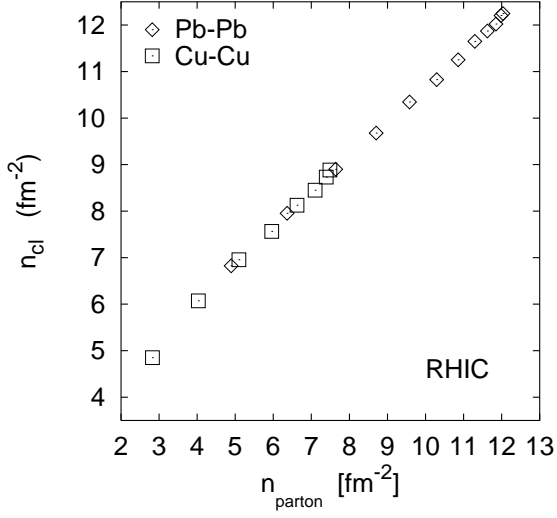


Figure 41: Cluster density vs. parton density for different centralities and different $A-B$ configurations at RHIC energy.

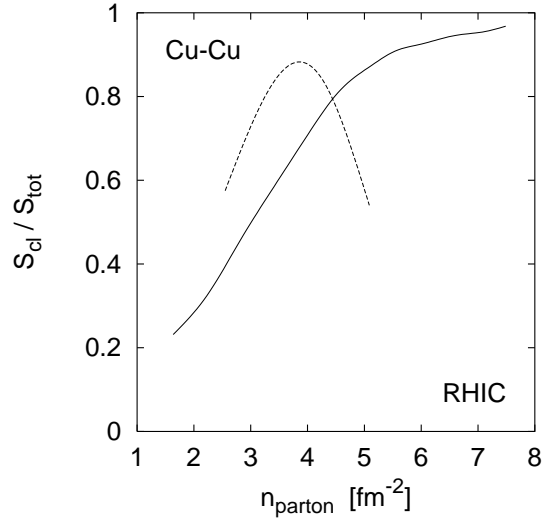


Figure 42: Fractional cluster size vs. parton density, together with its derivative, for $Cu-Cu$ collisions at RHIC energy.

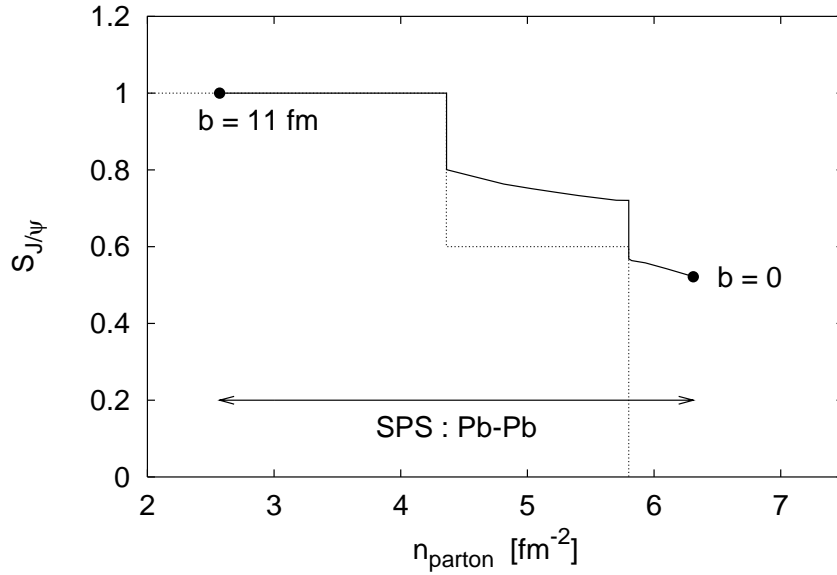


Figure 43: The J/ψ survival probability as function of the parton density for $Pb-Pb$ collisions at SPS energy; the dotted line corresponds to a medium of uniform parton density, the solid line to collisions with parton densities determined by the profiles of the colliding nuclei.

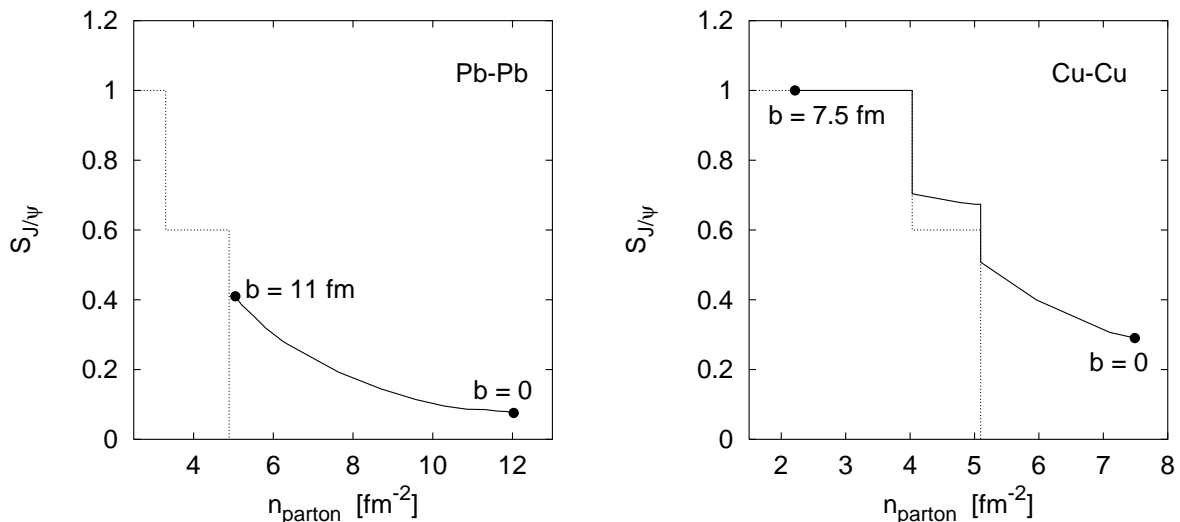


Figure 44: The J/ψ survival probability as function of the parton density for $Pb-Pb$ (left) and for $Cu-Cu$ (right) collisions at RHIC energy; the dotted line corresponds to a medium of uniform parton density, the solid line to collisions with parton densities determined by the profiles of the colliding nuclei.

size at deconfinement, which is about 45 % for $Pb-Pb$ at the SPS, about 70 % for $Cu-Cu$ at RHIC and effectively 100 % for $Pb-Pb$ at RHIC. At deconfinement, the corresponding fractions of J/ψ production through intermediate χ_c states should thus be suppressed.

As already noted, the dissociation of directly produced J/ψ 's requires a larger screening mass and thus higher density than available at the point of deconfinement. On a microscopic level, J/ψ break-up becomes possible only for harder than average gluons at deconfinement. In principle, the relevant quantities can be determined by lattice QCD studies; however, this requires computer capabilities which are being reached only now. For the moment, we therefore choose $r^{J/\psi} = 0.22$ fm and $n_{\text{cl}}^{J/\psi} = 7.8 \text{ fm}^{-2}$; this corresponds to a ratio of transverse dissociation energy densities $\epsilon_T(J/\psi)/\epsilon_T(\chi_c) \simeq 1.6$, in accord in studies combining potential theory and lattice results [64, 121]. With these parameters, one obtains 20% direct J/ψ suppression in $Pb-Pb$ collisions at SPS energy, once the required cluster density is reached. The corresponding fractions for RHIC are 30% for $Cu-Cu$ and 35% for $Pb-Pb$ collisions.

Schematically, one thus obtains a suppression pattern as illustrated in Fig. 43, where it is assumed that 40% of the observed J/ψ 's come from χ_c decay and 60% are produced directly. For clarity purposes, we ignore here the small fraction (about 8%) coming from ψ' decay. The dotted curve corresponds to the suppression which would take place in a uniform medium of precisely specified parton density: at the deconfinement point, all χ_c 's are dissociated, so that the corresponding fraction of decay J/ψ 's is gone; when the density for direct J/ψ melting is reached, these disappear as well, leading to complete

J/ψ suppression. In actual nuclear collisions, the medium is not uniform, with denser ‘inner’ and less dense ‘outer’ regions in the transverse plane. Suppression now occurs only in the fraction $S_{\chi_c}/S_{\text{total}}$ for the χ_c part and $S_{J/\psi}/S_{\text{total}}$ for the direct J/ψ part, where S_{χ_c} and $S_{J/\psi}$ denote the clusters in which the respective dissociation density is reached. Since these fractions depend on energy and nuclear geometry, the suppression curves are different for different experimental configurations. In Fig. 43, the result is shown for $Pb-Pb$ collisions at the SPS, from impact parameter $b = 11$ fm to $b = 0$ fm. The difference between this curve and the one for a uniform medium thus reflects the surviving J/ψ ’s produced in the less dense outer regions.

In Fig. 44, similar calculations are shown for $Cu-Cu$ and $Pb-Pb$ at RHIC energy. Here we note in particular that $Pb-Pb$ collisions are for all meaningful centralities ($b \leq 11$ fm) above both the χ_c and the direct J/ψ threshold, so that we get a smooth anomalous suppression increasing from about 60% at $b = 11$ fm to about 90% at $b = 0$. Combining this suppression with the ‘normal’ pre-resonance absorption in nuclear matter, we thus predict for central $Pb-Pb$ collisions at RHIC a J/ψ production rate of less than 5% the corresponding unsuppressed rate (excluding possible B decay contributions). It should also be noted that this result is based on twice the number of gluons per wounded nucleon at RHIC, compared to the SPS value. A larger increase, based on a possible larger hadron multiplicity at RHIC, would lead to more J/ψ suppression. Similarly, we assume an average number $(dN_g/dy)_{y=0}$ of gluons per wounded nucleon. It is conceivable that very central collisions reach into the tail part of the multiplicity distribution, with a larger number of hadrons and hence also gluons. This would lead to a larger suppression for very central collisions. At the SPS, the NA50 collaboration can check if the basis for this exists. By combining measurements of hadron multiplicity, transverse energy E_T and forward energy E_{ZDC} , it is possible to study the number of hadrons per wounded nucleon as function of E_T and check if there is an increase at highest E_T values.

Finally we can then turn to a comparison of our results on parton percolation to the E_T -dependence of the actual data, which contain an additional smearing due to the fact that a given E_T bin corresponds to a range of impact parameters and hence parton densities. Including this effect in the standard way [52], we obtain the result shown in Fig. 45. Included in this figure are the 1997 and 1998 data [124, 61] with minimum bias determined Drell-Yan reference. While reproducing the overall trend, our results clearly show deviations from the data in detail. As mentioned, the levelling-off of our curve at high E_T would have to be modified if an increase in the multiplicity per wounded nucleon at high E_T should be observed. Another possible modification could enter through a density-dependent charmonium dissociation. We have here assumed that all χ_c ’s melt once the critical density is reached. Allowing a partial survival chance, which decreases with increasing density, would lead to a steeper drop of the suppression with n_{parton} as well as with E_T . One possible source for such an effect could be the finite life-time of the deconfining medium in actual nuclear collisions.

Summarizing this section, we note that parton percolation provides a consistent framework to study the onset of deconfinement as well as the onset of charmonium suppression as a signature of the transition. It is clear that the compatibility of the parton basis with other, soft hadron production processes has to be checked; we return to this in section 6.

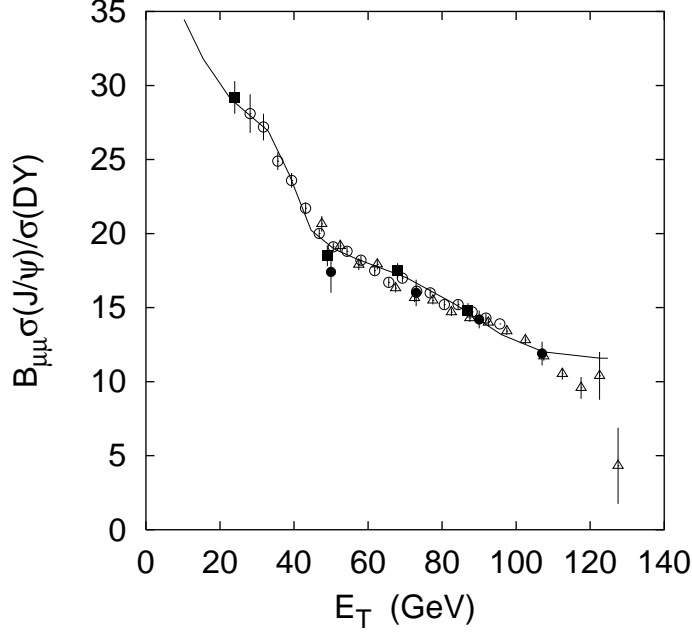


Figure 45: J/ψ production in $Pb - Pb$ collisions [61, 124], compared to colour deconfinement in the parton percolation model [128].

5.4 P_T Dependence

In this section, we want to consider the dependence of anomalous J/ψ suppression on the transverse momentum of the J/ψ . It is well known that the transverse momenta of secondaries from hadron-nucleus collisions quite generally show a p_T -broadening. This means that the universal parameter $\lambda \simeq 0.15$ GeV in Eq. (30) now depends on the size of the target nucleus. For secondary hadrons, this is the Cronin effect [129]; a similar behaviour is observed also in Drell-Yan and charmonium production [97]. The natural basis for all such broadening is initial state parton scattering, and it was in fact shown some time ago [130] - [133], [119] that this describes quite well the p_T -dependence observed in J/ψ production from $p - A$ to central $S - U$ collisions.

Consider J/ψ production in $p - A$ collisions, assuming gluon fusion as the dominant process for the creation of a $c\bar{c}$ pair. Parametrizing the intrinsic transverse momentum distribution $f(q_T)$ of a gluon in a nucleon as

$$f(q_T) = \frac{1}{\pi \langle q_T^2 \rangle} \exp \left\{ -\frac{q_T^2}{\langle q_T^2 \rangle} \right\}, \quad (79)$$

we obtain by convolution for the transverse momentum distribution $F_{pA}(P_T)$ of the resulting J/ψ

$$F_{pA}(P_T) = \frac{1}{\pi \langle P_T^2 \rangle_{pA}} \exp \left\{ -\frac{P_T^2}{\langle P_T^2 \rangle_{pA}} \right\}, \quad (80)$$

with

$$\langle P_T^2 \rangle_{pA} = \langle q_T^2 \rangle_A + \langle q_T^2 \rangle_p. \quad (81)$$

The quantity

$$\delta_{pA} \equiv \langle P_T^2 \rangle_{pA} - \langle P_T^2 \rangle_{pp} = \langle q_T^2 \rangle_A - \langle q_T^2 \rangle_p \quad (82)$$

is thus a suitable measure for the observed nuclear broadening. Note that the Gaussian form of Eq. (82) is obtained from Eq. (30) for $P_T^2 \ll m_{J/\psi}^2$. For J/ψ production in pp collisions, with the universal $\lambda^{-1} \simeq 0.15$, this leads to $\langle P_T^2 \rangle \simeq 2m_{J/\psi}/\lambda \simeq 1 \text{ GeV}^2$, which is slightly lower than the observed value of 1.23 ± 0.05 [97].

Assume now that in the passage of the projectile proton through the nuclear target, successive interactions broaden the intrinsic momentum distribution of the corresponding projectile gluon which will eventually fuse with a target gluon to form a J/ψ . If the process of P_T broadening during the passage is a random walk, then the relevant parameter of the Gaussian distribution (80) becomes

$$\delta_{pA} = N_c^A \delta_0, \quad (83)$$

where N_c^A is the average number of collisions the projectile undergoes on its passage through the target up to the fusion point, and δ_0 the average broadening of the intrinsic gluon distribution per collision.

In nucleus-nucleus collisions, a corresponding broadening occurs for both target and projectile gluon distributions; here, however, measurements at fixed transverse hadronic energy E_T can determine the broadening for collisions at a given centrality. Hence at fixed impact parameter b we have

$$\delta_{AB}(b) = \langle P_T^2 \rangle_{AB}(b) - \langle P_T^2 \rangle_{pp} = N_c^{AB}(b) \delta_0, \quad (84)$$

with $N_c^{AB}(b)$ denoting the average number of collisions for projectile nucleons in the target and vice versa, at fixed b . $N_c^{AB}(b)$ has a maximum at small b and then decreases with increasing b ; for a hard sphere nuclear model, it would vanish when $b = R_A + R_B$.

In Glauber theory, the quantity $N_c^{AB}(b)/\sigma$ can be calculated parameter-free from the established nuclear distributions [127]; here σ denotes the cross section for the interaction of the nucleon on its passage through the target. We shall determine $\sigma\delta_0$ from data, so that σ never enters explicitly. Once $\sigma\delta_0$ is fixed, the broadening by initial state parton scattering is given for all $p-A$ and $A-B$ interactions. For Drell-Yan production (with quarks instead of gluons in the partonic interaction), this would be the observed effect, since the final state virtual photon does not undergo any further (strong) interactions. A produced nascent J/ψ will, however, experience pre-resonance nuclear absorption; this suppresses J/ψ 's produced early along the path of the projectile, since they traverse more nuclear matter and hence are absorbed more than those produced later. As a net result, this shifts the effective production point to a later stage. In $p-A$ collisions, a Drell-Yan pair will on the average be produced in the center of the target. In contrast, nuclear absorption shifts the average $c\bar{c}$ production point further down-stream. This effectively lengthens the path for initial state parton scattering and hence increases the resulting broadening.

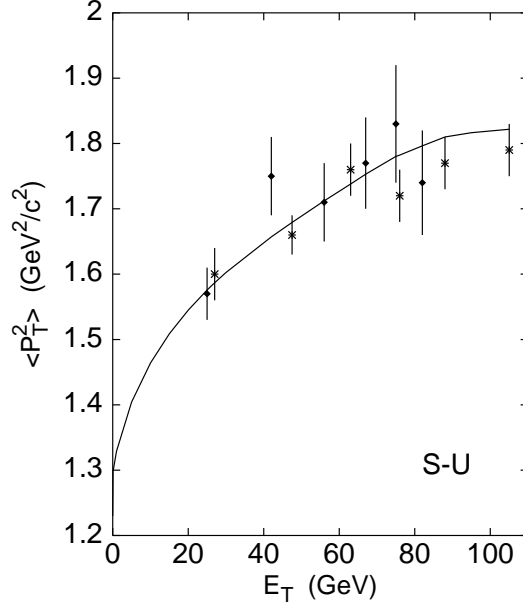


Figure 46: P_T in $S - U$ collisions, compared to NA38 data [134].

The transverse momentum behaviour of normal J/ψ production in nuclear collisions is thus a combination of initial state parton scattering before the production of the basic $c\bar{c}$ state, and pre-resonance nuclear absorption afterwards; both lead to a broadening of a P_T -distribution. A further broadening could come from elastic random walk scattering of the charmonium state itself in nuclear matter; however, the effect of this can be taken into account by fitting $\sigma\delta_0$ to the data. The essential task is then to calculate the number of collisions per cross section, N_c/σ , for $p-A$ and $A-B$ interactions, taking into account the effect of pre-resonance nuclear absorption. The result contains as only open parameter the quantity $\sigma\delta$; for details, see [136].

Ideally, one would use $p-A$ data to fix $\sigma\delta_0$; the broadening for $A-B$ interactions would then be fully predicted. Unfortunately there are $p-A$ data only for three values of A [97, 99], and these have rather large errors. It is therefore better to attempt a consistent description of all existing $p-A$ [97, 134] and $A-B$ data [134], up to central $S-U$, in terms of a common $\sigma\delta_0$. Using $\langle P_T^2 \rangle_{pp} = 1.23 \pm 0.05 \text{ GeV}^2$, a best fit to $p-A$, $O-Cu$, $O-U$ and $S-U$ data [136] gives $\sigma\delta_0 = 9.4 \pm 0.7$, with a $\chi^2/d.f.$ of 1.1. In Fig. 46 we show the resulting description of the $S-U$ data.

We then turn to $Pb-Pb$ collisions; the corresponding “normal” transverse momentum behaviour is shown in Fig. 47. Also shown here is the amount of broadening obtained from initial state parton scattering alone; we see that nuclear absorption increases $\langle P_T^2 \rangle_{PbPb}$ by about 15 %. Since the functional forms in the two cases are quite similar, nuclear absorption can be simulated by choosing a somewhat larger δ_0 . The basic feature of normal absorption thus remains the monotonic increase of $\langle P_T^2 \rangle$ with E_T , even though the collision geometry makes this slightly weaker for $Pb-Pb$ than for $S-U$ interactions [135].

The onset of anomalous suppression results in a striking modification of this pattern. If the J/ψ 's in the hot interior of the medium produced in the collision are suppressed,

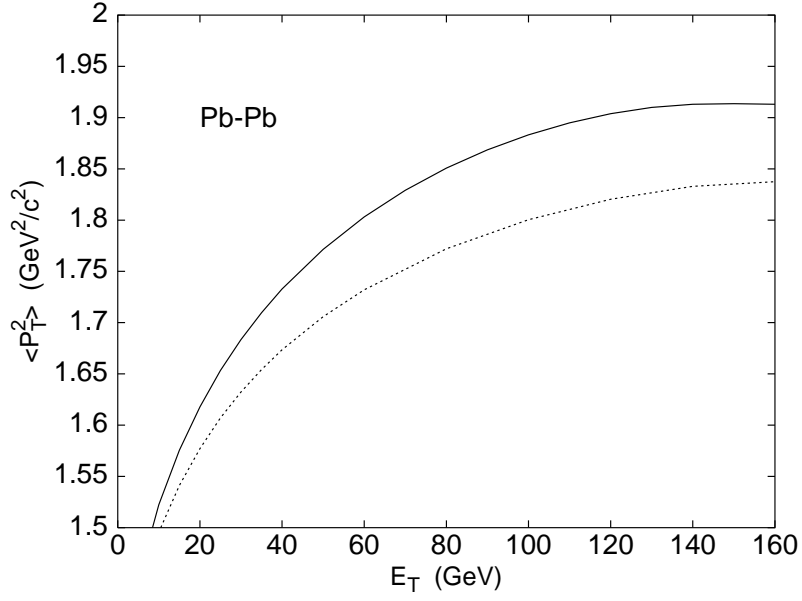


Figure 47: Normal P_T broadening in $Pb - Pb$ collisions with (solid line) and without (dashed line) pre-resonance nuclear absorption.

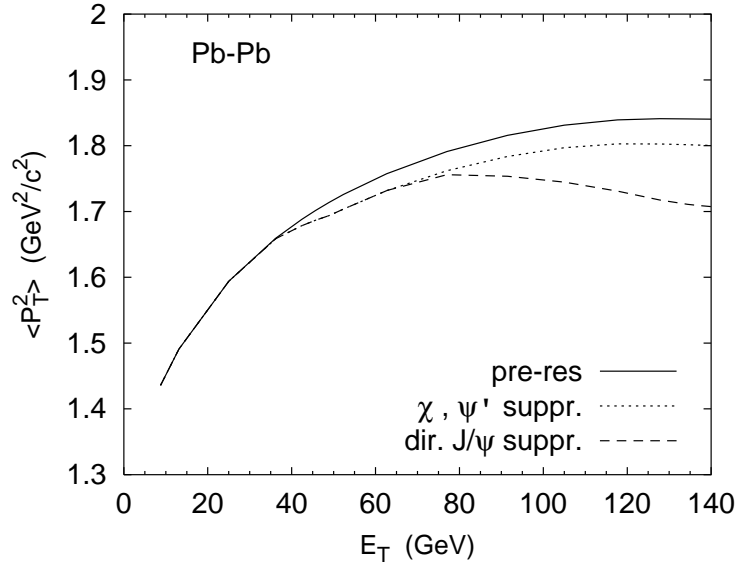


Figure 48: P_T broadening in $Pb - Pb$ collisions. The solid line shows normal broadening, the dotted line the effect of anomalous χ_c and ψ' suppression, and the dashed line the effect the onset of direct J/ψ suppression.

then this will reduce their contribution from the part of phase space leading to the most broadening. To illustrate the effect, we assume suppression by deconfinement; in this case the result is readily calculable [119, 132]. To be specific, we assume deconfinement to start once the number of collisions per wounded nucleon exceeds a certain critical value κ_c [52]

$$\frac{N_c(b, s)}{N_w(b, s)} \geq \kappa_c. \quad (85)$$

This defines for each collision configuration cool outer and hot inner regions, resulting in charmonium survival or dissociation, respectively. In Fig. 48 we compare the resulting patterns for several value of κ_c to that of normal absorption; the change of behaviour is qualitatively evident and due solely to anomalous J/ψ suppression. Moreover, abrupt onsets of anomalous χ_c and direct J/ψ suppression would also show up here; they have not yet been included in Fig. 48. The observation of such anomalous transverse momentum behaviour for J/ψ suppression would thus constitute another tool to study the onset of deconfinement in $Pb - Pb$ collisions.

6. SOFT HADRONIC PROBES

In this final section, we want to address the possible supporting evidence which can be obtained by measuring soft hadronic probes, i.e., mesons and baryons made up of the light u, d and s quarks and produced at low transverse momenta. Since there is no large intrinsic mass or momentum scale, their production occurs over comparatively large space-time regions determined by Λ_{QCD} and cannot be described perturbatively. The large intrinsic size of soft hadrons requires relatively low energy densities to make their existence conceptually meaningful: five mesons need a volume of at least roughly five meson volumes in order to exist [53]. As discussed in section 4.1, this implies that they are formed late in the collision evolution, when the high initial energy density has dropped to a sufficiently low value $\epsilon_h \lesssim 0.3 - 0.5 \text{ GeV/fm}^3$, taking the energy density of a typical hadron as indicator.

What features of the produced medium can one then study with the help of soft hadronic probes? It is clear, as also noted in section 4.1, that they provide direct information about the state of the medium at the energy density ϵ_h . In addition, one may hope to obtain ‘retrospectively’ also information about earlier stages at higher ϵ . In the following, we shall first consider two specific instances of such retrospective probing and then discuss the study of the medium at hadronization.

6.1 Retrospective Probes

The onset of anomalous J/ψ suppression occurs at a certain associated transverse energy of secondary hadrons. We would like to translate this into a value of the corresponding primordial energy density. In principle, this can be done in the same way as was used to derive Eq. (36) in section 3.2. It is clear, however, that the result will be

model dependent. Instead of the assumed free flow leading to Eq. (36), one could assume an isentropic flow [137], leading to

$$s_0 = \frac{1}{\pi R_A^2 \tau_0} \left(\frac{dN_h}{dy} \right)_{y=0}^{AA} \quad (86)$$

as initial entropy density. It turns out that with Eq. (35) for the multiplicity and for an ideal gas of massless partons, the two different expansion patterns result in very similar initial energy densities up to $\sqrt{s} \simeq 200$ GeV. At much higher \sqrt{s} , isentropic expansion leads to a somewhat higher energy density, but even at LHC energy, the difference is only about 20 % [138].

To obtain an estimate of the energy densities in the region of anomalous J/ψ suppression, we thus make use of Eq. (36). For the 5% most central $Pb - Pb$ collisions, one finds on the average about 800 secondaries at central rapidity; their average energy is about 0.5 GeV [144]. This leads to an initial energy density of about 2.8 GeV/fm³. Note that this value corresponds to ϵ averaged over the collision profile; the ‘hot’ central value, associated to the region of highest density of participating nucleons, will be around 30% higher, around 3.7 GeV/fm³ [52]. This is then the value of ϵ at the point of maximum J/ψ suppression in the SPS data. To study in detail the onset of deconfinement, the multiplicity of soft secondaries must be known as function of centrality. Until a detailed study of this is available, we can estimate the result by assuming the $\epsilon(b)$ (and hence $\epsilon(E_T)$) is approximately linear in E_T . This leads to $\epsilon_c \simeq 2$ GeV/fm³ at the onset of anomalous J/ψ suppression, which presumably occurs at the onset of χ_c dissociation and hence at deconfinement. Such a critical energy density is in reasonable agreement with the values predicted in section 2.

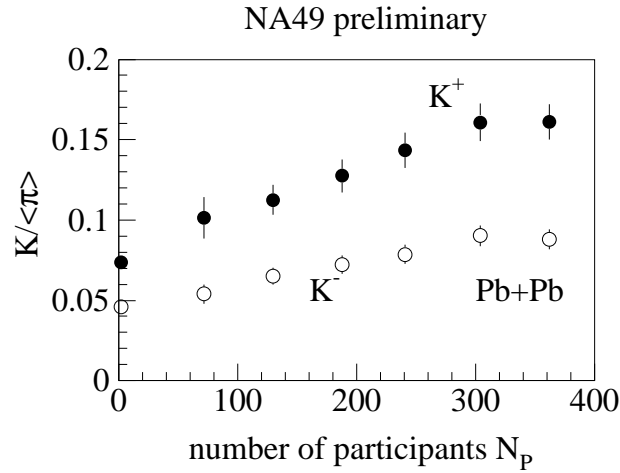


Figure 49: The K/π ratio in $Pb - Pb$ collisions as function of the number of participating nucleons [141].

A second and particularly interesting retrospective probe could well be the strangeness abundance in nuclear collisions [139]. We had seen in section 3.1 that the relative abundances of the secondary species in $p - p$ collisions were determined by the freeze-out

temperature T_h of a hadronic resonance gas, with the restriction that strangeness production was suppressed by a factor γ_s . In nuclear collisions, the non-vanishing baryon number density of the system requires that a corresponding analysis specifies temperature T_h and baryochemical potential μ_h at freeze-out, and in addition a possible strangeness suppression factor γ_s . In central nuclear collisions, strangeness production is found to be much more abundant than in $p-p$ collisions at the same \sqrt{s} . As illustration, we show in Fig. 49 the K/π ratio in $Pb-Pb$ collisions at the SPS as function of the number of participating nucleons [141, 142]. If we assume, as discussed in section 3.1, that the suppression factor γ_s is determined by the relative formation rate of the heavier strange quarks in an earlier partonic medium of higher temperature $T > T_h$, then $\gamma_s(T)$ could provide a thermometer for this early temperature T . The behaviour seen in Fig. 49 would thus indicate a significant increase with centrality for the initial temperature of the partonic medium in $Pb-Pb$ collisions at $\sqrt{s} = 20$ GeV. Comparing Fig. 49 with Fig. 11, we see that the strangeness increase with centrality in nuclear collisions is very similar to that found as function of \sqrt{s} or as function of multiplicity at fixed \sqrt{s} in the $p-p/p-\bar{p}$ interactions. This supports an increase of the initial energy density as the underlying mechanism for increased strangeness production; but further comparative studies seem necessary to fully specify the origin of the effect. If the model for $\gamma_s(T)$ discussed here is correct, we would expect that with increasing collision energy, at RHIC and LHC, $\gamma_s \rightarrow 1$. We also note that in accord with the interpretation of γ_s as thermometer, there is so far no indication of a threshold or sudden increase in the relative strangeness production.

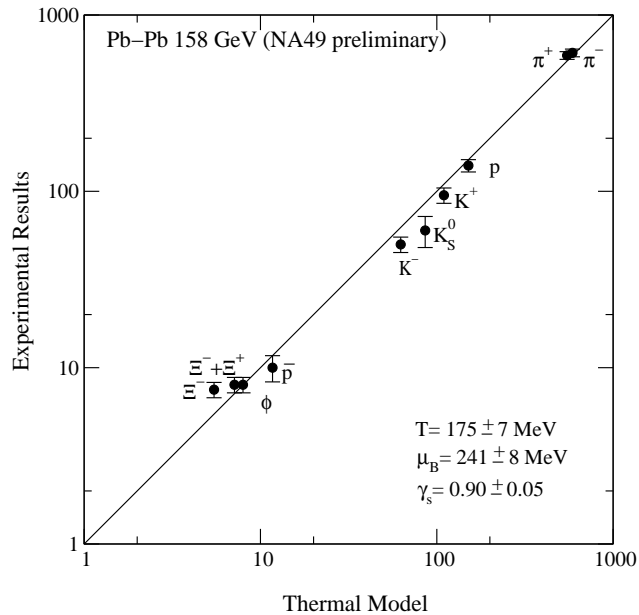


Figure 50: Experimental hadron production multiplicities compared to those in a resonance gas model [146].

6.2 Hadronisation and Freeze-Out

After strongly interacting matter has cooled off to reach the hadronization point, its freeze-out into free hadrons should be a universal phenomenon, depending only on the freeze-out temperature and baryon density. In view of the expansion of the produced medium, this universality can only be ‘local’, e.g., volume elements moving relative to each other can lead to different effective temperatures. In general terms, such an expansion scenario leads intuitively to three specific predictions [143]

- relative hadron abundances specified by a equilibrated hadronic resonance gas, most likely with $\gamma_s \rightarrow 1$,
- a mass-dependent transverse momentum broadening of hadron spectra due to radial hydrodynamic flow,
- a source size for hadron emission which increases with increased expansion due to increased initial energy density.

All three effects are indeed observed.

For the relative abundances of the soft hadron species, there are indications for the validity of a resonance gas distribution in $A - A$ collisions [144] - [146]. In Fig. 50, this is illustrated for $Pb - Pb$ collisions at the SPS; we note that now γ_s is indeed quite close to unity. The latest analysis shows some open questions concerning the universality of the resulting values of T_h , μ_h and γ_s [146]. We note here that all studies so far have assumed that for a given collision configuration, such a ‘hadrochemical’ equilibrium exists globally over the entire volume of produced matter. In view of the collision profile of participating nuclei, however, it seems quite possible that such an equilibrium exists only locally, making the triplet of values T_h , μ_h and γ_s dependent on the distance r from the collision axis. Since most expansion models start from such local equilibrium, it seems natural that species abundances would also be affected by it.

In Fig. 51, we see that there is indeed a significant (and mass-dependent) broadening in the transverse mass distribution of hadronic secondaries from $Pb - Pb$ collisions at the SPS [144]. Clearly it would be interesting to study the kinematic counterpart of a resonance gas freeze-out and check if the momentum distributions of secondaries become thermal and if the expanding system leads to the expected hydrodynamic flow [143]. Such an endeavor is confronted, however, by a specific problem. Besides collective final state effects, there are also initial state effects such as multiple state parton scattering which can and will modify the transverse momentum distribution Eq. (36) of secondaries [33]. Hence it is not so easy to separate the possible origins of the observed transverse momentum broadening in nuclear collisions [144] and to associate them to specific aspects of the produced state. Nevertheless, considerable effort has been devoted to this aspect [143]. For the purpose of our primary question, colour deconfinement, we note it does not seem possible to identify the initial state of the produced medium from the hydrodynamic expansion pattern alone [147].

Because of expansion and momentum-dependent effects, the source size situation is somewhat more complex, although an increase with incident collision energy has been observed [148]; for recent discussions, see [143, 144].

All three phenomena listed above are present already in $p-p/p-\bar{p}$ collisions for either increasing collision energy or increasing hadron multiplicity. For hadron abundances, this was shown in Fig. 11; transverse momentum broadening in hadronic collisions is illustrated in Fig. 52, and the the growth of the source size with multiplicity is shown in [140]. Evidently this supports strongly the idea that increased initial energy density is the common origin of the three effects. However, to identify the different underlying mechanisms quantitatively, it seems necessary carry out a comprehensive systematic comparison of $p-p$, $p-A$ and $A-A$ collisions, which so far is lacking. As a result, a full understanding of the properties of strongly interacting matter at freeze-out and their origin seems to require considerable further experimental as well as theoretical studies. Microscopic models based on partonic interactions may well provide a suitable tool to formulate a consistent picture.

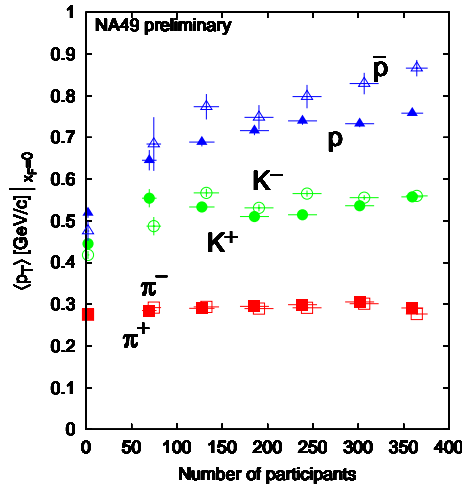


Figure 51: The average transverse momentum of different hadronic secondaries in $Pb-Pb$ interactions at the SPS [144].

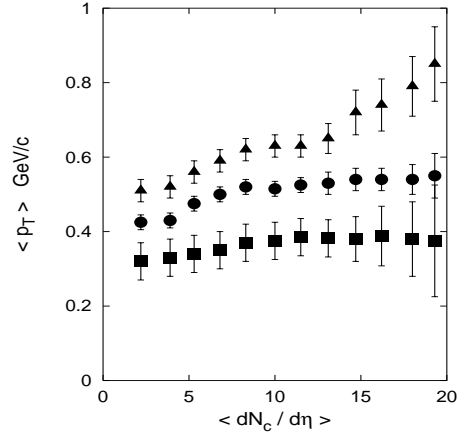


Figure 52: The average transverse momenta of antiprotons, kaons and pions produced in $p-\bar{p}$ collisions at $\sqrt{s} = 1.8$ TeV and central rapidity as function of the associated charged multiplicity [43].

6.3 Parton Cascade Models

For systems evolving in thermal equilibrium, later stages carry no information of the early history. In case of a non-equilibrium evolution, such information can be passed on to a certain extent. A study of the onset of deconfinement in a microscopic, non-equilibrium space-time picture would therefore be of great help in understanding if and to what extent the formation and the properties of the quark-gluon plasma are related to experiments observing the different evolution stages. The aim of partonic cascade models [50, 51] is to describe through perturbative partonic interactions embedded in a relativistic transport theory the evolution of a high energy nucleus-nucleus collision. Hence such models seem to be a good starting point for a dynamic study of deconfinement and the subsequent evolution of the produced systems.

We had seen above in section 5.3 that the initial state of two colliding nucleons can be pictured as colliding beams of confined partons. The incident partons have a distribution in intrinsic transverse momentum, leading to some average value $\langle k_T \rangle$, which in turn defines an average transverse parton size $r_T = 1/\langle k_T \rangle$. When two nuclei collide at high energy, the transverse parton density increases considerably, since now we have a superposition of nucleon-nucleon collisions. In this medium, colour screening will destroy the association of partons to particular hadrons, since for sufficiently high density of colour charges, the colour screening radius becomes much smaller than the typical hadronic scale. Hence we expect the onset of deconfinement for some characteristic density or for an equivalent screening scale. In perturbative QCD, the method to calculate the colour screening mass μ (the inverse of the screening radius r_D) is well-known; an extension to the non-equilibrium medium provided by cascade models has also been proposed [149] and allows a calculation of the time evolution of the screening mass $\mu(t)$ [151].

Given $\mu(t)$, we have to specify for what value deconfinement sets in; parton cascade models themselves does not identify such a point. They just introduce the primary collisions between the ‘confined’ partons of the incident nucleons, followed by successive interactions between primary as well as produced partons and eventually by the hadronisation of partons according to some given scheme. There are two possible ways to specify deconfinement in such a scheme. One can obtain at any given time the transverse density profile of the parton distribution, and a natural onset of deconfinement is the percolation point of partonic discs in the transverse plane, as discussed in section 5.3b. A more global approach is to calculate the screening mass μ and identify as critical point μ_c the value obtained from lattice studies. These provide the temperature dependence of μ and in particular also its value at the deconfinement point T_c , where one has $\mu_c \equiv \mu(T_c) \simeq 0.4 - 0.6$ GeV [65]. It is not obvious that such an equilibrium value can really be used in the non-equilibrium situation provided by the parton cascade model. A good check would be to compare in this model the transverse parton density at μ_c to the percolation value.

We now briefly recall the most important features of the parton cascade model; to be specific, we consider the version proposed in [50].

- The initial nucleus-nucleus system is treated as two colliding clouds of partons, whose distribution is fixed by the nucleonic parton distribution functions determined in deep inelastic lepton-nucleon scattering, and by the nucleon density distribution in the nuclei.

- The parton cascade development starts when the initial parton clouds inter-penetrate and traces their space-time development due to interactions. The model includes multiple elastic and inelastic interactions described as sequences of $2 \rightarrow 2$ scatterings, $1 \rightarrow 2$ emissions, and $2 \rightarrow 1$ fusions. It moreover explicitly accounts for the individual time scale of each parton-parton collision, the formation time of the parton radiation, the effective suppression of radiation from virtual partons due to an enhanced absorption probability by others in regions of dense phase space occupation, and the effect of soft gluon interference in low energy gluon emission.
- Finally, the hadronization in terms of a parton coalescence to colour neutral clusters is described as a local statistical process that depends on the spatial separation and colour of the nearest-neighbour partons [150]. These pre-hadronic clusters then decay to form hadrons.

This model can now be used to calculate characteristic features at different stages of the evolution process. As an illustration we show in Fig. 53 the evolution of the colour screening mass as function of the proper time τ of the system. It is seen that for sufficiently early times, the hot interior of a central $Pb - Pb$ collision leads to $\mu(\tau) > \mu_c$ and thus to deconfinement [151]. One can now follow the evolution of the model and study features of the system beyond the confinement point, such as in-medium hadron mass modifications or momentum distributions of soft secondaries [152].

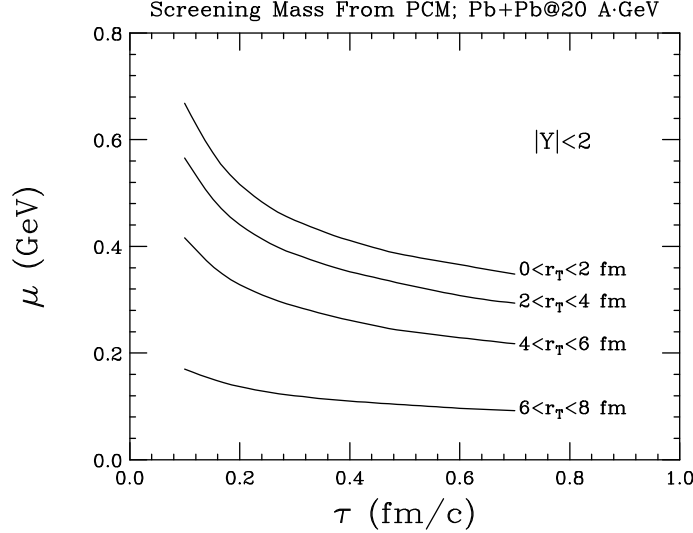


Figure 53: The time dependence of the colour screening mass in central $Pb - Pb$ collisions at SPS energy in different radial collision zones [151].

It is clear that such a description is necessarily model-dependent. Nevertheless, a coherent picture of this kind, accompanied by empirical cross-checks for the different evolution stages, provides an excellent visualisation of the expansion process and could thus lead to further predictions. It also allows an investigation of problems, such as the comparison to $p - p$ and $p - A$ collisions or the onset of thermalisation, for which so far no other tools exist.

7. SUMMARY

We summarize here what we take to be the main conclusions reached during the past two decades in the study of colour deconfinement and its manifestation in high energy nuclear collisions.

- QCD, in particular through finite temperature lattice studies, predicts the onset of colour deconfinement (quark-gluon plasma formation) for strongly interacting matter of vanishing baryon number, once energy densities in the range 1 - 3 GeV are reached.
- High energy nuclear collisions produce in their early stages sufficiently high energy densities for deconfinement; however, the produced systems expand and cool rapidly. Hence the crucial problem is the specification of probes which can unambiguously test the confinement/deconfinement status of the produced early medium.
- For a direct test, the high density, short distance nature of the quark-gluon plasma requires hard probes which can distinguish between confined and deconfined media. Two such probes are:
 - quarkonium dissociation, which for fully formed physical resonances can only occur in a deconfined medium, and
 - jet quenching, manifested by a much higher energy loss of hard transverse jets in a quark-gluon plasma than in hadronic matter.
- Charmonium suppression provides a particularly well-studied example, for which today there exist both an established theoretical framework and quite conclusive experimental results from nuclear collisions.
 - The hadroproduction of charmonium is understood as perturbative $c\bar{c}$ formation by interaction of partons whose distribution functions are determined in deep inelastic scattering; the colour neutralization of the $c\bar{c}$ pair can be described quantitatively in terms of colour evaporation.
 - Charmonium production in a confined medium is studied in $p - A$ collisions, and the resulting A -dependent decrease in production rate is understood in terms of pre-resonance absorption in standard nuclear matter.
 - Since about 60% of the observed J/ψ 's are directly produced, while the rest comes from decay of higher $c\bar{c}$ excitations (mainly χ_c), the onset of deconfinement in nucleus-nucleus collisions should lead to a suppression hierarchy. In a first step, essentially at the deconfinement point, the higher excitations are suppressed. In a second step at clearly higher energy density, the smaller direct J/ψ 's are dissociated.
 - J/ψ production in nucleus-nucleus collisions up to central $S - U$ collisions shows only the normal pre-resonance absorption known from $p - A$ collisions. While peripheral $Pb - Pb$ collisions also follow this pattern, there is with increasing centrality an abrupt first onset of some 30% further 'anomalous' suppression, followed by a later second further drop of some 20% in the observed J/ψ suppression. This step-wise sudden onset of anomalous J/ψ suppression disagrees with all conventional hadronic

suppression models and is understandable only as the onset of colour deconfinement.

- The onset of deconfinement is supported by multiplicity data of soft hadronic secondaries, which can be used to estimate the initial energy densities of the collision. With values of up to 3.7 GeV/fm^3 in the inner region of central $Pb - Pb$ collisions, the deconfinement range of energy densities is indeed attained.

The relative strangeness abundance could provide another check of the initial energy density. If the strangeness suppression observed in $p - p$ collisions of average associated multiplicity is due to the relatively low energy density of the early medium, it can be expected to end when in $A - A$ interactions the initial energy density becomes high enough. There are indications that this is happening.

J/ψ production experiments at the CERN-SPS [107, 108] thus provide first evidence for the predicted new state of deconfined quarks and gluons. Future experiments at the RHIC in Brookhaven and the LHC at CERN, making use of charmonium, bottomonium and jet production, are expected to extend these results and study the quark-gluon plasma in more detail and up to much higher energy densities. Soft probes, in particular the strangeness abundance, can serve to determine these initial energy densities quantitatively and study their effects on the final hadronic state of matter.

ACKNOWLEDGEMENTS

This report owes very much to stimulating discussions with numerous colleagues, and I want to express my sincere gratitude to all of them. Some have contributed decisively to different aspects of the work presented here, and so it is a particular pleasure to thank R. Baier, P. Braun-Munzinger, J. Cleymans, M. Gonin, F. Karsch, D. Kharzeev, L. Kluberg, C. Lourenço, M. Nardi, J. Schukraft, J. Stachel, R. Stock, D. Srivastava and R. Vogt for help, challenge and inspiration – without implying that they agree with all points of my interpretation of the state of the field. – For different parts of this work, financial support by DFG contract Ka 1198/4-1, BMBF contract 06BI804/5 and GSI contract BISATT is gratefully acknowledged.

References

- [1] N. F. Mott, Proc. Phys. Soc. (London) A62 (1949) 416.
- [2] V. V. Dixit, Mod. Phys. Lett. A 5 (1990) 227.
- [3] H. Satz, Nucl. Phys. A418 (1984) 447c.

- [4] D. Bailin and A. Love, Phys. Rep. 107 (1984) 325; for surveys of recent work, see
E. Shuryak, Nucl. Phys. A 642 (1998) 14c;
K. Rajagopal, Nucl. Phys. A 642 (1998) 26c;
Th. Schäfer, Nucl. Phys. A 642 (1998) 26c.
F. Karsch and M. P. Lombardo (Eds.), *QCD at Finite Baryon Density*, Nucl. Phys.
A 642 (1998).
- [5] M. Asakawa and T. Hatsuda, Nucl. Phys. A 610 (1996) 470c.
- [6] K. G. Wilson, Phys. Rev. D 10 (1974) 2445.
- [7] M. Creutz, Phys. Rev. D 21 (1980) 2308.
- [8] F. Karsch and E. Laermann, Rep. Prog. Phys. 56 (1993) 1347.
- [9] L. D. McLerran and B. Svetitsky, Phys. Lett. 98 B (1981) 195 and Phys. Rev. D
24 (1981) 450.
- [10] J. Kuti, J. Polónyi and K. Szlachányi, Phys. Lett. 98B (1981) 199.
- [11] F. Karsch and E. Laermann, Phys. Rev. D 50 (1994) 6954.
- [12] T. Blum et al., Phys. Rev. D 51 (1995) 5153.
- [13] J. Engels et al., Z. Phys. C 42 (1989) 341.
- [14] V. Goloviznin and H. Satz, Z. Phys. C 57 (1993) 671.
- [15] F. Karsch, A. Patkos and P. Petreczky, Phys. Lett. B 401 (1997) 69.
- [16] B. Svetitsky and L. G. Yaffe, Nucl. Phys. B 210 [FS6] (1982) 423.
- [17] P. Hasenfratz, F. Karsch and I. O. Stamatescu, Phys. Rev. 133 B (1983) 221.
- [18] R. V. Gavai, A. Goksch and M. Ogilvie, Phys. Rev. Lett. 56 (1986) 815.
- [19] M. Ogilvie, Phys. Lett. B 231 (1989) 161.
- [20] H. Satz, Nucl. Phys. A 642 (1998) 130c.
- [21] S. Digal, E. Laermann and H. Satz, in preparation.
- [22] G. Baym, Physica 96 A (1979) 131.
- [23] T. Çelik, F. Karsch and H. Satz, Phys. Lett. 97 B (1980) 128.
- [24] For a recent survey, see D. Stauffer and A. Aharony, *Introduction to Percolation
Theory*, Taylor & Francis, London 1994.
- [25] U. Alon, A. Drory and I. Balberg, Phys. Rev. A 42 (1990) 4634.

- [26] O. Alvarez, Phys. Rev. D24 (1981) 440.
- [27] For recent precision studies, see G. Bali, K. Schilling and C. Schlichter, Phys. Rev. 51 (1995) 5165 and Nucl. Phys. B (Proc. Supp.) 42 (1995) 273.
- [28] E. J. Garboczi et al., Phys. Rev. E 52 (1995) 819.
- [29] S. Fortunato and H. Satz, Nucl. Phys. Proc. Supp. 83 - 84 (2000) 452;
S. Fortunato and H. Satz, Phys. Lett. B 475 (2000) 311.
- [30] H. Satz, Nucl. Phys. A 661 (1999) 104c.
- [31] O. V. Kancheli, JETP Lett. 18 (1973) 274.
- [32] J. D. Bjorken, in *Lectures at the 1975 DESY Summer Institute*, J. G. Körner et al. (Eds.), Springer Verlag, Berlin 1976. Bjorken 1976
- [33] A. Leonidov, M. Nardi and H. Satz, Z. Phys. 74 (1997) 535.
- [34] R. Feynman, Phys. Rev. Lett. 23 (1969) 1415.
- [35] J. D. Bjorken, Phys. Rev. D27 (1983) 140.
- [36] R. Hagedorn, Nuovo Cim. Suppl. 3 (1965) 147, and Nuovo Cim. 56A (1968) 1027.
- [37] S. Fubini and G. Veneziano, Nuovo Cim. 64 A (1969) 811;
K. Bardakçi and S. Mandelstam, Phys. Rev. 184 (1969) 1640.
- [38] F. Becattini and U. Heinz, Z. Phys. C 76 (1997) 269.
- [39] J. Cleymans and H. Satz, Z. Phys. C 5 (1993) 135.
- [40] J. Rafelski, Phys. Lett. B 262 (1991) 153.
- [41] F. Becattini, Z. Phys. C 69 (1996) 485.
- [42] R. E. Ansorge et al. (UA5), Z. Phys. C 41 (1988) 179.
- [43] T. Alexopoulos et al., Phys. Rev. Lett. 64 (1990) 991.
- [44] F. Abe et al. (CDF), Phys. Rev. D 41 (1990) 2330.
- [45] A. Białas, M. Bleszyński and W. Czyz, Nucl. Phys. B 111 (1976) 461.
- [46] W. M. Geist, Nucl. Phys. A 525 (1991) 149c.
- [47] W. Albrecht et al. (WA80), Z. Phys. C 55 (1992) 52.
- [48] M. C. Abreu et al. (NA38), Nucl. Phys. A 544 (1992) 209c.
- [49] T. Alber et al. (NA49), Phys. Rev. Lett. 75 (1995) 3814.

- [50] K. Geiger and B. Müller, Nucl. Phys. B369 (1992) 600;
K. Geiger, Phys. Rev. D46 (1992) 4965 and 4986;
for surveys, see
K. Geiger, Phys. Rep. 258 (1995) 376;
K. Geiger, in *Quark-Gluon Plasma 2*, R. C. Hwa (Ed.), World Scientific, Singapore 1998.
- [51] M. Gyulassy and X.-N. Wang, Phys. Rev. D44 (1992) 3501. for a survey, see
X.-N. Wang in *Quark-Gluon Plasma 2*, R. C. Hwa (Ed.), World Scientific, Singapore 1998.
- [52] D. Kharzeev, C. Lourenço, M. Nardi and H. Satz, Z. Phys. C 74 (1997) 307.
- [53] I. Ya. Pomeranchuk, Doklady Akad. Nauk. SSSR 78 (1951) 889.
- [54] See H. Leutwyler, in *QCD 20 Years Later*, P. M. Zerwas and H. A. Kastrup (Eds.), World Scientific, Singapore 1993
- [55] G. E. Brown and M. Rho, Phys. Rev. Lett. 66 (1991) 2720.
- [56] N. Maserà et al. (HELIOS-3), Nucl. Phys. A 590 (1995) 93c.
- [57] B. Lenkeit (CERES), Nucl. Phys. A 654 (1999) 627c.
- [58] M. C. Abreu et al. (NA38), Phys. Lett. B 368 (1996) 230.
- [59] J. Wambach and R. Rapp, Nucl. Phys. A 638 (1998) 171c.
- [60] G. Boyd et al., Phys. Lett. B 349 (1995) 170.
- [61] For the most recent survey, see L. Kluberg (NA50), Proceedings of *Quark Matter '99*, May 1999, Torino/Italy; Nucl. Phys. A, in press.
- [62] T. Matsui and H. Satz, Phys. Lett. 178 B (1986) 416.
- [63] S. Jacobs, M. G. Olsson and C. Suchyta, Phys. Rev. D 33 (1986) 3338.
- [64] F. Karsch, M. T. Mehr and H. Satz, Z. Phys. C 37 (1988) 617.
- [65] U. Heller, F. Karsch and J. Rank, Phys. Lett. B 355 (1995) 511 and Phys. Rev. D 57 (1998) 1438.
- [66] K. Kajantie, Nucl. Phys. A 498 (1989) 355c.
- [67] M. E. Peskin, Nucl. Phys. B156 (1979) 365;
G. Bhanot and M. E. Peskin, Nucl. Phys. B156 (1979) 391.

- [68] M. A. Shifman, A. I. Vainshtein and V. I. Zakharov, Phys. Lett. 65B (1976) 255;
V. A. Novikov et al., Nucl. Phys. B136 (1978) 125.
- [69] A. Kaidalov, in *QCD and High Energy Hadronic Interactions*, J. Tran Thanh Van (Ed.), Editions Frontieres, Gif-sur-Yvette, 1993.
- [70] D. Kharzeev and H. Satz, Phys. Lett. B 334 (1994) 155.
- [71] D. Kharzeev et al., Eur. Phys. J.C 9 (1999) 459.
- [72] K. Martins, D. Blaschke and E. Quack, Phys. Rev. C 51 (1995) 2723.
- [73] S. G. Matinyan and B. Müller, Phys. Rev. C 58 (1998) 2994.
- [74] K. L. Haglin, nucl-th/9907034 (1999).
- [75] C.-Y. Wong, E. S. Swanson and T. Barnes, hep-ph/9912431 (1999)
- [76] Z. Lin and C. M. Ko, nucl-th/9912046 (1999).
- [77] M. Gyulassy and X.-N. Wang, Nucl. Phys. B 420 (1994) 583;
M. Gyulassy, M. Plümer and X.-N. Wang, Phys. Rev. D 51 (1995) 3436.
- [78] R. Baier et al., Phys. Lett. B 345 (1995) 277; Nucl. Phys. B 483 (1997) 291; Nucl. Phys. B484 (1997) 265; Nucl. Phys. B 531 (1998) 403.
- [79] B. G. Zakharov, JETP Letters 63 (1996) 952; JETP Lett. 65 (1997) 615.
- [80] L. P. Landau and I. Ya. Pomeranchuk, Doklad. Akad. Nauk SSSR 92 (1953) 535, 735;
A. B. Migdal, Phys. Rev. 103 (1956) 1811;
E. L. Feinberg and I. Ya. Pomeranchuk, Suppl. Nuovo Cim. III, Ser. X, No. 4 (1956) 652.
- [81] D. Schiff, Lectures at the 1999 Zakopane Summer School, to appear in the Proceedings.
- [82] J. D. Bjorken, Fermilab-Pub-82/59-THY (1982) and Erratum, unpublished.
- [83] Yu. L. Dokshitzer, Nucl. Phys. A 638 (1998) 291c.
- [84] R. Baier et al., Phys. Rev. C 60 (1999) 064902.
- [85] M. B. Einhorn and S. D. Ellis, Phys. Rev. D12 (1975) 2007;
H. Fritzsch, Phys. Lett. 67B (1977) 217;
M. Glück, J. F. Owens and E. Reya, Phys. Rev. D17 (1978) 2324;
J. Babcock, D. Sivers and S. Wolfram, Phys. Rev. D18 (1978) 162.

- [86] P. Braun-Munzinger et al., Eur. Phys. J.C 1 (1998) 123.
- [87] R. V. Gavai et al., Int. J. Mod. Phys. A 10 (1995) 3043.
- [88] A. D. Martin, R. G. Roberts and W. J. Stirling, Phys. Lett. B 306 (1993) 145.
- [89] M. Glück, E. Reya and A. Vogt, Z. Phys. C53 (1993) 127.
- [90] G. Schuler and R. Vogt, Phys. Lett. B 387 (1996) 181.
- [91] R. Baier and R. Rückl, Z. Phys. C 19 (1983) 251.
- [92] See e.g., A. Sansoni (CDF), Nucl. Phys. A 610 (1996) 373c, and references given there.
- [93] G. T. Bodwin, E. Braaten and G. P. Lepage, Phys. Rev. D 51 (1995) 1125.
- [94] E. Braaten and S. Fleming, Phys. Rev. Lett. 74 (1995) 3327.
- [95] See e.g., M. Mangano, hep-ph/9507353 (1995);
E Braaten, S. Fleming and T.-C. Yuan, Ann. Rev. Nucl. Sci. 46 (1996) 197,
- [96] D. Kharzeev and H. Satz, Z. Phys. C 60 (1993) 389.
- [97] J. Badier et al. (NA3), Z. Phys. C 20 (1983) 101.
- [98] D. M. Alde et al. (E772), Phys. Rev. Lett. 66 (1991) 133.
- [99] M. C. Abreu et al. (NA38), Phys. Lett. B 438 (1998) 35; Phys. Lett. B 444 (1998) 516.
- [100] C. Baglin et al. (NA38), Phys. Lett. B 446 (1999) 408.
- [101] C. Gerschel and J. Hüfner, Z. Phys. C 56 (1992) 171.
- [102] D. Kharzeev and H. Satz, Phys. Lett. B 366 (1996) 316.
- [103] This value is the result of applying the analysis of [52] to the most recent NA38 data [99]; M. Nardi, private communication.
- [104] C. Baglin et al. (NA38), Phys. Lett. B 220 (1989) 471; B 251 (1990) 465, 472; B 255 (1991) 459;
M. C. Abreu et al. (NA38), Phys. Lett. B 449 (1999) 128.
- [105] C. Baglin et al. (NA38), Phys. Lett. B345 (1995) 617; Phys. Lett. B 466 (1999) 128.
- [106] S. J. Brodsky and A. H. Mueller, Phys. Lett. 206 B (1988) 685;
- [107] M. C. Abreu et al. (NA50), Phys. Lett. B 410 (1997) 337.

- [108] M. C. Abreu et al. (NA50), Phys. Lett. B 450 (1999) 456.
- [109] M. Nardi, private communication.
- [110] J. Ftáčnik, P. Lichard and J. Pišut, Phys. Lett. 207 (1998) 194;
S. Gavin, M. Gyulassy and A. Jackson, Phys. Lett. 207 B (1988) 257;
R. Vogt, M. Prakash, P. Koch and T. H. Hansen, PL 207 B (1988) 263
J.-P. Blaizot and J.-Y. Ollitrault, Phys. Rev. D 39 (1989) 232;
J. Ftáčnik, P. Lichard, N. Pišutova and J. Pišut, Z. Phys. C 42 (1989) 132.
- [111] A. Capella, J. A. Casado, C. Pajares, A. V. Ramallo and J. Tran Thanh Van, Phys. Lett. 206 B (1988) 354;
C. Gerschel and J. Hüfner, Phys. Lett. 207 B (1988) 253.
- [112] S. Gupta and H. Satz, Z. Phys. C 55 (1992) 391.
- [113] R. C. Hwa and J. Pišut, Phys. Rev. C 58 (1998) 434.
- [114] J.W. Qiu and J. P. Vary, hep-ph/9809442, 1998.
- [115] R. Vogt, Phys. Reports 310 (1999) 197.
- [116] R. Vogt and S. Gavin, Phys. Rev. Lett. 78 (1997) 1006.
- [117] D. Kharzeev and H. Satz, Phys. Lett. B 356 (1995) 365.
- [118] D. Kharzeev, Nucl. Phys. A 558 (1993) 331c;
K. K. Seth, Nucl. Phys. A 629 (1998) 358c.
- [119] S. Gupta and H. Satz, Phys. Lett. B 283 (1992) 439.
- [120] R. Vogt and S. Gavin, Nucl. Phys. B 345 (1990) 104.
- [121] F. Karsch and H. Satz, Z. Phys. C 51 (1991) 209. *tex* *gsi*
- [122] J.-P. Blaizot and J.-Y. Ollitrault, Phys. Rev. Lett. 77 (1996) 1703.
- [123] M. Gonin (NA50 95), Nucl. Phys. A 610 (1996) 404c.
- [124] C. Cicaló (NA50), Nucl. Phys. A 661 (1999) 93c.
- [125] N. Armesto, E. G. Ferreira and A. Capella, Phys. Rev. C 59 (1999) 395.
- [126] A. D. Martin, R. G. Roberts and W. J. Stirling, Int. Journal of Mod. Phys. A 10 (1995) 2885.
- [127] C. W. deJager, H. deVries and C. deVries, Atomic Data and Nuclear Data Tables 14 (1974) 485.

- [128] M. Nardi and H. Satz, Phys. Lett. B 442 (1998) 14.
- [129] J. W. Cronin et al., Phys. Rev. D 11 (1975) 3105.
- [130] S. Gavin and M. Gyulassy, Phys. Lett. 214B (1988) 241.
- [131] J. Hüfner, Y. Kurihara and H. J. Pirner, Phys. Lett. 215B (1988) 218.
- [132] J.-P. Blaizot and J.-Y. Ollitrault, Phys. Lett. 217B (1989) 386 and 392.
- [133] N. P. Zotov and V. A. Saleev, Sov. J. Nucl. Phys. 53 (1991) 523.
- [134] C. Baglin et al. (NA38), Phys. Lett. B 262 (1991) 362.
- [135] S. Gavin and R. Vogt, hep-ph/9610432, Oct. 96
- [136] D. Kharzeev, M. Nardi and H. Satz, Phys. Lett. B 405 (1997) 14.
- [137] R. C. Hwa and K. Kajantie, Phys. Rev. D 32 (1985) 1109.
- [138] H. Satz, in *Large Hadron Collider Workshop*, G. Jarlskog and D. Rein (Eds.), Aachen 1990, CERN 90-10/ECFA 90-133.
- [139] J. Rafelski, Phys. Reports 88 (1982) 331.
- [140] A. Breakstone et al., Z. Phys. C 33 (1987) 333;
for a survey, see R. Stock, Annalen Phys. 48 (1991) 195.
- [141] C. Hoehne (NA49), Nucl. Phys. A 661 (1999) 485c.
- [142] J. Bachler et al. (NA49), J. Phys. G 25 (1998) 199;
R. Stock, Nucl. Phys. A 661 (1999) 282c;
F. Sikler, Nucl. Phys. A 661 (1999) 45c.
- [143] See e.g., U. Heinz, Nucl. Phys. A 368 (1998) 357c, and further references there.
- [144] G. Roland et al. (NA49), Nucl. Phys. A 638 (1998) 91c.
- [145] P. Braun-Munzinger, I. Heppe and J. Stachel, Phys. Lett. B 465 (1999) 15.
- [146] J. Cleymans, private communication.
- [147] J. Cleymans, K. Redlich and D. K. Srivastava, Phys. Rev. C 55 (1997) 1431.
- [148] See e.g. R. Stock, Nucl. Phys. A 544 (1992) 405c.
- [149] T. S. Biro, B. Müller, and X.-N. Wang, Phys. Lett. B 283 (1992) 171.
- [150] J. Ellis and K. Geiger, Phys. Rev. D 52 (1995) and Phys. Rev. D 54 (1996) 1967.
- [151] H. Satz and D. K. Srivastava, Phys. Lett. B 475 (2000) 225.

- [152] K. Geiger and D. K. Srivastava, Phys. Rev. C 56 (1997) 2718 and Phys. Lett. B 422 (1998) 39.